AD NUMBER
AD460593
LIMITATION CHANGES
TO: **Approved for public release; distribution is unlimited.**
FROM: **Distribution authorized to U.S. Gov't. agencies and their contractors; Administrative/Operational Use; JAN 1965. Other requests shall be referred to Office of Naval Research, Washington, DC 20360.**
AUTHORITY
onr ltr, 28 jul 1977

SU-SEL-65-002

The Synthesis of Sweep-Frequency Ground Backscatter by Digital Computer

by
T. A. Croft

460593

January 1965

Technical Report No. 84

Prepared under
Office of Naval Research Contract
Nonr-225(64), NR 088 019, and
Advanced Research Projects Agency ARPA Order 196-65

RADIOSCIENCE LABORATORY

STANFORD ELECTRONICS LABORATORIES

STANFORD UNIVERSITY · STANFORD, CALIFORNIA

SEL-65-002

THE SYNTHESIS OF SWEEP-FREQUENCY GROUND BACKSCATTER BY DIGITAL COMPUTER

by

T. A. Croft

January 1965

Technical Report No. 84

Prepared under
Office of Naval Research Contract
Nonr-225(64), NR 088 019, and
Advanced Research Projects Agency ARPA Order 196-65

Radioscience Laboratory
Stanford Electronics Laboratories
Stanford University Stanford, California

ABSTRACT

A high-frequency pulse radar often receives energy which has propagated through the ionosphere to the ground, scattered, and then returned to the radar again via the ionosphere. When this energy is displayed as a function of both time delay and operating frequency, the record is called sweep-frequency backscatter. In this report a digital computer technique is devised to synthesize such records in a manner which is quantitative in all parameters.

The synthesis is designed so that very few approximations are needed. Full allowance is made for the following: a spherical earth and ionosphere; a wide variety of electron-density variations in height and range; ionospheric absorption which varies with frequency, range, and the ray angle; radar antenna gain as a function of frequency, azimuth, and elevation; ground-scattering characteristics which vary with frequency, range, and the angle of incidence; ground-reflection coefficients which vary with frequency and range; the transmitted pulse shape, duration, and power level; receiver bandwidth and total received noise power. Only three approximations are made: the discrete number system is substituted for continuous numbers; ray theory is used with the assumption that energy is distributed uniformly between adjacent closely spaced raypaths; the effect of the geomagnetic field on raypath range and group time delay is neglected.

The digital synthesis has two major uses. First, it is possible to vary a single parameter in a known way and then see the effect that the variation should have on ground backscatter. For example, a ripple of known characteristics can be inserted in the ionosphere at a known range and the resulting perturbation in the ground backscatter can be calculated.

The second major use of the program is the synthesis of a close likeness of a specific experimental record. This synthetic record serves to confirm knowledge of the mechanisms which play a part in ground backscatter. For example, the ground-scatter coefficient varies with frequency, terrain type, and incidence angle in a manner which is not presently well understood. The process of making a synthetic record to

match an experimental record will involve the trial of several hypothetical scatter functions until one is found which duplicates observed behavior. Since most of the other contributing mechanisms exhibit a predictable behavior, it will thus be possible to isolate the scatter pattern and study it independently.

CONTENTS

TABLES

Number

ILLUSTRATIONS

Figure

ACKNOWLEDGMENT

The author wishes to acknowledge his indebtedness to Professor O. G. Villard, Jr. and Professor A. M. Peterson, under whose guidance this research was carried out, and to Dr. G. H. Barry, who gave some crucial assistance in the early development. Many thanks are also due Mr. C. R. Gilliland, who was primarily responsible for assembly and operation of the calibrated radar, and Mrs. L. Gregory for her excellent digital programming.

I. INTRODUCTION

In the study and use of radio frequencies in the high-frequency band, a commonly encountered phenomenon is the reception of energy which is scattered off the ground and propagated to the receiver after ionospheric refraction. This "ground backscatter" arises in an easily recognized form when the source of energy is a pulse transmitter located near the receiver. Echoes of ragged and fading structure are often found after a time delay of a few milliseconds.

When backscatter was first discovered, it was attributed to the action of reflectors of some sort located in the ionosphere [Ref. 1]. Only in recent years was it firmly established that the predominant source of such echoes is scatter from the ground itself, after propagation through the ionosphere [Refs. 2 and 3]. Several historical accounts of backscatter studies are available [Refs. 4, 5, and 6], so another will not be given here.

A. DEFINITION OF THE PROBLEM

The term "backscatter" will be used here in a restricted sense to mean ionospherically propagated energy scattered by the ground. The phenomenon which will be analyzed is the echo which would be received by a pulse radar in the high-frequency band when the sole source of returning energy is ground scatter. This source accounts for most of the echoes which are received by hf radar, and other echoing sources have been analyzed in considerable detail elsewhere. Examples are the following: field-aligned ionization in the vicinity of the auroral zone [Ref. 7], in the temperature latitudes [Refs. 8 and 9], and near the equator [Ref. 10]; direct echoes from sporadic E patches [Ref. 11]; apparent echo surfaces due to local dense regions or turbulence in the E and F regions [Ref. 12]; man-made regions of dense ionization [Ref. 13]; incoherent electron scatter [Ref. 14]. The analysis of these phenomena is in most cases less complex than it is for the case of ground backscatter because they involve the interaction of fewer mechanisms. A

great deal has been written about ground backscatter, and it is well summarized in the four lists of abstracts which are available [Refs. 15, 16, 17, and 18].

Below the maximum plasma frequency of the ionosphere, f_c, the strongest source of echo is the multiple return from vertical incidence. This return is usually so strong that it masks the backscatter echo. Consequently this analysis will be limited to frequencies above f_c (usually 3 to 6 Mc) where backscatter can commonly be seen.

These frequencies are well above the electron gyrofrequency, which remains below 1.5 Mc in all the regions traversed by energy which plays a part in backscattering [Ref. 19]. Other workers have investigated this matter and concluded that the geomagnetic field causes changes in the raypath parameters which are so small that the field may safely be neglected [Ref. 20]. This is an extremely fortunate circumstance because it leads to a considerable simplification in the mathematics with an attendant decrease in the cost of computation. The upper frequency limit of interest is established by the maximum frequency that can be refracted back to the ground by the ionosphere under the average conditions, roughly 25-35 Mc.

With the understanding of the nature of ground backscatter came a realization of its potential value as a means for study of the refracting characteristics of the ionosphere. Using a pulse radar in the high-frequency band, one can acquire a considerable amount of information about the nature of the ionosphere at a distance from the equipment in a desired direction [Ref. 21]. This technique shows its greatest promise when the transmitter and receiver are made to sweep through the high-frequency band so that the backscatter can be studied as a function of both time delay and the frequency of the radio waves [Refs. 22 and 23]. These "sweep-frequency ground-backscatter" records have been gathered for a number of years; the details of their structure are complex and interesting although not now well understood.

If sweep-frequency ground-backscatter records could be properly interpreted to shed light on the nature of the ionosphere in the region of refraction, they would be of great use to the many organizations which

use the high-frequency band as a means of communication. These organizations form an important and large segment of the communications industry, primarily by virtue of the large bandwidth available and the ability of these waves to refract off the ionosphere to reach around the curvature of the earth.

Also, it should be noted that the proper interpretation of backscatter records would be valuable in the study of the upper atmosphere, a region of increasing importance with the advent of nuclear weapons and rocket travel. The ability of a backscatter sounder to examine the ionosphere at considerable lateral distance permits study of areas which are otherwise inaccessible due to geographical or political limitations. Backscatter techniques offer the possibility of examining the ionosphere at a distance from a single station which operates at a fixed location without remote assistance or use of remote equipment (Fig. 1). This single fact holds out so much promise that considerable effort is justified in an attempt to understand the phenomenon. It may prove feasible

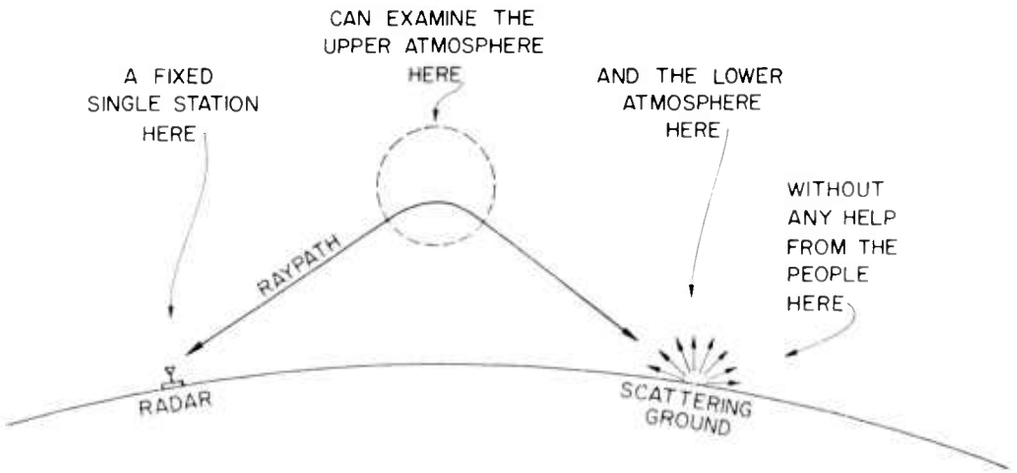

FIG. 1. THE PRIMARY ADVANTAGE OF BACKSCATTER.

to study the detailed behavior of the ionosphere at a distance over areas that are inaccessible; even over accessible areas the backscatter technique offers the advantage of technical simplicity when compared to the various alternate methods that use multiple cooperating stations.

The theoretical study of the phenomenon has led to a rather disappointing lack of success. In fact, the reader will find that this paper gives the first analysis of such records which is realistically quantitative regarding signal strength. Since a backscatter record is merely a time history of signal strength, it can be seen that this is a rather basic quantity which must be understood if the data are to be properly interpreted.

Most of the information successfully derived from backscatter records has been taken from a study of the frequency dependence of the leading edge of the echo. This parameter can be studied without analysis of the signal strength because a phenomenon called "time-delay focusing" usually causes the backscatter echoes to begin abruptly so that the skip-distance portion of the return can be identified with some confidence [Ref. 24]. One useful application of this has been the determination of the MUF of a propagation path by means of the equipment located solely at one end of the path [Ref. 25].

B. METHOD OF STUDY

The backscatter phenomenon is a complex interaction of so many different mechanisms that the most practical approach to its study is the use of a modern high-speed digital computer. The present method taxes the capability of an IBM 7090--a fairly modern machine, which may be one of the primary reasons why it has taken so long to acquire an ability to study backscatter signal strength. Analytic and graphical methods are useful only if the investigator is willing to make some extreme simplifying assumptions (i.e., a parabolic ionosphere) or if he is interested in just those aspects of the phenomenon which can be attacked by some non-computer technique (i.e., the time delay of the leading edge of the echo). Some authors have attempted to calculate the signal strength, but their methods have either been too difficult for practical use [Ref. 26] or else they have made the calculation short by means of unrealistic simplifying approximations [Refs. 20 and 27].

Work has been done in determining skip-distance time delay of simple ionospheres by analog computer [Ref. 28], but the method did not give any information about signal amplitude and so its usefulness was limited.

The approach to be described begins with a rather detailed analysis of the backscatter phenomenon. Subsequently, the results of this analysis are used to devise a computer program which will simulate the various mechanisms that comprise backscatter, leading to a synthetic radio record which might be acquired by a high-frequency pulse radar. The program is run at a number of frequencies, and finally a simple manual operation is used to combine many such records into a single "sweep-frequency ground-backscatter record."

Both analysis and synthesis make use of raypaths that are calculated through a known ionosphere by computer. The synthesis process makes use of "raysets," which are groups of numbers stored on punched cards in such a manner as to permit the subsequent reconstruction of the characteristics of a family of raypaths at low cost.

Since raypaths may be considered to be streamlines in a flux of energy, the basic assumption is made that energy which starts out between closely spaced raypaths will stay between them, uniformly spaced in both range and time, and thus the computer can calculate the direction of travel and the distribution of energy in space and time. This approximation approaches truth so long as the rays are closely spaced. A considerable cost reduction is achieved by neglecting the magnetic field, an approximation which is good in this application. These approximations, together with the use of a discrete rather than a continuous number system, are the only ones needed; thus the "rayset method" is shown to be an economical approach for the realistic calculation of the amplitude of a ground-backscatter signal. Each run costs about two dollars, and the result is automatically plotted for an extra dollar.

C. APPLICATIONS OF THE TECHNIQUE

The backscatter synthesis program can be used as a means of studying the phenomenon itself. Because the synthesis technique is so realistic, calculations can show the effect on ground backscatter of changes in the following:

1. The shape and elevation angle of the lobes in antenna gain patterns.
2. Secondary lobes in the gain patterns.

3. The degree of ionospheric absorption.

4. Changes in the absorption as a function of range, such as when the radar looks across a twilight zone.

5. The duration of the transmitted pulse.

6. The shape of the transmitted pulse, including the effect of limited receiver bandwidth which tends to smooth the pulse.

7. The absolute magnitude of the scattering coefficient of the ground.

8. The dependence of this scattering coefficient with ground range as, for example, when a radar looks out over flat land, mountains, and sea.

9. The dependence of the scattering coefficient on the angle at which energy strikes the ground.

10. Variation of scattering coefficient with frequency.

11. The reflecting coefficient of the ground, which is a measure of the amount of energy specularly reflected. This affects the relative power of multiple-hop backscatter echoes.

12. Variation of the reflecting coefficient as a function of ground range due to the presence of the various types of terrain which also affect the scattering coefficient.

The effect of changes in the nature of the ionosphere can also be studied by this technique. The kinds of changes that can be studied are limited only by the versatility of the raytracing program used to generate the raysets. Practically any raytracing program can be adapted to this purpose; the particular one used to support these calculations would permit investigations of the following changes in the ionosphere:

13. Chapman layers, parabolic layers, E, F_1, and F_2 layers in various combinations and relative proportions; in fact, any ionosphere which can be adequately described by 3000 sample points. (Usually, 300 serve the purpose.)

14. Horizontal gradients of electron density (ionospheric tilts) which are gentle but widespread, similar to those which are normally present in the ionosphere near dawn or twilight.

15. An isolated irregularity in an otherwise undisturbed ionosphere. The irregularity can be some kind of localized dense or rarefied region. By carrying out the synthesis with the irregularity at a succession of different ranges, it is possible to simulate the time history of the effect of a traveling irregularity on sweep-frequency ground backscatter.

II. FOUNDATIONS OF THE BACKSCATTER ANALYSIS

In preparation for the analysis of backscatter, three pertinent subjects will be discussed:

1. The concept of a rayset as a means of storing raypath characteristics.
2. Experimental measurements of the ground-backscatter coefficient.
3. Nondeviative absorption formulas, manipulated into a useful form.

A. THE METHOD OF CALCULATION BY MEANS OF RAYSETS

Before proceeding with analysis of backscatter, it is necessary to introduce a mathematical concept which has been called the "rayset." Calculations will be keyed to the utilization of this concept.

It is assumed that there exists a digital computer program which traces the paths of radio waves in the ionosphere. Such programs are in operation at several institutions [Ref. 29] and they form the basis of a rapidly advancing technology in the study of the ionosphere. The particular raytracing program is largely immaterial, so long as it has the requisite versatility, accuracy, and sufficient speed to be run at a reasonable price. The program used to support this work has been described in a previous publication [Ref. 30]; basically, it is a successive series of solutions of Snell's Law in a concentrically stratified ionosphere. The index of refraction is a scalar which varies vertically and horizontally as indicated on Fig. 2.

This program is able to present its results in any combination of three forms: the raypaths will be drawn in curved earth coordinates; selected numerical data can be printed out to show the ray trajectory parameters; or the computer may punch the data into the rayset cards. Figure 3 shows the automatically drawn raypaths which were calculated through a Chapman ionosphere whose vertical-incidence critical frequency was 4 Mc. These raypaths were originally drawn by a small x-y plotter controlled by a tape from the IBM 7090. The true shapes of the rays are shown over a curved earth. To the author's knowledge, this is the only raytracing program which directly plots its resulting raypaths in an undistorted coordinate system.

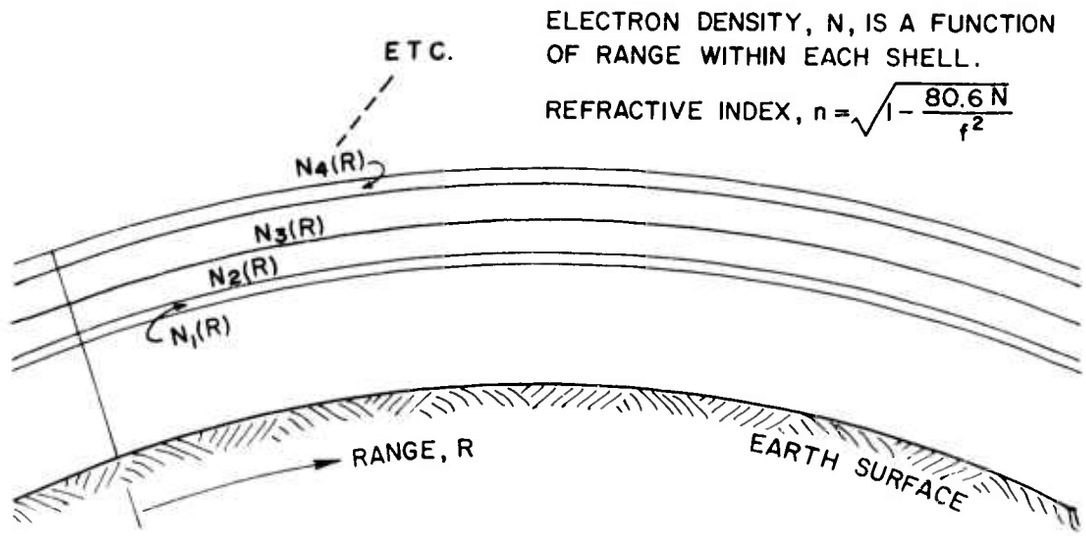

FIG. 2. METHOD OF PROGRAMMING ELECTRON-DENSITY VARIATIONS.

A rayset is a set of eleven numbers which characterize a particular hop of a particular calculated raypath. This set is stored in one punched card; the system is so devised that a deck of appropriately related punched cards will contain sufficient organized information that the user can extract practically anything he wishes to know concerning the interrelationships of the various raypaths that have been computed. Thus, decks of raysets can be used as input data in subsequent computer programs. In this way, the information which was acquired by raytracing can be used over and over at practically no cost.

New programs can be written based on the assumption that the relationships between raypath parameters are known quantities. For example, the derivative which relates the change in raypath ground range that arises from an associated change in the raypath takeoff angle can be considered as a known number; this derivative appears in most expressions for energy density which reaches the ground. Consequently, the analysis which follows may stop when it encounters such a quantity.

This is a tremendous advantage because it is usually the unknown variations of such parameters which make other forms of analysis either difficult or impossible. The rayset method was previously used by the author for the synthesis of oblique ionograms [Ref. 31]. In that case

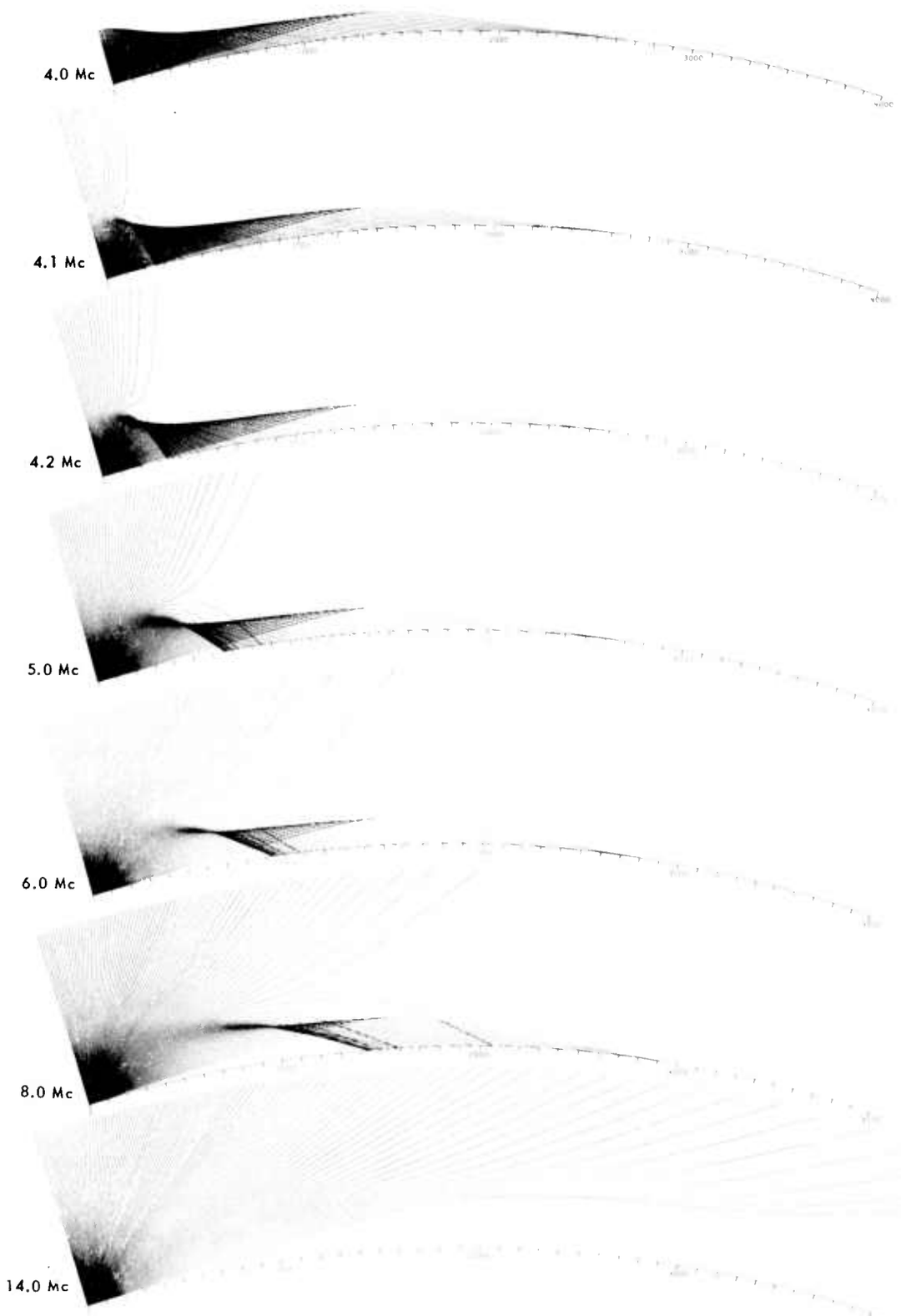

FIG. 3. EXAMPLES OF CALCULATED RAYPATHS AUTOMATICALLY DRAWN.

the analysis was very simple and the subsequent synthesis was made almost trivial by the use of raysets.

The nature of a rayset can best be understood by consideration of the process which goes on inside a digital computer when raytracing is taking place. Each ray is calculated individually; the computer is instructed to go to a designated starting point and calculate the path originating at that point which propagates at a given initial takeoff angle above the surface of the earth as indicated in Fig. 4. Using circular coordinates and appropriate equations, the computer calculates the curved path of the ray as it traverses a medium of varying index of refraction.

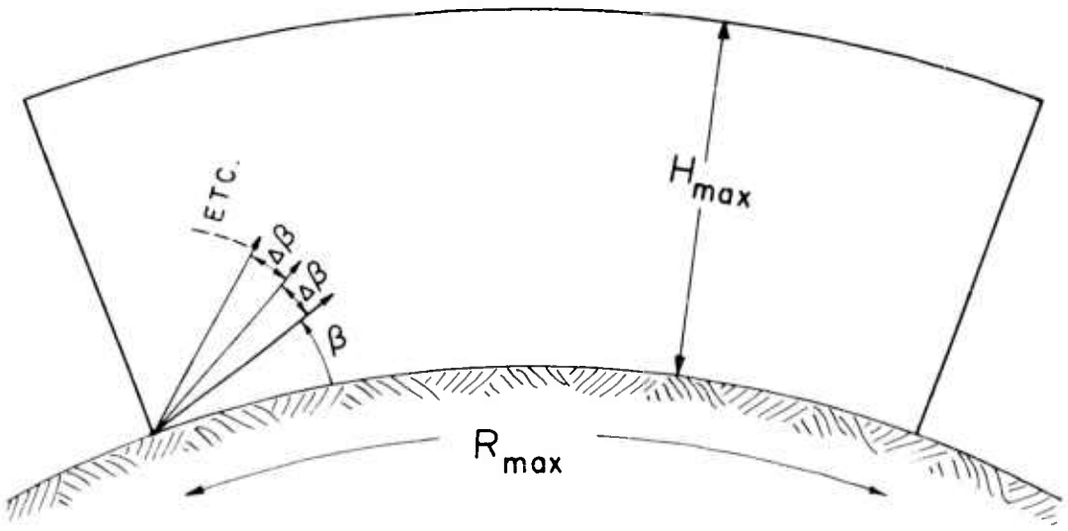

FIG. 4. ILLUSTRATION OF SOME LOGIC CONTROLS USED IN RAYTRACING.

Many things can happen to the ray; it can refract off the ionosphere and execute normal hops. It may go so far that it exceeds a specified maximum range, R_{max} on Fig. 4, in which event the computer will be instructed to shut off. Similarly, there might be a specified maximum altitude, H_{max}, at which raypath calculations would be terminated. If the index of refraction varies in the horizontal direction, the ray may climb into the ionosphere only to come down on top of a densely ionized area; if the ray then refracts upward off this area, it is said

to have executed a "perigee." This sometimes happens when rays are calculated in an ionosphere with an E layer whose electron density increases with increasing range.

Usually, a ray trapped between the E and F layers will either escape or reach the maximum range. However, there may be a buildup in the electron density between the E and F layers of sufficient magnitude that the index of refraction becomes imaginary in all forward directions. This electron-density distribution is called a "closed trap" by the author, and rays are terminated when they encounter this circumstance. However, in the actual situation, the energy must reflect and come back out.

Each time a ray encounters the earth, a perigee, or a raypath termination instruction, the computer stops temporarily to store on magnetic tape a set of numbers which will later be punched into a card to be called a rayset. These parameters are illustrated on Fig. 5. Consider the first hop of the ray shown. When the computer finds that the ray strikes the earth, it stores the numbers shown in the top row on the

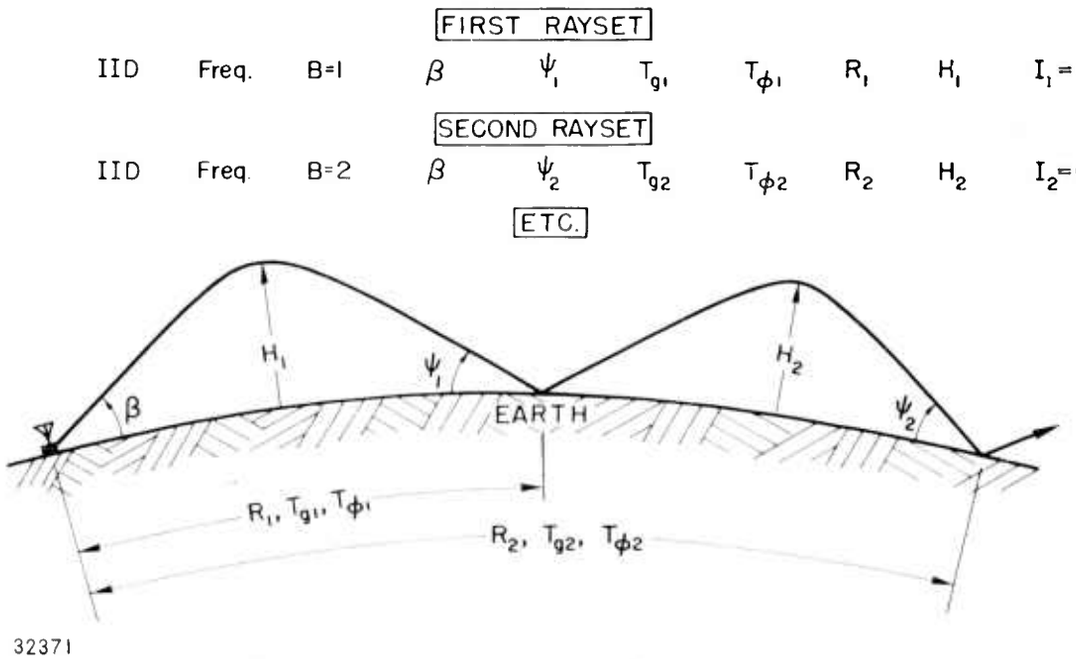

FIG. 5. PARAMETERS INCLUDED IN A RAYSET.

figure. The parameter IID (ionosphere identification) is a three-digit number that identifies the particular ionosphere used for calculation. The frequency F is given in kilocycles. The parameter B (bounce) is given the value 1 because this is the first time the ray has hit the earth. The parameter β is the takeoff angle, and ψ_1 is the landing angle as shown on the figure. The ground range from the transmitter to the point of impact of the ray, R_1, is given in kilometers. The group and phase time delays, T_{g1} and $T_{\phi 1}$, are given in milliseconds. The height H_1 is the height of the apogee of the ray as shown. The parameter I_1 (indicator) is a number which is coded 0 through 6 and serves to identify the general nature of the raypath. Notice that $I = 0$ when the ray hits the earth; $I = 1$ if the ray exceeds maximum height and $I = 2$ or 3 if the ray exceeds maximum range. Similarly, $I = 4$ or 5 if the ray executes perigees, and $I = 6$ if the ray encounters a closed trap.

After the computer has stored the rayset described above, it continues calculating the ray until it again encounters the earth, a perigee, or a raypath termination instruction. In the example shown on Fig. 5, the ray hit the ground for a second time and the computer stored the rayset shown as the second row in the figure. Here the information is similar to the first rayset except that $B = 2$, because this is the second encounter with the ground. Also, the range, group time delay, and phase time delay are all given as accumulated totals counted from the transmitter.

As a matter of interest, the definitions of the various parameters as shown on Fig. 5 apply only when $I = 0$. When I is nonzero, the ranges, times, and angles are defined differently so as to maximize the ability of the user to reconstruct the ray trajectories. For example, if the third hop of the ray exceeded maximum range going upward, as it appears to do in Fig. 5, the time and range would be measured to the point of ray termination. The height would be the height of termination and ψ would be the terminal angle of the ray relative to horizontal. The indicator would be $I = 2$. If the ray had exceeded maximum range coming down, the same definitions would apply except that the indicator would be $I = 3$. Actually, the change in the indicator number

serves only to establish the algebraic sign of the angle ψ. This procedure conserves one column on the punched card and thus maximizes the amount of information it can convey.

Figure 6 shows the appearance of a family of rayset cards when they are printed out. The family shown has been calculated through a Chapman ionosphere with a 100-km scale height and a 4-Mc critical frequency. Thus, the operating frequency is twice the critical frequency. The height of the maximum occurs at 300 km and there were no horizontal gradients of electron density in this example. The corresponding rays are drawn in the sixth plot on Fig. 3.

IID	FREQ KC	HOP	BETA DEG	PSI DEG	GROUP TIME MS	PHASE TIME MS	RANGE KM	HT KM	INUMB
5 023	8000.	1	-0.	0.00000	10.8006718	10.7229493	3174.4673	160.34241	0
5 023	8000.	1	0.50000	0.50000	10.4383457	10.3605003	3065.8038	160.40894	0
5 023	8000.	1	1.00000	1.00000	10.0931543	10.0149453	2962.1877	160.62427	0
5 023	8000.	1	1.50000	1.50000	9.7616800	9.6830413	2862.6362	161.00000	0
5 023	8000.	1	2.00000	2.00000	9.4511156	9.3715227	2769.1909	161.51292	0
5 023	8000.	1	2.50000	2.50000	9.1565795	9.0758870	2680.4518	161.96838	0
5 023	8000.	1	3.00000	3.00000	8.8747151	8.7927719	2595.4536	162.51965	0
5 023	8000.	1	3.50000	3.50000	8.6090416	8.5256091	2515.1899	163.25287	0
5 023	8000.	1	4.00000	4.00000	8.3580719	8.2729403	2439.2286	164.12195	0
5 023	8000.	1	4.50000	4.50000	8.1214892	8.0344212	2367.4699	165.08350	0
5 023	8000.	1	5.00000	5.00000	7.8994121	7.8101246	2299.9374	166.11570	0
5 023	8000.	1	5.50000	5.50000	7.6906605	7.5989053	2236.2868	167.22662	0
5 023	8000.	1	6.00000	6.00000	7.4950919	7.4006006	2176.4666	168.44589	0
5 023	8000.	1	6.50000	6.50000	7.3120553	7.2145738	2120.2820	169.79730	0
5 023	8000.	1	7.00000	7.00000	7.1366974	7.0361863	2066.3518	171.09644	0
5 023	8000.	1	7.50000	7.50000	6.9761081	6.8720565	2016.6688	172.52197	0
5 023	8000.	1	8.00000	8.00000	6.8211829	6.7136837	1968.6552	174.04387	0
5 023	8000.	1	8.50000	8.50000	6.6816314	6.5697770	1925.0365	175.55908	0
5 023	8000.	1	9.00000	9.00000	6.5471288	6.4313715	1882.6925	177.14105	0
5 023	8000.	1	9.50000	9.50000	6.4254458	6.3050094	1844.4004	178.69294	0
5 023	8000.	1	10.00000	10.00000	6.3085191	6.1833240	1807.2891	180.53003	0
5 023	8000.	1	10.50000	10.50000	6.1989045	6.0687276	1772.2659	182.26644	0
5 023	8000.	1	11.00000	11.00000	6.0966413	5.9611966	1739.3330	184.09235	0
5 023	8000.	1	11.50000	11.50000	5.9998949	5.8590115	1707.9711	186.00690	0
5 023	8000.	1	12.00000	12.00000	5.9174750	5.7700701	1680.6109	187.74942	0
5 023	8000.	1	12.50000	12.50000	5.8367042	5.6828467	1652.7275	189.89101	0
5 023	8000.	1	13.00000	13.00000	5.7612810	5.6006715	1628.3387	191.89076	0
5 023	8000.	1	13.50000	13.50000	5.6931461	5.5252620	1604.9684	193.96210	0
5 023	8000.	1	14.00000	14.00000	5.6241665	5.4492497	1581.3771	196.01105	0
5 023	8000.	1	14.50000	14.50000	5.5711712	5.3875793	1562.1634	198.11729	0
5 023	8000.	1	15.00000	15.00000	5.5201049	5.3277348	1543.4552	200.31413	0
5 023	8000.	1	15.50000	15.50000	5.4783050	5.2761201	1527.2735	202.40007	0
5 023	8000.	1	16.00000	16.00000	5.4307674	5.2196226	1509.5049	204.63569	0
5 023	8000.	1	16.50000	16.50000	5.3997081	5.1773723	1496.1677	207.30565	0
5 023	8000.	1	17.00000	17.00000	5.3720572	5.1381271	1483.7071	209.85040	0
5 023	8000.	1	17.50000	17.50000	5.3449511	5.0997654	1471.3476	212.30439	0
5 023	8000.	1	18.00000	18.00000	5.3205684	5.0627803	1459.6703	215.01886	0
5 023	8000.	1	18.50000	18.50000	5.3181986	5.0447208	1453.7955	217.70148	0
5 023	8000.	1	19.00000	19.00000	5.3109953	5.0224124	1446.5447	220.44486	0
5 023	8000.	1	19.50000	19.50000	5.3124439	5.0071214	1441.5013	223.38347	0
5 023	8000.	1	20.00000	20.00000	5.3263789	5.0018914	1439.6528	226.47754	0
5 023	8000.	1	20.50000	20.50000	5.3434397	4.9986794	1438.4522	229.76542	0
5 023	8000.	1	21.00000	21.00000	5.3666864	5.0004777	1438.7448	233.07080	0
5 023	8000.	1	21.50000	21.50000	5.4146826	5.0215904	1445.3012	236.71454	0
5 023	8000.	1	22.00000	22.00000	5.4768993	5.0533617	1455.3116	240.57568	0
5 023	8000.	1	22.50000	22.50000	5.5651234	5.1049240	1471.7456	244.86542	0
5 023	8000.	1	23.00000	23.00000	5.6824797	5.1781853	1495.2950	249.67162	0
5 023	8000.	1	23.50000	23.50000	5.8460481	5.2860113	1532.1713	254.93618	0
5 023	8000.	1	24.00000	24.00000	6.0913021	5.4548047	1585.1261	261.07800	0
5 023	8000.	1	24.50000	24.50000	6.5525358	5.7854409	1693.4778	269.19989	0
5 023	8000.	1	25.00000	25.00000	8.1115361	6.9379462	2073.6387	284.97051	0
5 023	8000.	1	25.50000	37.67967	9.0622348	7.8930444	2188.9791	900.00000	1

FIG. 6. A SAMPLE FAMILY OF ONE-HOP RAYSETS.

Using the information on these raysets, one can reconstruct most of the useful information that describes all of the possible one-hop rays through this ionosphere. Raysets computed through a very simple ionosphere such as this will prove useful in later synthesis for study of the effect on backscatter of equipment changes without the added complication in the record which appears when the ionosphere has layers or tilts.

B. THE GROUND-SCATTER PATTERN

In 1959, Neilson et al [Ref. 32] and Hagn [Ref. 33] of the Stanford Research Institute (SRI) flew an instrumented aircraft over various terrain types, investigating the behavior of backscattered power at 32.8 Mc. Although the data are restricted to one frequency, they appear to be the only comprehensive data available. Therefore, as a starting point, the SRI data will be used at all frequencies; however, it should be noted that the technique of backscatter synthesis being invented here may open an avenue for the investigation of the actual behavior of the ground-backscatter coefficient as a function of frequency, since all the other necessary parameters will be seen to exhibit a predictable behavior during changes of frequency.

The SRI results were expressed in terms of a parameter, ρ. In this paper, ρ denotes a reflection coefficient, so scattering will be symbolized K. On page 51 of Ref. 33, K is explained (in paraphrase) as follows:

> "When K is viewed as a loss parameter, one simple interpretation is to consider it the ratio of the received power actually measured to the power that would have been measured with K equal to unity. The case of K being unity corresponds to the earth acting as an antenna (with aperture equal to the area actually illuminated by the pulse) which receives the incident power and isotropically retransmits it without depolarization or loss into a hemisphere."

As a consequence of the definition of K, the theoretical treatment of backscatter will begin with the assumption that the earth acts as a completely reradiating, hemispherically isotropic antenna. The power received (according to the resulting equations) will then be multiplied

by K in order to bring the theoretical predictions into line with the SRI measurements or other known measures.

On Fig. 7 are shown Hagn's curves depicting the behavior of the parameter K as a function of the angle of incidence ψ for various terrain types. Also shown on the figure are curves of $\sin \psi$, $\sin^2 \psi$, and $\sin^4 \psi$. The labels H and V refer to horizontal and vertical polarization of the radiation being measured. It is somewhat remarkable that in all cases the horizontal polarization seems to exhibit a shape which is quite close to that of the curve of $\sin^4 \psi$. Since the vertical axis of Fig. 7 is logarithmic, curves can be shifted up and down on the plot simply by use of a scalar multiplier.

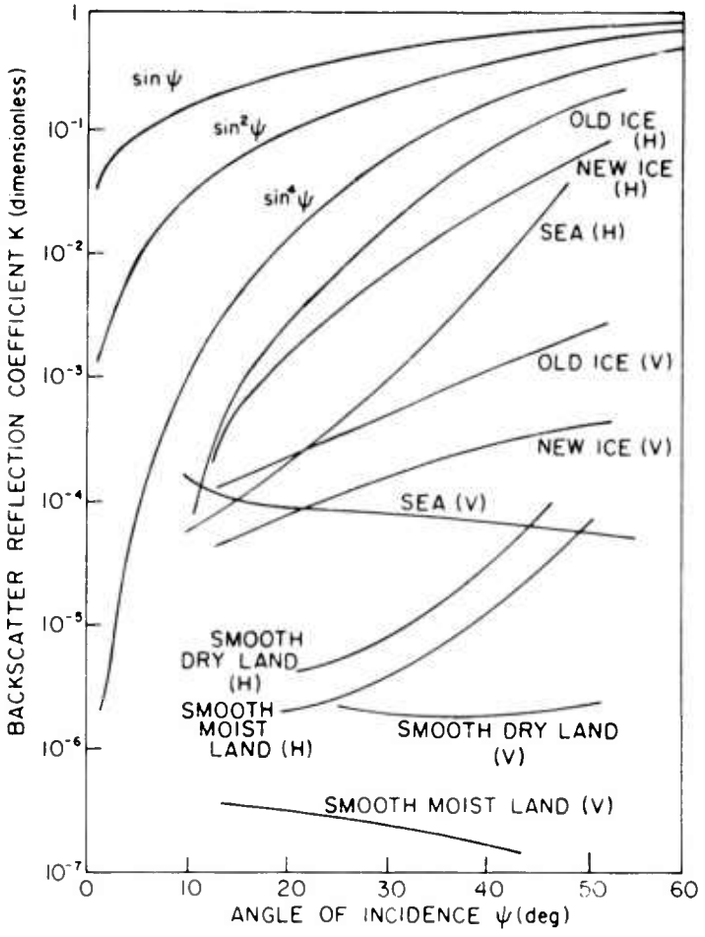

FIG. 7. 32-Mc BACKSCATTER COEFFICIENTS MEASURED BY AIRCRAFT.

For vertical polarization, the data are not so easily matched; in some cases it appears that the data will fit a $\sin^2\psi$ curve, whereas in other cases it appears that a constant would be more appropriate. Figure 8 shows the same curves separated by terrain type, together with analytic functions which have been selected as the closest reasonable match to each. It is seen that in some cases the agreement is quite close. The reader should not be excessively critical of small differences between the analytic function and the SRI measured curves, for the latter are actually smoothed representations of a wide variety of data and, in a sense, they reflect the judgment of Hagn.

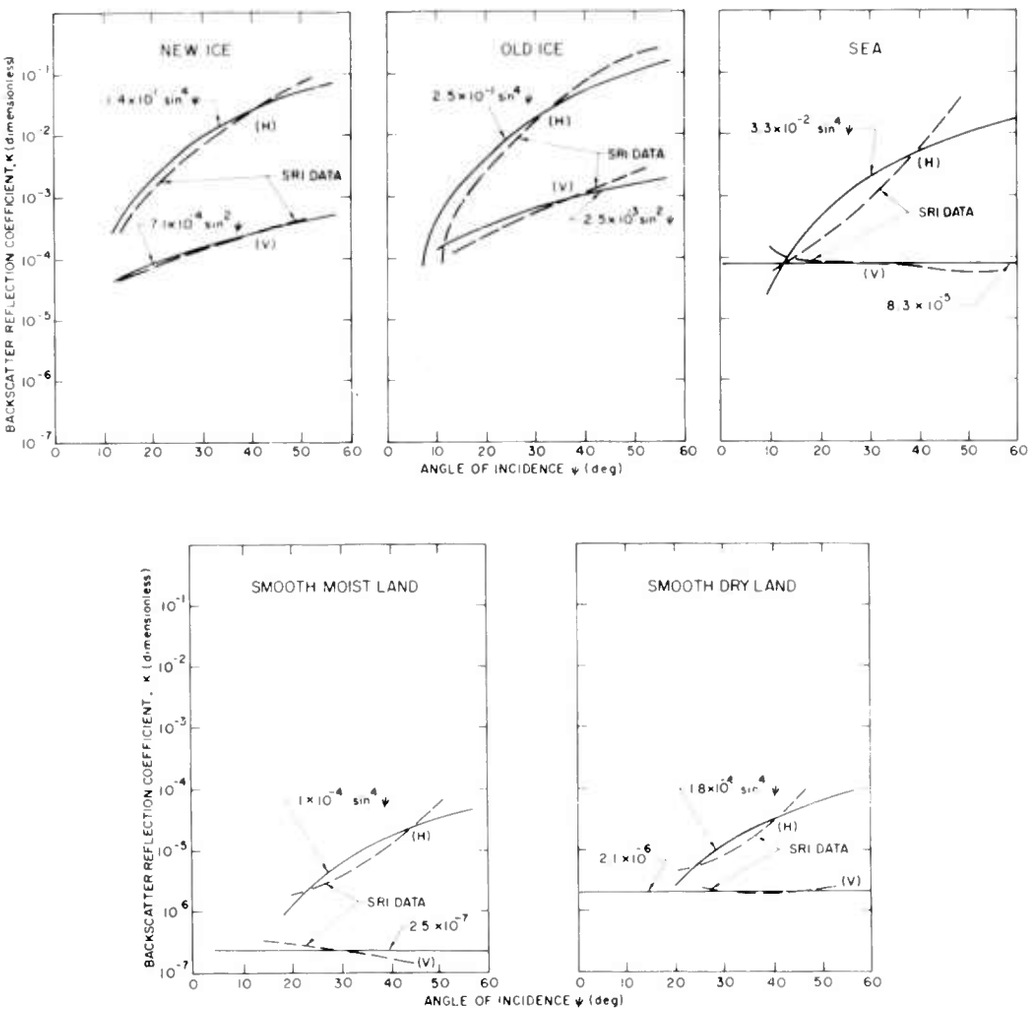

FIG. 8. ANALYTIC FUNCTIONS FITTED TO THE SCATTER DATA.

As a consequence of this curve-matching exercise, it was decided to represent the five types of terrain by the function

$$K(\psi) = K_1 \sin^4\psi + K_2 \sin^2\psi + K_3$$

where the values of K_1, K_2, and K_3 are as shown in Table 1, which gives the data used to produce Fig. 8.

TABLE 1. GROUND-REFLECTION COEFFICIENT FACTORS

Material	Horizontal Polarization	Vertical Polarization	
	K_1	K_2	K_3
New ice	1.4×10^{-1}	7.1×10^{-4}	0
Old ice	2.5×10^{-1}	2.5×10^{-3}	0
Sea	3.3×10^{-2}	0	8.3×10^{-5}
Smooth moist land	1×10^{-4}	0	2.5×10^{-7}
Smooth dry land	1.8×10^{-4}	0	2.1×10^{-6}

Although the SRI data are the only complete set, some other authors have mentioned isolated characteristics of ground scattering derived either from theory or experiment. The theoretical study of this subject is extremely difficult. It appears that those who try to analyze this phenomenon make approximations so severe that their results are questionable or else they are unable to solve the equations that they set up. There is a wide disagreement among the results which have been derived and so they will not be used here. However, the following items taken from the literature deserve mention:

1. Shearman [Ref. 20] states on theoretical grounds that the backscatter should vary as $\sin^4\psi$. It is also interesting to note that he made calculations which show that the magnetic field can

be neglected in backscatter calculations without introducing perceptible error in the location of the scatterers.

2. McCue [Ref. 6] acquired experimental data which indicated that land is a better scatterer than the sea when the angle ψ is small.

3. Ingalls and Stone [Ref. 34] made measurements at 18 and 24 Mc which seemed to indicate that the sea had a backscattering cross section of 10^{-4} m^2 for every square meter of sea.

4. Ranzi [Ref. 35] found that the sea was a better scatterer than the land by an amount which varied between 5 and 16 db. This same author [Ref. 36] found that the scattering coefficient of a mountain range depended very strongly on the particular characteristics of the troposphere. It appears that the refracting power of the troposphere varies slightly from day to day and makes small changes in the value of ψ at which the raypaths encounter the mountain range. If such small angular changes actually cause measurable changes of scattered power, this might be explained in terms of a scattering coefficient which varies quite strongly in the vicinity of $\psi = 0$ deg where Ranzi's measurements were made. Such a characteristic is exhibited by the functions $\sin^2\psi$ and $\sin^4\psi$.

5. Ament [Ref. 37] calculates theoretically that the scattering coefficient of a rough surface should vary in proportion to $\sin^2\psi$ and λ^{-1}, that is, inversely proportional to the wavelength of the radio frequency.

The mechanism for scattering of signals by terrain has been intensely studied, and the above references form only a partial view of the whole subject. The state of knowledge in this field, as of June 1961, is well summarized by a series of 77 abstracts which are given by Hagn, Neilson, and Smith [Ref. 15]. The most recent theoretical study of scattering at the time of this writing was made by Hagfors [Ref. 38]. His analysis applies only for values of ψ near 90 deg, so the results are of little use here; but he gives a lucid explanation of the common approach to this problem, together with a number of references more recent than those which were available in 1961 to Hagn et al.

C. THE METHOD OF TREATING ABSORPTION

One of the advantages of the technique developed here is that it permits use of the most basic theory as a source of information about the physical world. The processing of the data often involves a considerable

amount of arithmetic, but the application of the basic theories involved is seldom masked by complex mathematics or obscure approximations. The speed of the digital computer permits solution directly from the basic laws. Developments such as the Breit-Tuve theorem or Martyn's equivalence theorem are unnecessary approximations in this context.

The method by which absorption is taken into account should provide a clear example of the above. Absorption losses lead to a single, isolated factor in the final result, and so the analysis of absorption can be separated from the general backscatter problem and will be treated independently here.

The physical principle involved is that power is lost in proportion to that which remains, so that the amount which manages to penetrate an absorbing region varies as the factor

$$\exp\left(-\int k\, dz\right)$$

where k is called the absorption coefficient and z is the distance traversed. The quantity which is usually measured experimentally is the absorption index Ω, which is related to the coefficient by the equation

$$\Omega = \int k\, dh$$

where h is the vertical component of z. An assumption will be made that the absorbing region is centered about a height of 80 km, since this is the approximate height of the D layer, and only the nondeviative absorption will be considered here.

The above relations are basic and can be found, for example, in Ref. 39. There it is also shown that the coefficient of absorption should theoretically be inversely proportional to the square of the radio frequency in the absence of a magnetic field. If the magnetic field is taken into account, this proportion is approximately true provided the operating frequency exceeds the electron gyrofrequency (see, for example, Ref. 40), which will be a good approximation at the frequencies used throughout this study.

In actual practice, one of the best measures of absorption is obtained by observing successive multiple reflections of a pulse traveling vertically between the earth and the ionosphere. The technique is described in Ref. 39 where data from such an experiment are given. The technique yields good results but has two unfortunate limitations: (1) frequency is restricted to less than the vertical-incidence critical frequency of the most dense layer because total reflection must be obtained; (2) when frequency is near the critical frequency of any layer below the maximum, then the ray suffers a great deal of deviative absorption.

Nevertheless, such experimental data can be extrapolated so as to be useful in the prediction of the behavior of oblique propagated waves. In Fig. 9 the author has taken data from Ref. 39 and has attempted to make such an extrapolation from the cusped curve into a straight line where α is proportional to the inverse square of frequency. These data, it should be noted, applied in winter at noontime in a temperate zone at a time when the sunspot activity was low. On the extrapolated straight line, α equals 0.12 at a frequency of 10 Mc.

Unfortunately, there appear to be two different definitions in current use for the meaning of the index of absorption. In fact, both definitions are used in Ref. 39. The first definition, as given above, leads to the result that power is decreased by the factor $e^{-\alpha}$. However, field measurements of the absorption index are sometimes reduced through the use of a definition based on a power loss proportional to $10^{-\alpha}$ which facilitates use of the decibel as a unit. This latter definition is used in Fig. 9.

Let us call the former definition α_e and the latter α_{10}. Thus

$$e^{\alpha_e} = 10^{\alpha_{10}}$$

Comparison of the value of α_{10} from Fig. 9 with that which would be obtained if $\int k\, dh$ were measured, would reveal that two compensating

errors nearly cancel one another. That is, $\int k\, dh$ corresponds to $2\alpha_e$ (up and down) and since $2\alpha_e$ is only 15 percent larger than α_{10},

$$e^{2\alpha_e} \cong e^{\alpha_{10}}$$

Figure 10(a) shows the relation between an element of distance along an oblique raypath, Δz, and an element of distance along a vertical raypath, Δh, such as was used in the determination of the curve on Fig. 9. Here it is seen that

$$\Delta z = (\Delta h) \csc \zeta$$

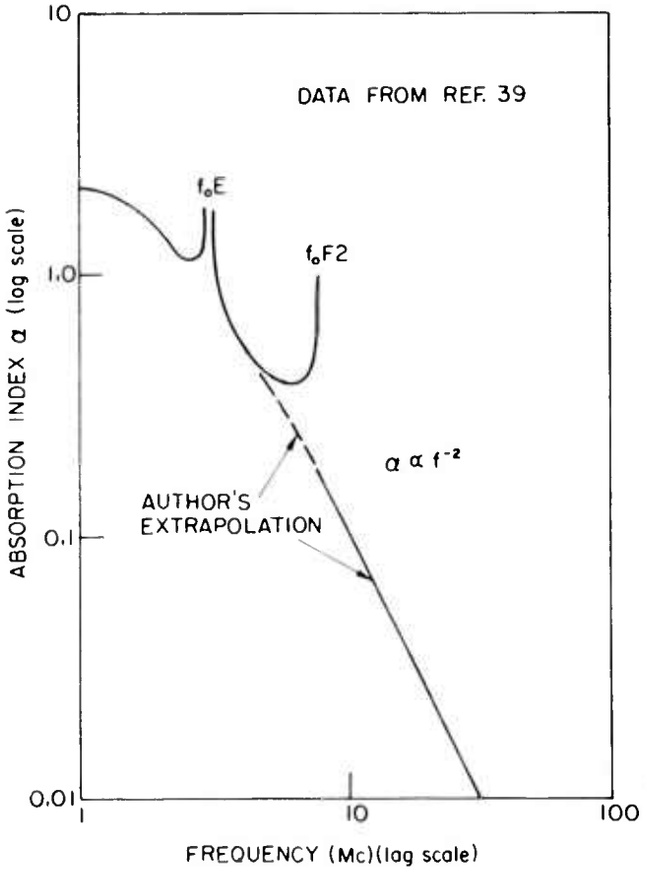

FIG. 9. FREQUENCY VARIATION OF THE ABSORPTION INDEX.

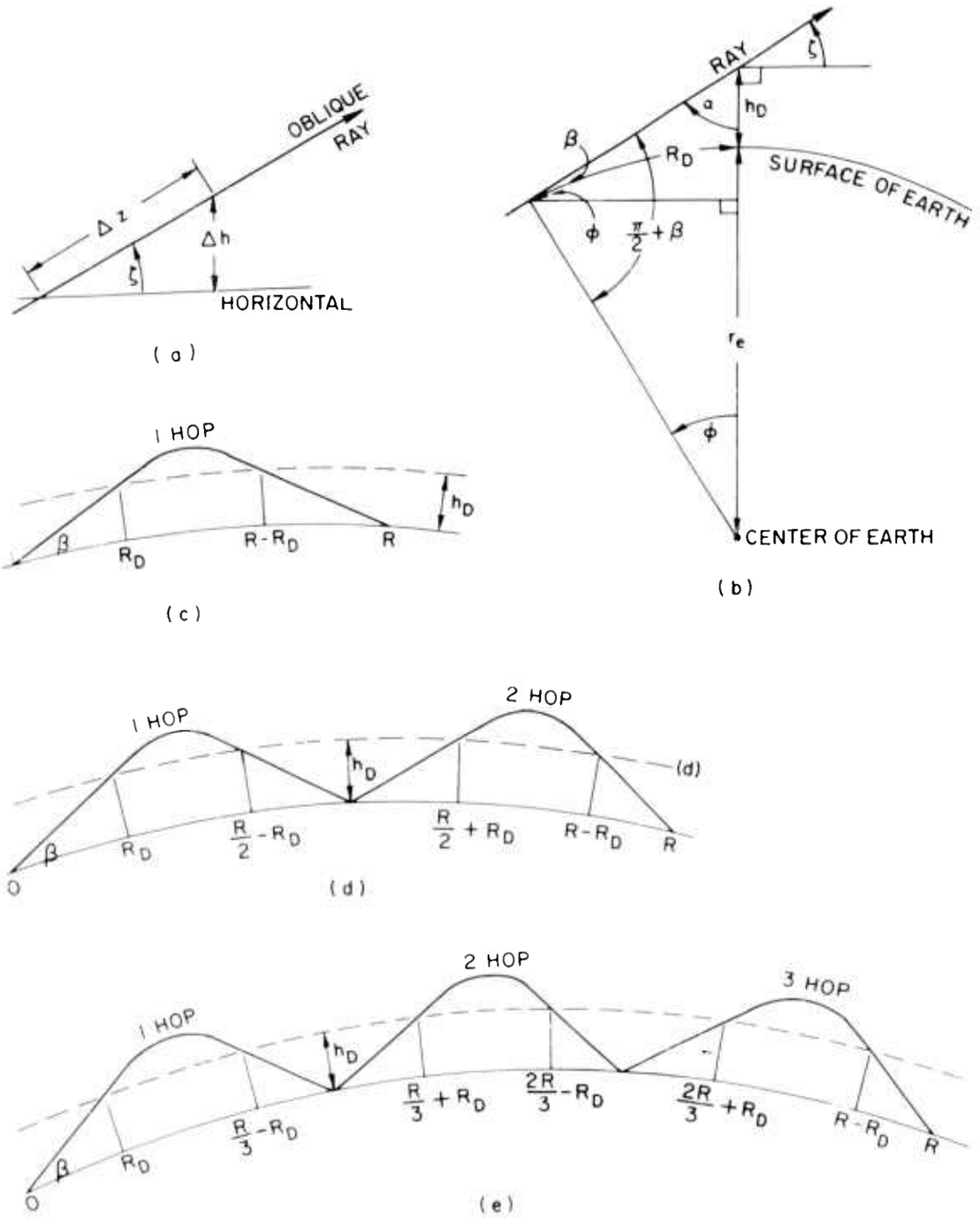

32693

FIG. 10. GEOMETRY USED IN ABSORPTION CALCULATIONS.

rom which it follows that absorption loss is

$$e^{-\alpha \csc \zeta}$$

Now, since α is proportional to the inverse of frequency squared, it will be more convenient to define a new parameter, E, which obeys the relation

$$E = F^2\alpha = 1.38 \times 10^7 \quad \text{for} \quad \alpha_{10} = 0.12 \quad \text{at} \quad 10 \text{ Mc}$$

This new factor is not frequency dependent except near the gyrofrequency, and the work which follows is restricted to frequencies of several megacycles, well above the gyrofrequency.

It is desirable to program the computer so that the severity of absorption may change with horizontal range. This will happen, for example, if a backscatter radar looks toward or away from the sun across a twilight zone. Thus the factor E_α will be a function of range. A cubic equation for E_α provides enough flexibility, so absorption is described by the expression

$$E(R) = E_\alpha\left(1 + e_1R + e_2R^2 + e_3R^3\right)$$

where E_α, e_1, e_2, and e_3 can be specified independently each time the program is run. This equation has proven to be more than adequate.

In the equations above, it is necessary to specify ζ, the angle at which the raypath penetrates the absorbing region. It may be assumed that the raypath from earth to the D region is a straight line as shown in Fig. 10(b). In the figure, β is a known takeoff angle, r_e is the radius of the earth (6370 km), and h_D is the height of the absorbing region (80 km). From this figure it is seen that

$$\frac{\sin \alpha}{r_e} = \frac{\sin (\pi/2 + \beta)}{r_e + h_D} = \frac{\cos \beta}{r_e + h_D}$$

$$\zeta = \pi/2 - \alpha, \quad \text{so} \quad \sin \alpha = \cos \zeta$$

$$\zeta = \arccos \left(\frac{r_e \cos \beta}{h_D + r_e} \right)$$

Since E varies with range, it will be necessary to locate the range at which every ray penetrates the absorbing layer going up and coming down for each hop. For example, if an element of backscattering ground is illuminated by a two-hop ray and the energy returns to the receiver by a one-hop ray, then the calculation of the received power will include six factors, one going up and one coming down for each of the three hops. This sounds difficult, but it is actually little more than a bookkeeping operation to the computer which can simply add exponents, thanks to the relation:

$$e^a \cdot e^b \cdot e^c \cdot e^d = e^{a+b+c+d} \quad \text{etc.}$$

Since E will be a slowly varying function of range, it is assumed that a ray which reaches a given range travels by hops which are equal and symmetrical. This approximation is made only for the purpose of evaluating E; in other stages of the analysis, it would be altogether unacceptable. Here, its effect is quite minor and the approximation does lead to an increase of computer speed.

It is necessary to know, for a ray which leaves the ground at angle β, how much ground range it traverses before reaching the D region. This calculation is straightforward as shown on Fig. 10(b). The ground range in question is symbolized R_D. In this figure it can be seen that

$$R_D = r_e \zeta$$

It can also be seen that

$$\Phi = \zeta - \beta$$

Therefore the instruction given to the computer is

$$R_D = r_e(\zeta - \beta)$$

Using this value of R_D, the computer evaluates $E(R)$ at the two locations shown in Fig. 10(c) for the case of a one-hop ray. Here, the symbol R stands for the total range reached by the one-hop ray. For the two-hop ray, the computer is instructed to evaluate E at the four locations shown in Fig. 10(d). Similarly, for a three-hop ray, the computer evaluates E at six places as shown in Fig. 10(e). No more than three hops were included in any portion of the entire analysis, primarily because the author has seldom seen on any experimental record the fourth hop of ground backscatter. (The fourth or fifth hop could easily be included, if desired.)

Let us recapitulate what has been done here:

1. The absorption has been programmed so that it can be made to vary with range in any manner matched by a cubic equation.
2. Absorption has been corrected so that the index is inversely proportional to the square of the radio frequency.
3. Absorption is calculated to allow for the angle at which the raypaths penetrate the D region.
4. Absorption is calculated once each time a ray penetrates the region going out to the backscattering ground and once each time the ray penetrates the region coming back from the same ground, both when the ray goes up and when it comes down.

The above is simply an expression of the fact that the energy content of a ray decreases exponentially as it passes through an absorbing region. Further complexity could have been built into the program, but this set of choices is optimum for the objectives at hand and refinements can be added if they become desirable. In the following analysis, the factor written e^{α} will signify an instruction to the computer to calculate absorption according to the criteria outlined here.

III. ANALYSIS OF BACKSCATTER

The factors which must be taken into account in this discussion of the ground-backscatter phenomenon are sketched in Fig. 11. It is assumed that there are on the earth+s surface a transmitter, receiver, and an associated antenna which are to be simulated. The transmitter operation may be described by specification of the transmitted power level as a function of time. In general, the pulse shape will not be rectangular and, when scattered and received, it will be further modified by the smoothing effect of limited receiver bandwidth and ionospheric dispersion.

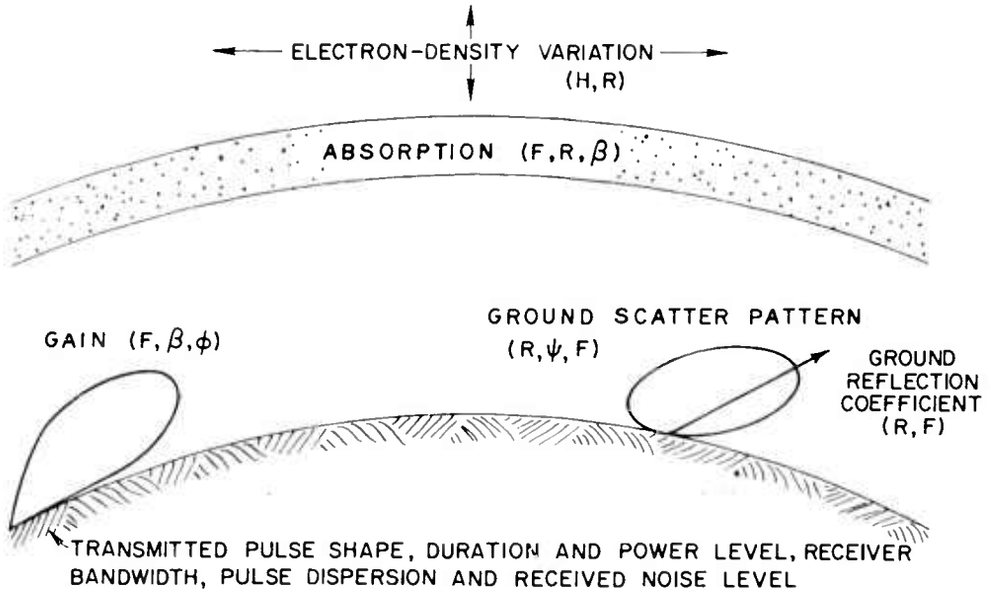

32690

FIG. 11. FACTORS WHICH INFLUENCE THE AMPLITUDE OF GROUND BACKSCATTER.

The electron density can vary with both altitude and range. However, the raytracing program used here does not permit electron-density gradients in the direction transverse to the propagation path, since it is two-dimensional. Such gradients can be simulated by carrying out the entire synthesis process a number of times for different azimuths (assuming no transverse variation within any single azimuth sector), and the final results can be added.

At the lower edge of the ionosphere, a certain amount of the energy will be absorbed, and this absorption will depend on the radio frequency. Also, the amount absorbed depends on β because shallow raypaths stay in the absorbing region for a longer distance. Since calculations will cover many thousands of kilometers, provisions are made for the variation of absorption with horizontal range.

Antenna gain will generally be a fairly complex function of frequency, azimuth, and elevation angle. The exact nature of its variation exerts quite a strong control over the backscatter amplitude pattern and so a good deal of effort is justified in the simulation of its effect [Ref. 25]. The ground scatter pattern and reflection coefficient have been discussed, and the provision will be made so that they can be changed as a function of range to simulate the changing surface of the earth. Since the radio wavelength is comparable to the scale of irregularities on the earth's surface, these parameters may vary with frequency. Also, the data previously discussed give a clear indication that the scatter pattern varies as a function of the angle ψ.

A. THE FLUX OF ENERGY

Figure 12 contains sketches showing raypaths, areas, and dimensions of interest over the same "block" of the earth. In part (a) are shown the raypaths and measurements which apply to the energy which travels outward from the radar to the backscattering ground. In part (b), attention is focused on the rays which return from the backscattering ground to the radar.

Notice in particular that it is <u>not</u> being assumed that energy which travels out by a certain raypath must return by the <u>same</u> raypath. To emphasize this fact, part (a) shows one hop and part (b) shows two hops. However, it could equally well be that both the transmission and reception propagation paths consist of the same number of hops. For instance, the energy could go out by one-hop-E and return by one-hop-F or the same one-hop-E. As the reader will see, it is not necessary to make any restriction and thus, in this regard, the program will be able to synthesize a portion of backscatter which has previously been completely neglected.

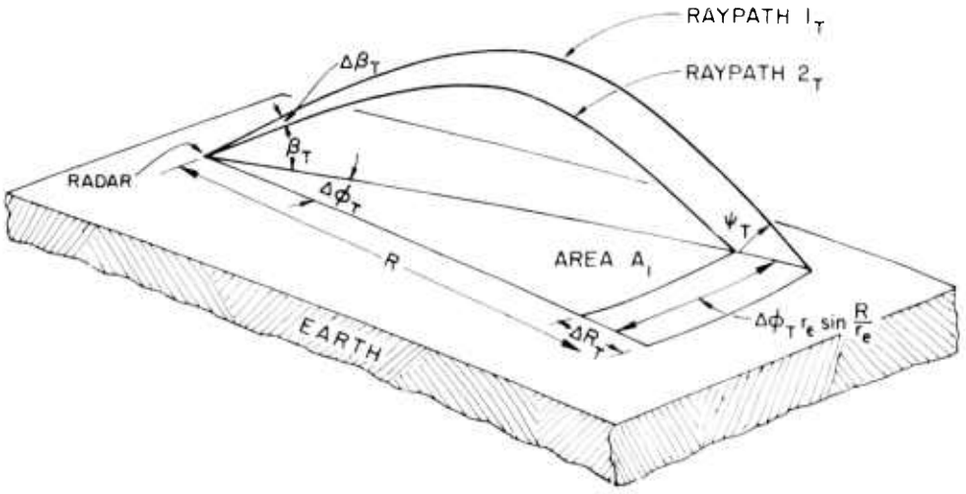

a. Transmitted rays

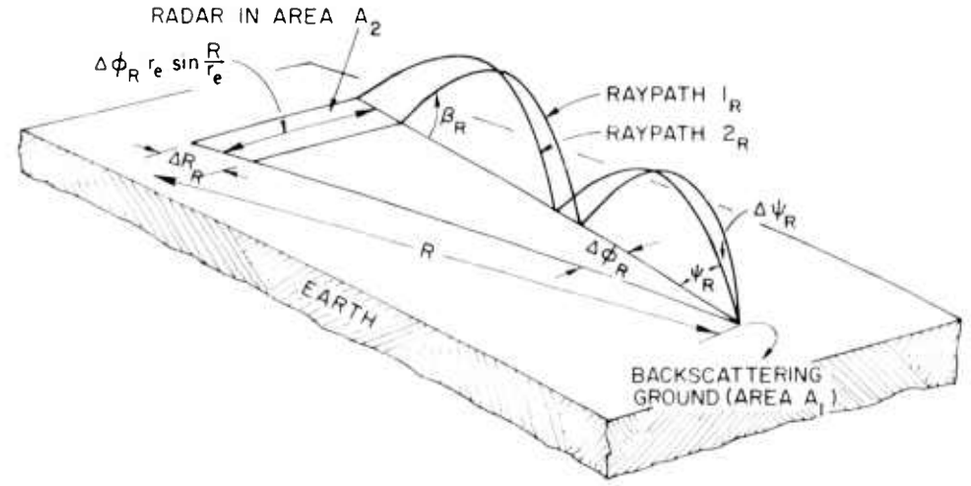

32686

b. Backscattered rays

FIG. 12. ILLUSTRATION OF THE BACKSCATTER POWER-DENSITY CALCULATION.

In order to lend clarity to the next few pages, a convention is adopted whereby the subscript T means that the subscripted parameter is associated with the transmitted rays, and the subscript R implies association with the received (backscattered) rays. In other words, parameters associated with Fig. 12a will have a T subscript and those associated with Fig. 12b will have an R subscript.

Now consider the transmitted rays. Since raypaths are streamlines in a flux of energy, it is assumed that all of the energy which leaves the radar within elevation angle increment $\Delta\beta_T$ and within azimuth angle increment $\Delta\phi_T$ will travel up into the ionosphere confined between raypaths 1_T and 2_T and the two great circles defined by $\Delta\phi_T$. This energy will refract downward and strike the ground within area A_1. The angle increments are considered to be small, so that the energy striking A_1 is uniformly distributed. Then, since raypaths 1_T and 2_T are calculated by the raytracing program, it is possible to calculate the energy density which strikes area A_1 directly from a set of known parameters, including the antenna gain specified at elevation angle β_T.

Area A_1 may be illuminated by other raypaths which leave the transmitter at different values of β_T. This eventuality will be covered under the assumption of linearity so that superposition may be used. In other words, the <u>percentage</u> of energy backscattered by the ground will be assumed to be independent of the <u>amount</u> of energy striking the ground in that particular region. This appears to be an extremely safe assumption, but it should be noted that this is an assumption. Notice also that use of the SRI data implicitly assumes that the backscattered energy is incoherent. This is generally accepted; see, for example, Ref. 41. A detailed theoretical exposition on this subject is given in Ref. 5.

If the earth were flat, the width of area A_1 would simply be $(R)\ (\Delta\phi_T)$, where R is the mean distance from the radar to the area. However, the earth's transverse curvature requires a correction that cannot be ignored. Consider Fig. 13a which shows the earth in cross section with the radar situated to give an elevation view. The distance from the radar to the area A_1 is R. The earth's radius is r_e, and the geocentric angle subtended by R is α. From the figure, it can be seen that $R = r_e \alpha$ and that $\sin \alpha = \rho / r_e$. Now in part (b) of Fig. 13, the same radar is shown in plan view. The distance from the radar to the ground area appears to be ρ, not R. The width of area A_1 appears undistorted in this view and is seen to be $\rho\Delta\phi$. Combining all these results, the width of the area is to be:

$$\text{width of } A_1 = \Delta\Phi_T \, r_e \sin \frac{R}{r_e}$$

The earth is not a sphere, of course, and so the selection of a value for r_e is somewhat subjective. At the poles it is 6357 km; at the equator it is 6378; the average of these two is 6368; a sphere whose circumference is 40,000 km would have radius 6366; the selection of 6370 is used here in order to reflect the uncertainty in the last digit (values from Ref. 42).

Looking back at area A_1, it is seen that ΔR_T can be computed directly from the parameters associated with the raypaths 1_T and 2_T. The equation for A_1 is

$$A_1 = \Delta R_T \, \Delta\Phi_T \, r_e \sin \frac{R}{r_e}$$

All of these parameters can be obtained from the raysets. Associated with these particular raypaths, there will be a certain amount of energy injected into area A_1 within the small solid angle between $\Delta\beta_T$ and $\Delta\Phi_T$. The actual solid angle subtended by A_1 as seen from the radar via raypaths 1_T and 2_T is then $\Delta\beta_T \, \Delta\Phi_T \cos\beta_T$.

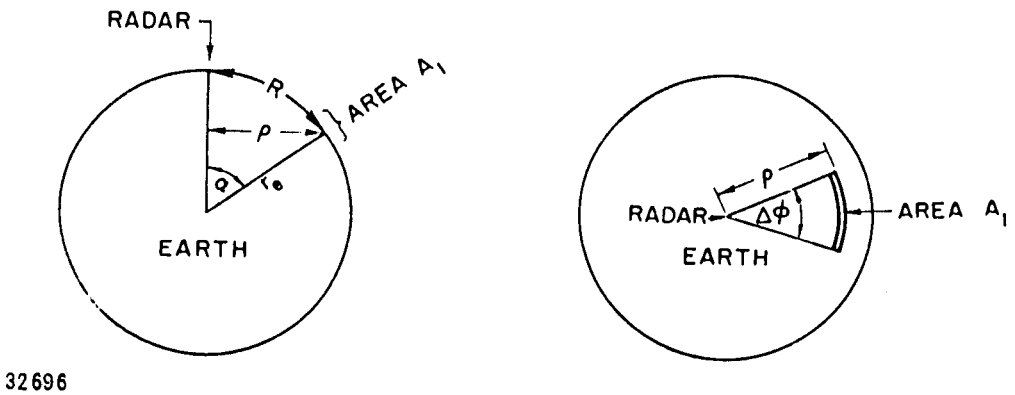

a. Elevation view

b. Plan view

FIG. 13. GEOMETRY USED IN CALCULATING A CORRECTION FOR THE SPHERICAL EARTH.

Although actual interest will be centered on power levels, this analysis will be simplified if attention is initially restricted to the accounting of energy. Later a refinement will produce the time distribution of a known amount of energy, thereby giving the desired answers in terms of power. Thus, the pulse duration will initially be set at ϵ, which is a time interval so short that errors of the order of ϵ are acceptable.

Let the amount of energy which impinges on area A_1 and which travels between raypaths 1_T and 2_T be symbolized E_1. Let the gain of the transmitting antenna be symbolized G_T when it is evaluated in the direction of raypaths 1_T and 2_T. Then the total energy transmitted toward A_1 by these raypaths is

$$E_1 = \epsilon P_T G_T \frac{\Delta\beta_T \, \Delta\phi_T \cos \beta_T}{4\pi}$$

where P_T is the transmitted power. All of this energy will strike A_1, except that reductions must be made for the power lost to absorption and, if more than one hop is involved, for the power lost due to the incompleteness of reflection off the surface of the earth. The latter factor will be taken into account as follows. It will be assumed that the earth, in addition to backscattering, specularly reflects (100ρ) percent of the energy incident upon it. The parameter ρ is thus a power ratio and will always be less than unity. Since ρ is probably strongly dependent on the type of terrain, the final program will incorporate an ability to vary ρ with distance from the radar.

When E_1 is corrected for absorption and incomplete reflection, it represents the amount of energy which impinges on area A_1 due to propagation between raypaths 1_T and 2_T. Many different propagation modes may illuminate the same area on the ground and these must be accounted for in the final result.

Despite the appearance of Fig. 12a, recall that area A_1 is considered to be infinitesimal. In fact, it is shown as only a point of backscattering ground in Fig. 12b. Here are shown raypaths 1_R and 2_R

which represent one of the possible propagation modes by which the energy which strikes area A_1 can return to the radar.

Suppose, for the moment, that raypaths 1_R and 2_R are actually known. Then it can be seen by analogy to A_1 that the area A_2 is

$$A_2 = \Delta R_R \, \Delta \phi_R \, r_e \sin \frac{R}{r_e}$$

However, this equation is not directly useful since the quantity ΔR_R cannot be found in the raysets. It is associated with rays which return from the scattering ground, and the raysets describe only the rays which go out <u>from</u> the radar. It might be possible to perform a raytracing which originates at the scattering ground area, but this would be cumbersome and expensive. Fortunately a more logical solution exists, which is as follows. First, note that

$$\Delta R_R = \frac{\partial R_R}{\partial \psi_R} \Delta \psi_R$$

This relation shows promise because an opportunity will arise for the cancellation of the factor $\Delta \psi_R$. Thus, if the derivative can be determined, the area A_2 will be known.

Although this analysis concerns simulation of a monostatic radar, it will be convenient to digress temporarily and consider the bistatic system shown on Fig. 14a for the study of the needed derivative. Assume that a raypath exists which joins the transmitter and receiver, and that this raypath strikes the ground at angles β and ψ as shown. Constructed at the transmitter and receiver are antennas whose gains are equal and arbitrarily large. These theoretical antennas will be considered to have a single lobe at the appropriate elevation angle, β or ψ, so that they have maximum gain along the raypath. Each of these antennas has an effective receiving area, A, related to gain by the equation

$$G = \frac{4\pi A}{\lambda^2}$$

The areas of these two imaginary antennas are normal to the raypath, by definition.

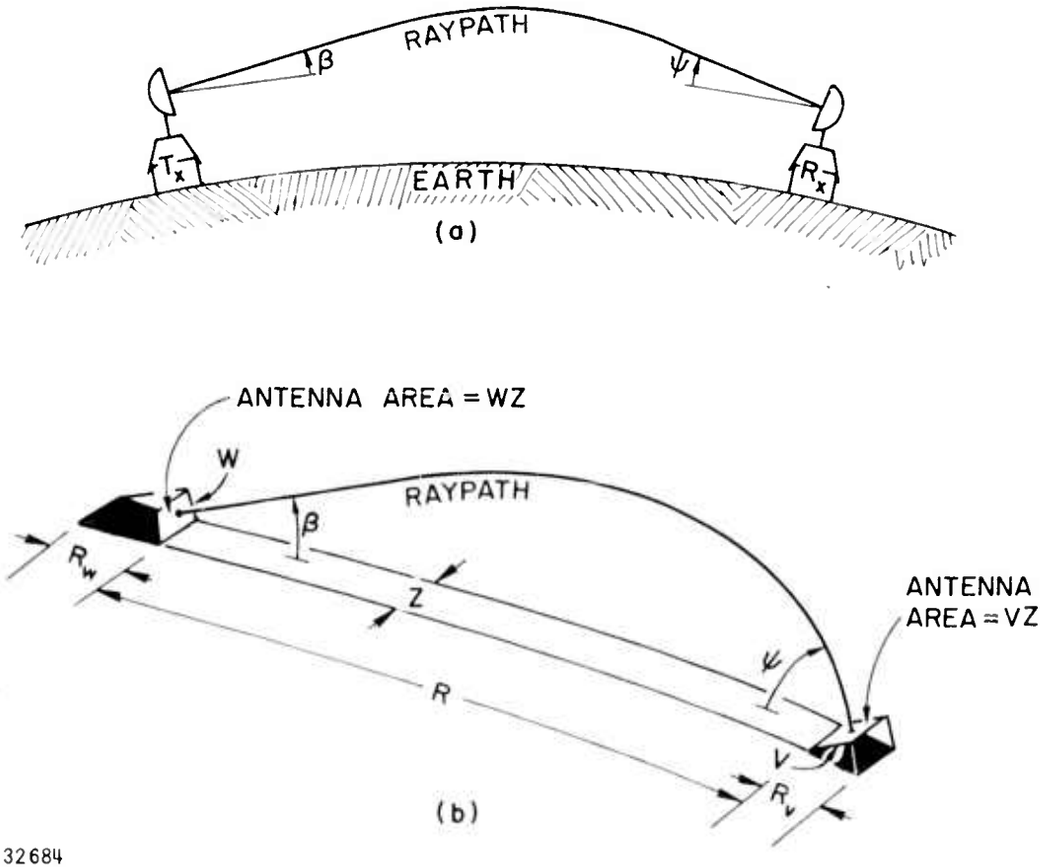

FIG. 14. RELATIONS USED TO PERMIT APPLICATION OF RECIPROCITY.

Suppose one has calculated rays which originate at the transmitter end of this path; then from the raysets one has a measure of the spreading of energy as it travels from transmitter to receiver. The measure most accessible is the change in the range at which the rays return to earth when a small change in takeoff angle occurs. For example, suppose a raytracing at $\beta = 26°$ and $27°$ produces two rays which land at the

earth at $R = 2500$ and 2600 km, respectively. Assuming that these rays are flux streamlines, then the energy which leaves the transmitter in the 1-deg increment of takeoff angle hits the ground in a 100-km increment of ground range. The measure of spreading can then be written:

$$\Delta R/\Delta\beta = 100 \text{ km per degree}$$

If this parameter is large, the signal is weak, and vice versa.

Suppose now that the transmitter and receiver are switched without any change in the antennas or the ionosphere. Then, the measure of spreading would be $\Delta R/\Delta\psi$.

Notice in particular that for small $\Delta\psi$, $\Delta R/\Delta\psi \doteq \partial R/\partial\psi$, the desired derivative. We wish to calculate its value without raytracing so we turn to the Rayleigh-Carson reciprocity theorem, which was stated by Terman [Ref. 43] as follows:

> "If an electromotive force, E, inserted in antenna 1 causes a current, I, to flow at a certain point in a second antenna, 2, then the voltage, E, applied at this point in the second antenna will produce the same current, I (both in magnitude and phase), in a short circuit at a point in antenna 1 where the voltage, E, was originally applied. (This) fails to be true only when the propagation...is appreciably affected by the presence of the earth's magnetic field."

In other words the hypothetical switch of transmitter and receiver should not cause a change in the received signal level under the conditions assumed throughout this report. Now, for convenience of notation, assume that $\Delta\beta$ and $\Delta\psi$ are selected to make ΔR constant. Further, suppose that the antenna on the left side of the figure has an equivalent area WZ which is inclined at angle β so that it casts a shadow of length R_W as shown in part (b) of the figure. Similarly, let the antenna at the right end have area VZ inclined at angle ψ. When the transmitter is at the left end of this propagation path, let the received power (at the right) be P_V and when transmitter and receiver are switched, let the received power be P_W. If the transmitted power in both cases is P_T, then all of the following relations hold true:

$$V = R_v \sin \psi \qquad \text{and} \qquad W = R_w \sin \beta$$

$$P_v = \frac{P_T G \Delta\beta \cos \beta}{4\pi} \cdot \frac{VZ}{R\Delta R \sin \psi}$$

$$P_w = \frac{P_T G \Delta\psi \cos \psi}{4\pi} \cdot \frac{WZ}{R\Delta R \sin \beta}$$

Reciprocity indicates that $P_v = P_w$. Since $WZ = VZ$,

$$\frac{\Delta\beta}{\Delta\psi} = \frac{\sin \psi \cos \psi}{\sin \beta \cos \beta}$$

from which

$$\frac{\Delta R}{\Delta\psi} = \frac{\Delta R \sin \psi \cos \psi}{\Delta\beta \sin \beta \cos \beta}$$

All of the elements on the right side of this new equation are available from the raysets, and so the derivative can be calculated without further raytracing.

Returning to the monostatic backscatter radar, it is seen that an R subscript must be put on the R's, ψ's, and β's in the above equations to signify that the values are selected from the rayset that describes the returning raypath (which may be different from the outgoing raypath). Thus, the area A_2 is calculated according to the relation

$$A_2 = (\Delta\psi_R \, \Delta\phi_R) \left(\frac{\partial R_R}{\partial \beta_R} \, \frac{\sin \psi_R \cos \psi_R}{\sin \beta_R \cos \beta_R} \, r_e \sin \frac{R}{r_e} \right)$$

It is not necessary to worry about the algebraic sign in such expressions as these because they will all be factors in an expression for the absolute value of the received power, which is known to be positive.

Since the amount of energy striking area A_1 is known, the portion of this energy which returns toward the radar can be calculated by application of the ground backscattering coefficient, $K(\psi)$. Measurements such as those of SRI were taken by a single monostatic radar in an aircraft and therefore they apply only to the case where the angle of incidence is equal to the angle of scatter. In the problem being analyzed here, such a relation will not always hold true. For example, compare parts (a) and (b) of Fig. 12 where it can be seen that the angles ψ_T and ψ_R are not equal. In fact, they must be unequal for all cases except the commonly assumed one in which the energy travels to and from the backscattering ground via the same raypath. However, there is no experimental information known to this author which indicates the behavior of the backscattering coefficient when ψ_T and ψ_R are different, so it seems reasonable to calculate their average value and to use that as the argument of the backscattering coefficient.

Each time any ray penetrates the absorbing region, there will be an energy loss which must be calculated by the program. This loss will be accounted for by multiplication of the total energy by a constant whose value is between 0 and 1. This constant, calculated by the method previously described, will be symbolized e^{α_T} for the outgoing (transmitted) raypath. Similarly, the attenuation of the incoming (received) raypath will be symbolized e^{α_R}.

The factors which account for the incomplete reflection off the ground of the transmitted and received rays will be symbolized ρ_T and ρ_R.

Let E_2 represent the amount of energy which returns to area A_2. Then, the above arguments can be combined to show that

$$E_2 = \left[\frac{\epsilon P_T G_T \, \Delta\beta_T \, \Delta\phi_T \cos \beta_T}{4\pi} \rho_T \, e^{\alpha_T}\right] \left[K\left(\frac{\bar{\psi}_T + \bar{\psi}_R}{2}\right)\right]$$

$$\cdot \left[\frac{\Delta\psi_R \, \Delta\phi_R \cos \psi_R}{2\pi} \rho_R \, e^{\alpha_R}\right]$$

In this expression the 2π appears in the last denominator because the definition of the function $K(\psi)$ involves a power comparison against an ideal radiator which transmits isotropically into a hemisphere. If a complete sphere had been used, the factor would have been 4π and the parameter K would have been more closely analogous to a gain function.

Let the receiving antenna have an equivalent area symbolized A_R. The use of an equivalent area such as this implies that the area is oriented in space perpendicular to the direction of the incoming rays to be received. Thus, when comparisons are made between A_R and the area A_2 which lies flat in the earth, a correction must be made because A_2 is not perpendicular to the raypaths; the raypaths make an angle β_R with area A_2.

In a practical situation, the antenna used will transmit and receive only one of the two possible polarizations. Suppose, for example, that the antenna transmits and receives horizontal polarization only. During both the transmission and reception parts of the ray propagation, the plane of polarization will rotate. On the average, only half of the returning energy will exist in the form of horizontal polarization. Thus, a correction factor of $1/2$ must be inserted to account for the fact that half the energy is undetectable due to polarization rotation.

Returning to the analysis, let E_R represent the total received energy. The above reasoning then indicates that

$$E_R = \frac{E_2}{2} \frac{A_R}{A_2 \sin \beta_R}$$

Now $c = F\lambda$ and $G = 4\pi A/\lambda^2$, so $A_R = c^2 G_R / 4\pi F^2$. Also $G_T = G(\bar{\beta}_T)$ and $G_R = G(\bar{\beta}_R)$. With this notation it is finally possible to express the received energy in terms of known parameters as follows:

$$E_R = \frac{1}{2} \cdot \frac{c^2 G(\bar{\beta}_R)}{4\pi F^2} \cdot \frac{K\left(\frac{\bar{\psi}_T + \bar{\psi}_R}{2}\right) \frac{1}{2\pi} (\Delta\psi_R \, \Delta\phi_R \cos \psi_R) \, \epsilon P_T \, G(\bar{\beta}_T)}{(\Delta\psi_R \, \Delta\phi_R)\left(\frac{\partial R_R}{\partial \beta_R} \frac{\sin \psi_R \cos \psi_R}{\sin \beta_R \cos \beta_R} r_e \sin \frac{R}{r_e}\right)}$$

$$\cdot \frac{\Delta\beta_T \, \Delta\phi_T \cos \beta_T}{4\pi} \cdot \rho_T \, e^{\alpha_T} \cdot \rho_R \, e^{\alpha_R}$$

B. POWER; THE TIME DISTRIBUTION OF ENERGY

At this point it is necessary to include time in the analysis. The above equation gives the total amount of energy received by a selected combination of modes for a very short transmitted pulse length. Now the energy must be traced in both space and time, a process which is most easily visualized on a three-dimensional graph whose coordinates are range, time, and power. Such a plot is shown in Fig. 15 which sketches the distribution of energy on the ground after an ionospheric reflection

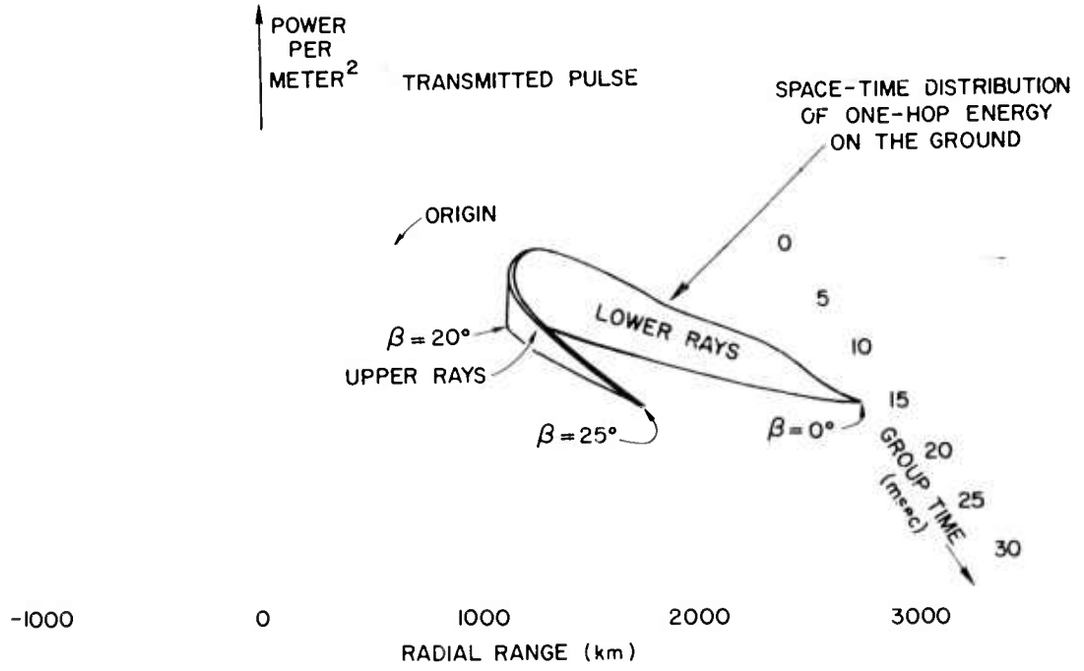

FIG. 15. THE DISTRIBUTION OF ENERGY IN SPACE AND TIME AFTER ONE HOP.

similar to the one described by the family of raysets printed on Fig. 6. Notice that volume on this particular three-dimensional graph will represent energy per meter, but it will not be necessary to calculate the energy quantitatively because the total received energy has already been expressed in terms of known parameters. Consequently, this discussion seeks only to clarify qualitatively the time distribution of received power.

The space and time distribution of energy shown on Fig. 15 will be affected by such things as the antenna gain and the ionospheric absorption. Ionospheric focusing and defocusing also play a strong part in many circumstances, but this simple Chapman layer shows only the defocusing of upper rays, which leads to the low power level.

Now consider a single scatterer taken along the lower-ray portion of the energy in Fig. 15. This scatterer is shown in Fig. 16 where it now assumes the role of a transmitter. The energy scattered back toward the radar assumes a space-time distribution like that in Fig. 15.

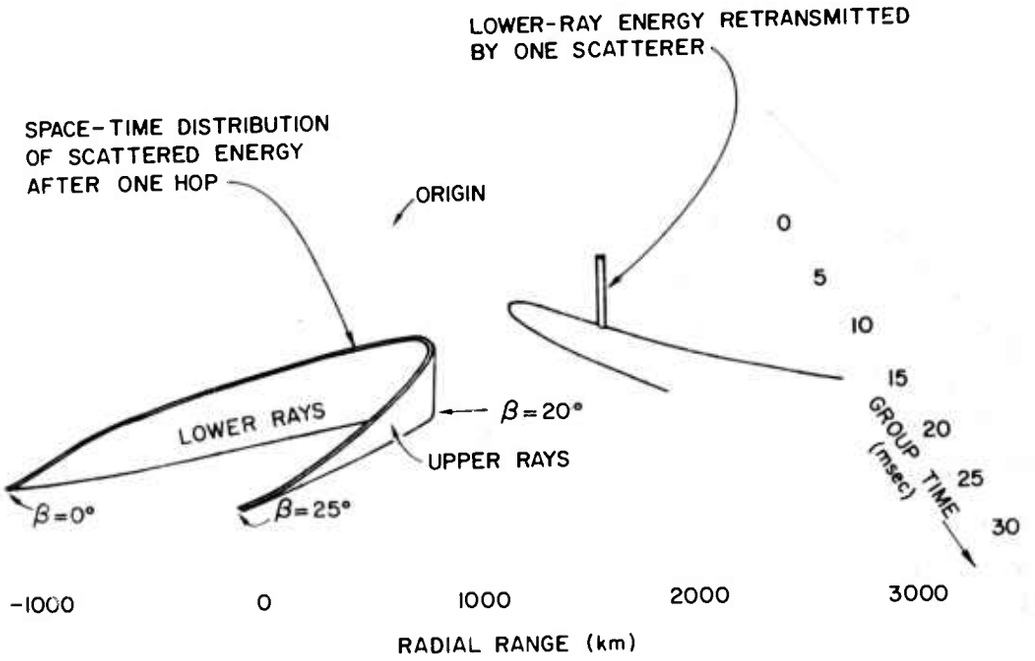

FIG. 16. THE DISTRIBUTION IN SPACE AND TIME OF THE ENERGY FROM A SINGLE SCATTERER.

Strictly speaking, the energy would go both to the right and left on these figures, but this fact will be ignored since it would serve no purpose here. Also, no attempt is being made to depict actual relative power levels from one hop to the next.

Since the radar is located only at range zero, it would receive energy only at the two time delays where the zero range line intersects the scattered energy distribution on Fig. 16. Actually, in this case the single scatterer would receive energy by two modes and would scatter it back by two modes, with a consequent reception of four different elements of energy at three different time delays.

Figure 17 is similar to Fig. 16 except that it describes the action of a group consisting of all scatterers in a strip of terrain. If only lower rays are considered, this energy scatters back toward the radar where it lands in a space-time distribution which appears to be a solid bar on the figure. The intersection of the zero-range plane with this solid bar, as shown in red, is therefore a pulse of energy which is very nearly rectangular. The power level in this pulse will be symbolized

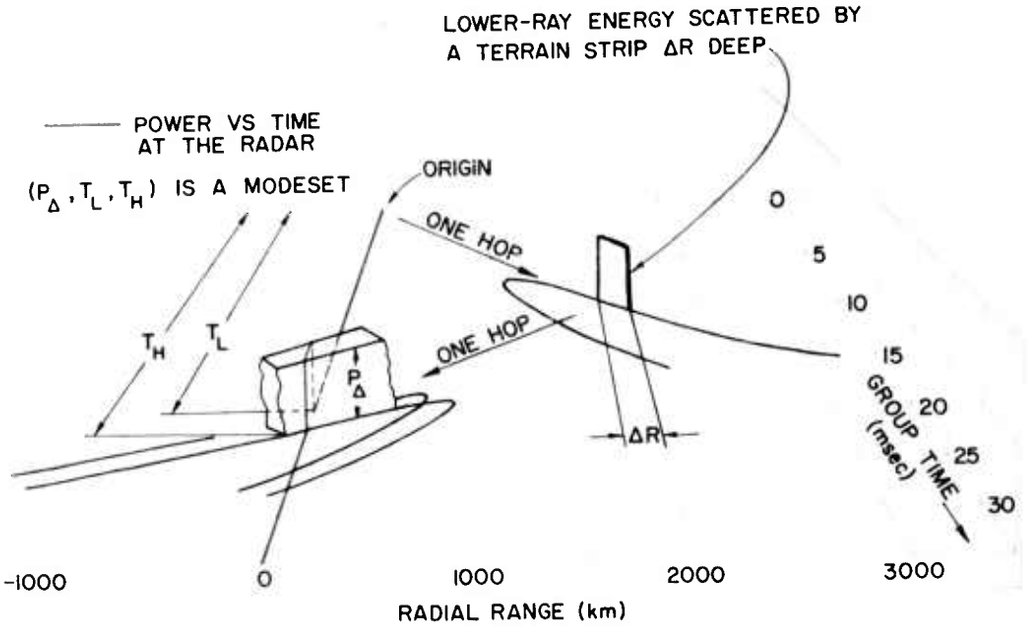

FIG. 17. THE TIME DISTRIBUTION OF ENERGY RECEIVED FROM ONE RANGE INCREMENT VIA SELECTED MODES: A MODESET.

P_{Δ}, and its beginning and ending times will be called T_L and T_H respectively. These three parameters, taken as a group, fully describe the energy which is received for a particular combination of modes, and so the threesome will be termed a "modeset."

In order to correlate the discussion which led to Fig. 17 with the discussion of energy centered around Fig. 12, a number of the parameters shared by these two figures are drawn in on Fig. 18.

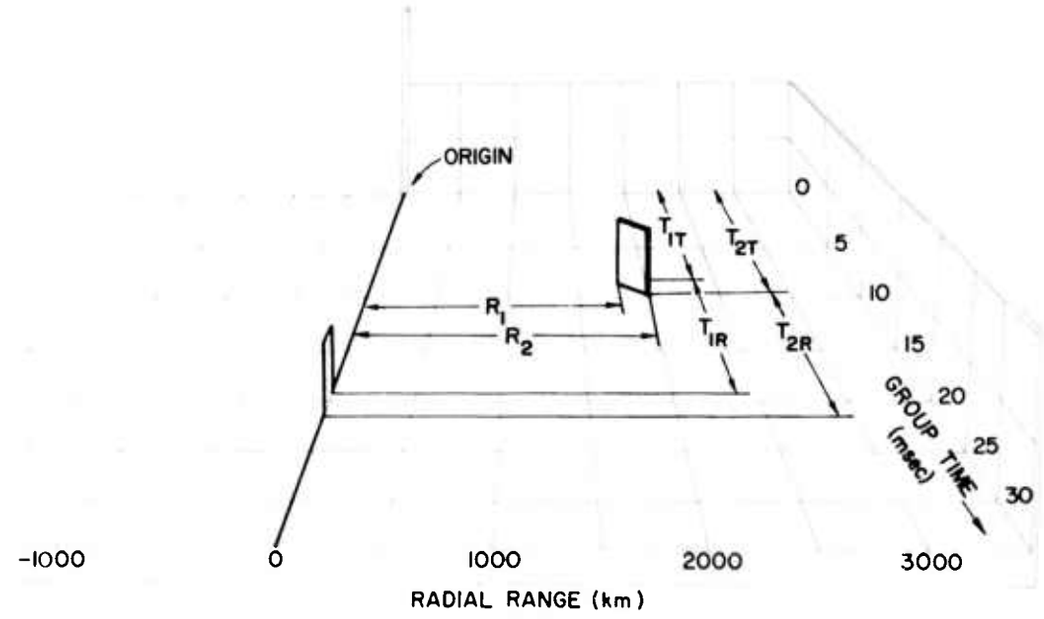

FIG. 18. KNOWN MEASURES OF THE ENERGY DISTRIBUTION.

From the arguments given, it can clearly be seen that

$$T_L = T_{1T} + T_{1R} \quad \text{and} \quad T_H = T_{2T} + T_{2R}$$

Thus, the energy bundle E_R will arrive in the time interval (T_L, T_H). Under the assumption of a uniform distribution of energy within a flux tube, it follows that the power level is

$$P_{\Delta} = \frac{E_R}{T_H - T_L} , \qquad T_L < t < T_H$$

$$P_{\Delta} = 0 , \qquad \text{otherwise}$$

C. SUMMATION IN AZIMUTH AND ELEVATION ANGLES

Next, it is necessary to carry out a summation in azimuth and elevation to account for all possible flux tubes to and from the backscattering ground. The summation in azimuth Φ is relatively easy because the only expression which varies in azimuth is the antenna gain so that the summation can be changed to an integration. The influence of antenna gain and its method of variation constitute a rather extensive subject and so the entire matter, including the integration in azimuth, is discussed in Chapter IV.

Although the summation of results with respect to azimuth can be changed into an integral, the same is not true of the summation with respect to elevation angle β, because the energy is a multiple-valued function of β. The complication arises for the following reason: Suppose three different flux tubes reach the same spot on the earth's surface, each with a different β. Then, energy contributions will exist for each possible combination of these three paths, and it will be necessary to calculate $(3^2 = 9)$ modesets.

The summation with respect to elevation angle will actually be carried out in terms of the parameter range R. The surface of the earth will be considered divided into a series of concentric rings as defined by the intersections with the ground of the individual raysets. All energy which strikes each ring will be accounted for in such a manner that every possible propagation mode is included.

In the section which discusses gain, it will be shown that the term $\Delta\Phi$ can be eliminated from the expression for P_{Δ} provided gain is replaced by a scalar multiplier g_i operating on the function $g(\beta)$. The factor g_i is a result of the integration in azimuth.

The computer will calculate the value of E_R and P_{Δ} for every possible combination of modes that can lead to an element of the received

backscattered power. It will add each of the resulting power levels along a time base between the values T_L and T_H. When this process is finished there will be some distribution of power as a function of time, which would represent the backscatter signal if the transmitted pulse were of short duration ϵ and if errors were permitted of the order of ϵ. However, the actual transmitted pulse has a measurable duration and a definite shape. Also, after this pulse has traveled out and been reflected off a scatterer, it will be received with a shape that is further modified by the influence of the receiver bandpass characteristics. These processes are simulated by the use of a weighted-summation scheme within the computer. The analogous procedure in the domain of continuous variables can be expressed by use of the convolution integral as indicated below.

Let the transmitted pulse shape, as modified by the receiver bandpass function, be symbolized $f(t)$ where t is time. Similarly, let the power level which was calculated for pulse duration ϵ be symbolized $P_\epsilon(t)$. The actual received power will be symbolized $P_r(t)$ and is related to known quantities by the convolution integral,

$$P_r(t) = \int_0^t P_\epsilon(\xi)\, f(t - \xi)\, d\xi$$

In the discrete number system, such as is used in the computer, the pulse shape $f(t)$ is given as a sequence of numbers. Similarly, the power distribution $P_\epsilon(t)$ is given as a sequence of numbers which represent the power level sampled at equal increments of time, each of which equals the "infinitesimal" duration ϵ. Another way of visualizing this is to consider that the transmitter power level changes its value abruptly at each increment of time ϵ. As with any computer solution, the method leads to errors in the time distribution of energy on the order of ϵ. Thus the value of ϵ must be selected small for good results and large for quick computation; there are a number of other parameters which must similarly be chosen as a compromise between conflicting requirements (e.g., $\Delta\beta$).

The underlying assumption here is that the elements of the backscattered signal add incoherently. If each element added coherently, it

would be possible to carry out the analysis using a convolution integral on the received voltage. If the actual situation lay somewhere between coherence and incoherence, the convolution approach probably would not work* because it is a mathematical model based on linearity [Ref. 44].

This essentially ends the analysis of ground backscatter, because all the factors in the expression P_Δ can be found by appropriate calculations starting from the rayset information. Now, it will be necessary to carry out the process of synthesis which in effect will close a loop when it arrives at the expression for P_Δ.

*The possibility exists that satisfactory results might be obtained using voltage raised to some power between 1 and 2.

IV. THE EFFECT OF ANTENNA GAIN PATTERNS

Since the objective of this study is synthesis of backscatter as it might be received by some particular radar, it is appropriate to consider some sources of information concerning the gain pattern of the antenna $G(\beta,\phi)$. The most commonly available information consists of graphs showing the gain as a function of elevation angle $g(\beta)$ and as a function of azimuth $q(\phi)$. The actual measurement of the gain of an antenna is an expensive and time-consuming project, so it is seldom carried out unless the antenna is part of a system where calibration is of sufficient importance to justify the effort [Ref. 45]. In most cases, the functions $g(\beta)$ and $q(\phi)$ are calculated on the basis of theory, empirical formulas, or measurements made on a small model. Such results are usually of acceptable accuracy as a description of the performance of high-frequency antennas.

In the equation which gives the energy contribution of a single modeset, the gain is entered in the calculation in an expression of the following form:

$$E_R = \sum_{\beta_T} \sum_{\phi_T} f(\beta_T,\beta_R)\ G_T(\beta_T,\phi_T)\ G_R(\beta_R,\phi_R)\ \Delta\beta_T\ \Delta\phi_T$$

where G_T is the gain of the transmitting antenna and G_R is the gain of the receiving antenna. Throughout this report it is assumed that there are no transverse tilts in the ionosphere, so it is permissible to drop the subscripts on ϕ because $\phi_T = \phi_R = \phi$; that is, all propagation is by great-circle routes, and a ray which starts out in one azimuth will return along the same azimuth. Also, most backscatter radars make use of a single antenna so that the subscripts on the G can be eliminated. However, it is not possible to ignore the subscripts on β because a large amount of energy actually leaves the radar at takeoff angle β_T and travels to and from the backscattering ground by different propagation modes. It will thus arrive back at the radar at an angle of arrival β_R which is not equal to β_T.

Now suppose that gain G can be represented by the product:

$$G(\beta,\phi) = ug(\beta)\, q(\phi)$$

where g and q are functions of arbitrary size but appropriate shape and u is a scalar multiplier. This equation implies that gain is a function which is separable in terms of the azimuth and elevation variables, a condition which is not always true. Nevertheless, it is an assumption which is made so commonly that it is not widely recognized to be an approximation. There are probably two reasons for this: (1) The actual gain is relatively difficult to determine, as was mentioned above, and (2) it is difficult to make any useful calculations using information which is better than that which can be represented by the assumption of separable variables. Most users of gain information are interested in either g or q but seldom have enough information about other system variables to make use of both functions simultaneously. Thus, if given G, they would find it necessary to calculate either g or q for use in solving the problems at hand.

One of the most gross departures of gain from a function which can be represented by separable variables exists in the form of side lobes which are centered about elevation angles <u>different</u> from the elevation angle of the main antenna lobe. In backscatter synthesis, it is fortunately practical to simulate this situation closely while still making use of the assumed separable variables. Because the elements of the backscattered signal add in a linear fashion, the superposition principle will allow separate calculations to be made for each lobe which cannot be simulated by a product such as $G = ugq$. Separate backscatter can be calculated for each such lobe and the resulting power levels can be added graphically in a simple manner. To state this mathematically, it would be said that

$$G(\beta,\phi) \approx u_1 g_1(\beta)\, q_1(\phi) + u_2 g_2(\beta)\, q_2(\phi) + \ldots$$

where the functions and constants are selected so that each term represents one or more of the actual antenna lobes. The number of terms which can thus be used are limited only by the patience of the user.

From the above arguments, it can then be said that gain enters into the backscatter calculation in the following manner:

$$E_R = \sum_{\beta_T} \sum_{\phi} f(\beta_T, \beta_R)\ u^2 g(\beta_T)\ g(\beta_R)\ q^2(\phi)\ \Delta\beta_T\ \Delta\phi$$

Notice that the summation in ϕ involves only the single-valued function $q^2(\phi)$. Thus, this summation can be transformed into an integral and taken outside the summation in β, as follows:

$$E_R = \left[u^2 \oint q^2(\phi)\ d\phi\right] \sum_{\beta_T} f(\beta_T, \beta_R)\ g(\beta_T)\ g(\beta_R)\ \Delta\beta_R$$

This operation permits the integration to be done analytically. The bracketed quantity is thus reduced to a scalar multiplier.

Gain is defined as the ratio of (the power transmitted in the direction β,ϕ) to (the power which would be transmitted in that direction if the antenna were lossless and isotropic). In this development the transmitted power will be considered as the total radiated power and thus the antenna may be assumed lossless.

From the above definition, it can be seen that conservation of energy requires

$$\int_{\beta=0}^{\pi/2} \oint_{\phi} G(\beta,\phi) \cos\beta\ d\beta\ d\phi = 4\pi$$

which can be written

$$(u)\left[\int_{\beta=0}^{\pi/2} g(\beta)\cos\beta\, d\beta\right]\left[\oint_{\phi} q(\phi)\, d\phi\right] = 4\pi$$

and this relation will hold true provided u is calculated according to the relation:

$$u^{-1} = \frac{1}{4\pi}\left[\int_{\beta=0}^{\pi/2} g(\beta)\cos\beta\, d\beta\right]\left[\oint_{\phi} q(\phi)\, d\phi\right]$$

Looking at the way in which gain enters the backscatter calculation, it can be seen that the mathematics will take on its simplest form if we choose to simulate gain according to the relation:

$$G(\beta,\phi) = u\left[\sqrt{\oint_{\phi} q^2(\phi)\, d\phi}\right] g(\beta)$$

The quantity in brackets is merely a calculated constant. If the value of u is inserted, the factors can be rearranged in the following form:

$$G = g_i g(\beta); \qquad g_i = \left[\frac{\sqrt{\oint_{\phi} q^2(\phi)\, d\phi}}{\oint_{\phi} q(\phi)\, d\phi}\right]\left[\frac{4\pi}{\int_{\beta=0}^{\pi/2} g(\beta)\cos\beta\, d\beta}\right]$$

Here it can be seen that the first factor in the expression for g_i is a constant calculated only from the azimuthal variation of gain. The second factor is calculated only from the variation of gain with elevation angle.

It is interesting to note that the first factor represents the only influence of $q(\phi)$ on the entire backscatter calculation. Thus the behavior of this factor is of exceptional interest and it will be discussed

at some length, both to illustrate how azimuthal gain affects backscatter and to derive a formula for mathematical simulation.

A. METHODS OF PROGRAMMING GAIN FUNCTIONS

In the computer program which makes synthetic backscatter records, it is sufficient to have a scalar multiplier g_i together with the function $g(\beta)$. The function is inserted into the program by two different methods, each of which is well suited to a particular form of input information.

In one approach the computer is actually given a rather complex analytic equation which has been designed so that a large number of different shapes of functions can be synthesized. Then, the user can insert various constants into the equation by means of punched cards.

Another separate computer program was designed to support this operation by carrying out the integration which leads to the second factor in g_i and at the same time making a graphical plot of the function $g(\beta)$. This form of computation is well suited to studies where one is most interested in other parameters and only cares that the gain is easily programmed, fairly realistic, and consistent with the known variation of a gain function.

The formulas used for the gain model can be selected from the following array which is built into the computer program:

$$G(\beta) = g_i \left\{ \begin{bmatrix} \cos^n a(\beta + \beta_1) \\ \\ \dfrac{\sin\,[a \sin b\,(\beta + \beta_1)]}{a \sin b\,(\beta + \beta_1)} \\ \\ \dfrac{\sin a\,(\beta + \beta_1)^n}{b(\beta + \beta_1)} \end{bmatrix} \begin{bmatrix} 1.0 \\ \\ \sin\,[k \sin\,(\beta + \beta_1)] \end{bmatrix} \right\}^2$$

In this formula g_i is the constant calculated according to the criteria mentioned previously. The parameter β_1 is used to raise or lower the

beam. The first array represents the free-space pattern of the antenna. The second array represents the effect of a perfectly conducting earth on the free-space pattern provided that the lower element in the brackets is selected. If unity is selected, then the shape of the antenna gain pattern is determined only by the square of the element selected from the first array. The parameter k allows for antenna height h through the relation:

$$k = \frac{2\pi h}{\lambda}$$

which is derived for horizontal polarization and for vertical polarization under the Brewster angle in Ref. 46.

The elements in the first factor were selected somewhat subjectively by the author in order to make maximum use of the constants n, a, b, while at the same time including as special cases some of the theoretically derived equations for free-space antenna patterns.

Perhaps of more interest is the programming technique which has been termed "itemized gain." This approach is better suited to the use of specific experimental or theoretical gain functions. As the name implies, the function $g(\beta)$ is fed into the computer by means of a large number of sample points along the function. The computer then performs interpolation between the data points to determine the value of the function at intermediate values of the takeoff angle. The integration of the function $g(\beta)$ must be done so often that it has been found convenient to invent a graphical technique which permits use of a planimeter. Figure 19 shows the graph devised for this purpose. The horizontal axis is foreshortened by the factor $\cos \beta$ and the vertical axis is labeled so that gain can be plotted in decibels, but the vertical axis scale is linear in power. Thus, if the itemized gain points are plotted on this graph and the planimeter is run along the curve defined by the points, the area measured will be proportional to

$$\int_{\beta=0}^{\pi/2} g(\beta) \cos \beta \, d\beta$$

A normalization area can be measured on the graph and the ratio of the two readings then used to calculate g_i.

B. AZIMUTHAL GAIN

The first factor in the expression for g_i warrants further discussion because it represents the only effect of azimuthal gain on the

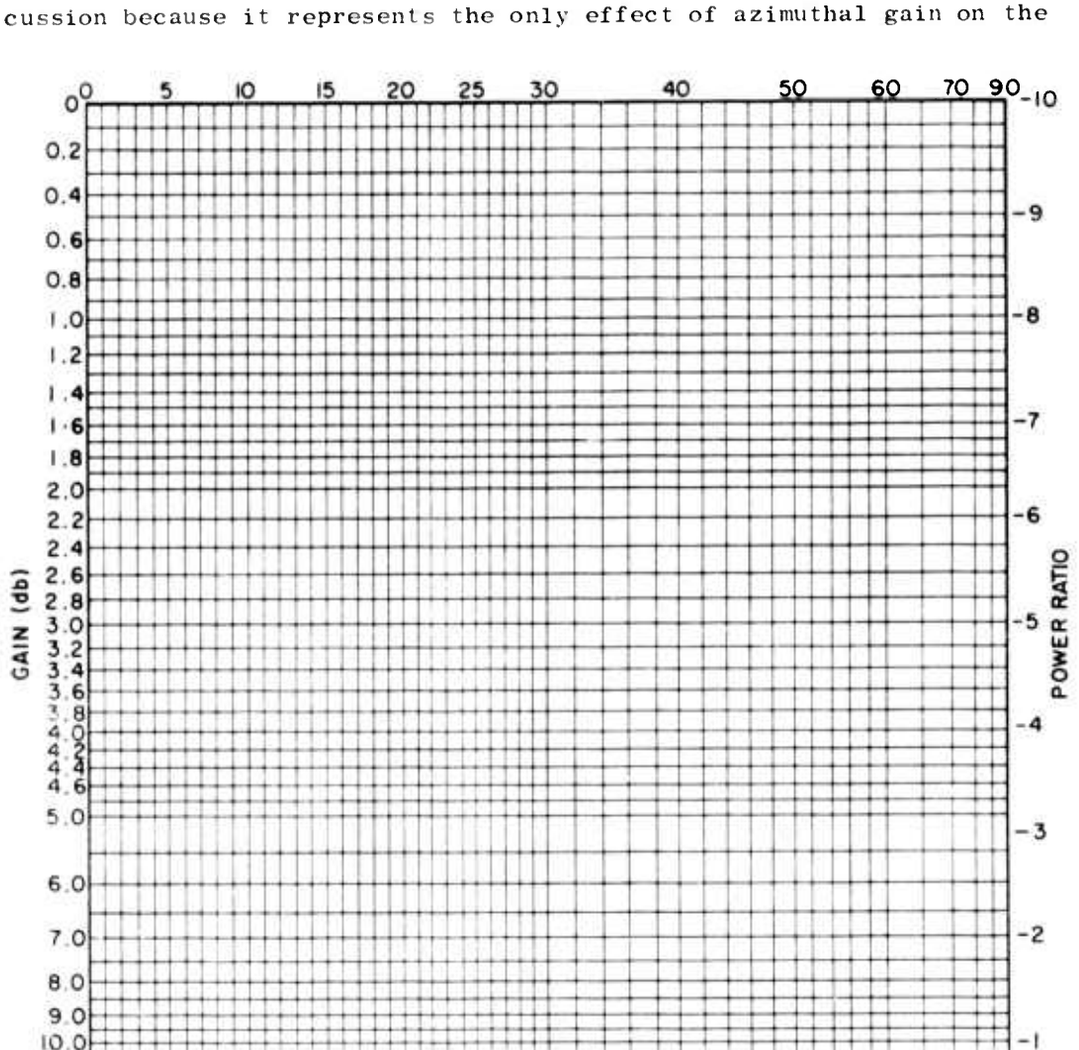

FIG. 19. A CHART DEVISED TO PERMIT USE OF A PLANIMETER FOR THE INTEGRATION OF GAIN.

backscatter, provided the underlying assumptions are valid. This excludes, for example, the effect of side lobes which can be calculated by a separate run of the same computer program. For convenience, define the numerator and denominator of the expression to be q_n and q_d, that is,

$$q_n = \sqrt{\oint_{\phi} q^2(\phi)\, d\phi} \; ; \quad q_d = \oint_{\phi} q(\phi)\, d\phi$$

The ratio of these factors will be calculated for various widths and shapes of the azimuthal gain pattern illustrated on Fig. 20. Here are shown three functions $q(\phi)$ of arbitrary width and varying shape. The first example, function q_a, has a constant value between two azimuths and is zero elsewhere: it might be termed rectangular. Shown on the drawing is the 3-db beamwidth, symbolized ϕ_{3db}, and the null-to-null beamwidth, symbolized ϕ_w. Each of the three examples on the figure was selected so that the first null falls at azimuth $\pm\pi/2n$, and thus the total width of these patterns between the nulls has the value of $\phi_w = \pi/n$. Similarly, let $\phi_{3db} = \pi/L$. Going back to Fig. 20a, it is seen that

$$q_n^2 = \frac{m^2\pi}{n} \; ; \qquad q_d = \frac{m\pi}{n}$$

$$q_n/q_d = \left(m\sqrt{\frac{\pi}{n}}\right)\left(\frac{n}{m\pi}\right) = \sqrt{\frac{1}{\pi} \cdot n} = 0.564\sqrt{n}$$

In this case, $L = n$ and so $q_n/q_d = 0.564\sqrt{L}$.

Now consider case (b) where $q_b(\phi)$ is a sinusoid. Here,

$$q_n^2 = \frac{m^2\pi}{2n} \; ; \qquad q_d = \frac{2m}{n}$$

$$q_n/q_d = \sqrt{\frac{\pi}{8} \cdot n} = 0.626\sqrt{n}$$

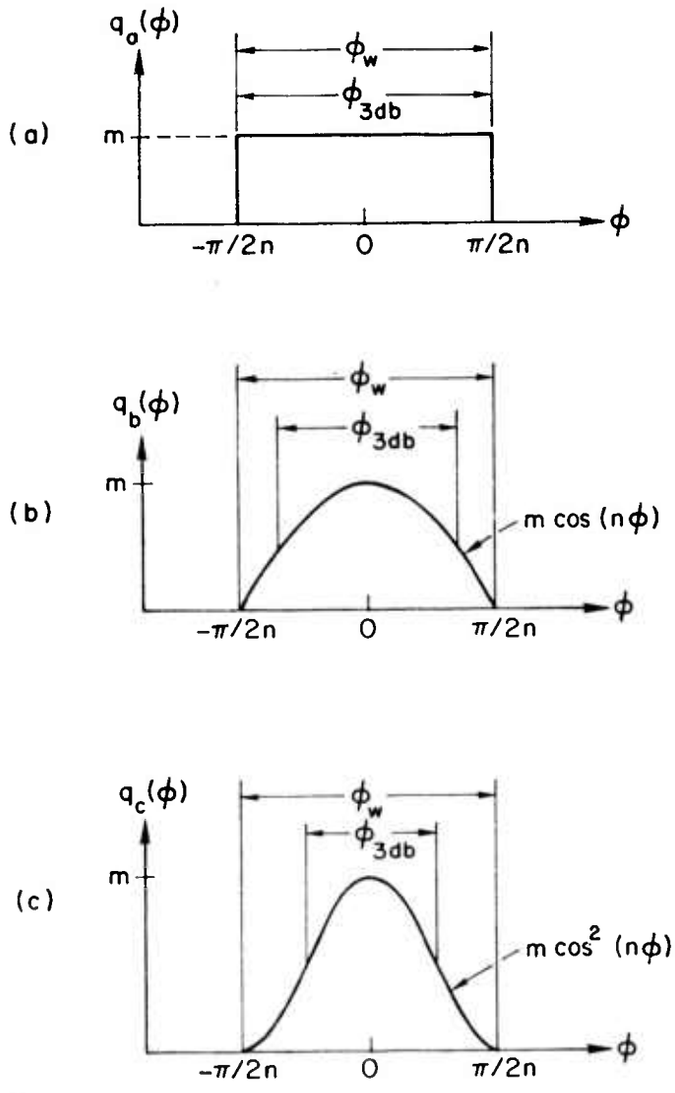

32683

FIG. 20. HYPOTHETICAL SHAPES USED FOR CALCULATING THE EFFECT OF THE AZIMUTHAL VARIATION OF GAIN.

Since the 3-db points occur at $\phi = \pm\pi/3$, $L = 3n/2$ and therefore

$$q_n/q_d = 0.513 \sqrt{L}$$

In case (c) the function is a squared sinusoid, probably the most realistic of the three patterns shown. Here,

$$q_n/q_d = 0.690 \sqrt{n} = 0.488 \sqrt{L}$$

These results can be summarized as follows:

Null-to-null beamwidth = π/n

3-db beamwidth = π/L

Shape of Gain Function, q	Value of q_n/q_d, Multiplier of $\sqrt{n}$	Value of q_n/q_d, Multiplier of $\sqrt{L}$
Square	0.564	0.564
Sine	0.626	0.513
Sine^2	0.690	0.488
Variation (%)	22	15

Two interesting conclusions follow from the argument given: (1) A high directivity in azimuth leads to a stronger backscatter signal in approximate proportion to the inverse of the square root of the beamwidth, and (2) the shape of the azimuthal gain function does not have a very strong effect on the backscatter signal strength for a given beamwidth. In fact, we have shown that the shape can undergo the drastic changes shown on Fig. 20 and that the backscatter signal strength will vary by only 30 percent provided the beamwidth remains constant in terms of the parameter L. [The variation would be reduced to 8 percent if $(\sqrt{n} + \sqrt{L})$ remained constant.]

Finally, this result is useful because it opens up a number of possibilities for the mathematical simulation of the effect of azimuthal gain patterns. Uncertainties in the experimental measurement of backscatter signal levels are usually far in excess of 30 percent and probably should be measured in orders of magnitude. Thus, if the only information available is a number giving the beamwidth of the azimuthal

pattern, a good approximation can be made to the value of the parameter q_n/q_d, by using either $0.69\sqrt{n}$ or $0.5\sqrt{L}$, depending on which of these factors is known. Of course, if the actual azimuthal pattern is known, the integration can be carried out and this approximation may be eliminated.

C. SUMMARY OF GAIN DISCUSSION

The effect of antenna gain on the backscatter signal-strength distribution has been analyzed in some detail. A single transmitting-receiving antenna is assumed, although this argument could be readily extended to cover use of separate antennas. The gain is mathematically broken down into the sum of several functions, each of which can be represented by a function which is separable in terms of the variables, azimuth and elevation angle. This procedure results in a marked simplification of the mathematics and yet utilizes all the information which is normally available concerning antenna gain patterns.

The effect of the elevation-angle variation in gain is thus separated out from the main problem and two different techniques are shown for simulating this pattern during computer operations. A graphical method of carrying out the needed integration is also given.

Backscatter signal strength is shown to vary approximately in inverse proportion to the square root of azimuthal beamwidth. The shape of the azimuthal gain pattern does not have a marked effect on the backscatter signal strength for a given beamwidth, assuming that the ionosphere and terrain do not vary in the direction transverse to the propagation path. Such variations can be simulated by means of separate computer calculations for each azimuth and subsequent addition of the results, by virtue of the fact that signals add incoherently in such a manner that superposition can be applied.

V. THE TECHNIQUE OF DIGITAL SYNTHESIS

This chapter describes the operation of the computer program which synthesizes backscatter, together with comments which illustrate the connection between some of the processes carried out digitally and the corresponding backscatter mechanisms. Input data to this program will include a deck of cards containing a sufficient number of raysets to describe a family of calculated raypaths through the ionosphere of interest. The number of hops can be varied between one and three, although it would be easy to modify this procedure to accommodate four or more hops.

The assumption is made that the raypaths represent streamlines in a flux of energy, and that the streamlines are sufficiently closely spaced that the energy can be considered to be uniformly spread between them in space and time. The energy tubes defined by these streamlines will begin at the transmitter where the energy density in each tube is determined by the antenna pattern. Then, as the tubes travel out into space, mix, spread, and cross in various ways, the energy within each tube is conserved. The flux-tube concept permits calculation of the density distribution of the energy in space and time as it strikes the ground after ionospheric refraction of some number of hops. Notice that two or more flux tubes may strike the same area on the ground.

As the energy travels outward within these flux tubes, corrections are made when it passes the D region to account for absorption at the particular range and angle of each such encounter. Also, corrections are made if the raypaths reflect off the earth, to account for the incomplete reflection coefficient at the particular terrain where the ray landed. For example, there may be synthesized a mountain range of high scatter coefficient but low reflection coefficient, which has a limited extent in radial range.

When the tube of flux arrives at the ground where it is to be scattered, the scattering coefficient $K(\psi)$ is used to determine how much of the energy is scattered back toward the transmitter, taking into account the angle of incidence and the angle of scatter necessary to

permit the energy to return to the transmitter. Geometrical relations applied to the rayset information provide full allowance for the effect of earth curvature and ionospheric curvature, both along and transverse to the propagation path.

On the return trip, the energy is again attenuated due to absorption in the D region and incomplete reflections off the earth. When it reaches the receiver location, it is corrected to account for the antenna gain at the elevation angle of arrival. Also, half the energy is lost because of polarization rotation in the ionosphere which causes it to be undetectable by the receiver antenna.

Typically there will be several thousand elements of energy calculated in this manner. Throughout this process, the time of flight of each element is accounted for and, finally, the convolution principle is applied to correct for the actual shape of the individual transmitted pulses as modified by the receiver bandpass characteristics.

The preceding discussion is a rough sketch of the digital computer process which is about to be described. During the actual computer operation, a number of complicating problems arise, such as the presence of raypaths that do not return to the earth because of a tilted ionosphere or because they penetrate and escape from the earth completely. Since such raypaths may form one of the boundaries of a flux tube, it is necessary to decide how to process the semibounded energy increments to maximize the similarity between the synthetic backscatter and that which would be obtained experimentally in such a situation.

A number of other complications arise because synthesis is done in the domain of discrete rather than continuous numbers. The particular computer in use, an IBM 7090, provides slightly more than eight decimal digits; consequently, round-off error is frequently a source of difficulty, particularly when it describes the height parameter which is measured from the center of the earth. In this case, the round-off error is approximately a meter, which is just large enough to cause occasional trouble.

The author hopes that others may wish to write similar computer programs and it is unlikely that the Fortran II version of this program would be directly useful. Consequently, this chapter will be given in sufficient detail to enable a scientific programmer to write a successful

backscatter synthesis program in another computer language if given some assistance by a person familiar with the physics of backscatter. A consistently successful program can be written in from two to four weeks starting from this description.

A. LIST OF SYMBOLS AND DEFINITIONS

At this point it is convenient to list and define the symbols used in this study, many of which have already been introduced.

Symbol	Description
A	the effective receiving area of an antenna
A_1, A_2	areas on the surface of the earth
a, b	constants used to calculate gain
B	bandwidth of a receiver, in cycles per second; also, in raytracing, the number of times a ray hit the earth
c	the speed of light, 299.7925 km/msec
D, E, F_1, F_2	conventional designation of ionospheric layers
$E, E_\alpha, e_1, e_2, e_3$	parameters which control the calculation of absorption according to the formula, $E = E_\alpha\left(1 + e_1 R + e_2 R^2 + e_3 R^3\right)$
E_R	the received energy in a single modeset
e	2.7182818, Napier's constant
F	frequency, usually given in kilocycles
f	general notation for a function
G	antenna gain as a function of azimuth and elevation

Symbol	Description
g	antenna gain separated to be a function of elevation alone
g_i	a constant used in gain calculations
H	a height punched into a rayset, usually the height of the last preceding apogee
h	height in general, always given in kilometers
h_D	the height of the D region
I	an indicator number in raysets giving general ray trajectory shape
K	a function of angle, terrain type, and frequency which determines backscatter coefficient
${}^{2}K_{3}$	when used with subscripts of presuperscripts, this is a constant used to calculate K
k	Boltzmann's constant; an arbitrary constant used to calculate gain; also, the absorption coefficient
k_1, k_2	constants used in the descriptions of ionospheric tilts
L, m	constants used in analysis of the gain function, q
n	a constant used to describe gain; also an identification number for timesets
n_1, n_2	specific values of the timeset identification
N	ionospheric electron density; electrons per cubic centimeter

Symbol	Description
N_m	maximum electron density in an ionosphere
P	power, measured in watts or milliwatts
P_n	noise power
P_Δ	the power level of a modeset
P_ϵ	received power, provided transmitted pulse is of "infinitesimal" duration, ϵ
q	gain as a function of azimuth, ϕ, according to the relation, $G = gq$
R	range in kilometers. However, if used as a subscript, this signifies association with the receiver.
R_L, R_H	the lowest and highest of two ranges compared by the computer
$^1R, ^2R$	arbitrary ranges used to establish the boundary between differing types of terrain for purposes of calculating K and ρ
R_p	the maximum range to be calculated
R_1, R_2	ranges calculated by the computer in establishing the identity of a modeset
$\bar{R}$	the center of the range interval reached by a particular energy flux tube
R_D	for a particular raypath, the ground range between encounters with the earth and the ionospheric D layer

Symbol	Description
R/R	the "received rayset," that is, the rayset used to describe the energy path on its return from the scattering ground
r_e	the radius of the earth, 6370 km
T	time, in milliseconds. However, when used as a subscript it signifies association with the transmitter.
T_g, T_ϕ	group and phase time delays, respectively, as given by the raysets
T_p	the maximum time used in calculating backscatter
T_1, T_2	the time limits which define the interval during which a particular flux tube encounters the earth
T_L, T_H	the time limits which define the interval spanned by a modeset
T/R	the "transmit rayset," that is, the rayset used to define the outgoing flux tube which strikes the ground
t	time, as a variable used in analysis
u	constant used in gain analysis
V, W	dimensions used in a reciprocity calculation
x, y	distance, usually in Cartesian coordinates
z	distance measured along a raypath; also used as a parameter in the formula for a Chapman ionospheric layer

Symbol	Description
α	an angle, usually measured from the center of the earth
$\alpha, \alpha_e, \alpha_{10}$	the ionospheric absorption index
β	the angle of a raypath, relative to the ground, measured at the radar end of the path
$\bar{\beta}$	the average beta of a flux tube
β_1	a constant used to raise or lower a mathematically synthesized antenna beam
γ	an angle used in absorption calculations
$\gamma_1, \gamma_2, \ldots, \gamma_{11}$	various intermediate products calculated during backscatter synthesis
Δ	used as a prefix to indicate the increment of some parameter
ϵ	in continuous numbers, an infinitesimal time increment; in discrete numbers, a short time increment on the order of 0.1 msec
ζ	an angle used in absorption calculations
θ	the geocentric angle subtended by the end points of a line; for example, $\theta = R \div r_e$
λ	the wavelength of the radio energy
ξ	in continuous numbers, a dummy variable
ξ, ξ_1, ξ_R, ξ_T	intermediate products calculated during back-scatter synthesis

Symbol	Description
ρ	the percentage of energy specularly reflected off the earth; also, the radius in circular or polar coordinates
${}^1\rho, {}^2\rho, {}^3\rho$	the reflection coefficient of the three types of terrain which are separated at ranges ${}^1R$ and ${}^2R$
ρ_T, ρ_R	the product of all the reflection coefficients encountered by a multiple-hop flux tube as it travels to or from the backscattering ground
τ	the duration of the transmitted pulse, if it is rectangular
ϕ	azimuth angle in polar coordinates; angle in circular coordinates
ϕ_W, ϕ_{3db}	the azimuthal beamwidth of the antenna, measured between nulls or 3-db points
ψ	the angle of a raypath relative to horizontal at the ground end of the path. (The analogous angle at the radar end is β.)
$\bar{\psi}$	the average landing (or takeoff) angle of an energy flux tube as it arrives at (or leaves) the scattering ground
' (prime)	The primed superscript on a rayset parameter means that it is selected from the next punched card in a deck of raysets.
Rayset	A set of numbers that describe a particular hop of a particular ray. It can also contain numbers that characterize the energy flux tube bounded by the ray and some other ray with a higher β.

Symbol	Description
Modeset	Each propagation mode to and from the backscattering ground leads to a small portion of the total received signal of power level P_Δ during the time interval bounded by T_L and T_H. The three parameters thus defined are termed a modeset.
Timeset	A set of approximately one thousand numbers which represent the received power distribution as a function of time sampled at intervals of ϵ.

B. REARRANGEMENT OF THE POWER EQUATION

Chapter III led to a long expression for P_Δ which may be rearranged into eleven factors, γ_1 through γ_{11}, as follows:

$$P_\Delta = \underbrace{\frac{1}{T_H - T_L}}_{\gamma_1} \cdot \underbrace{\cos \beta_T}_{\gamma_{2T}} \cdot \underbrace{\frac{\cos \bar{\beta}_R}{\sin \psi_R}}_{\gamma_{3R}} \cdot \underbrace{g_i^2 g(\bar{\beta}_T) g(\bar{\beta}_R)}_{\gamma_4} \cdot \underbrace{\frac{\epsilon P_T c^2}{(4\pi)^3 r_e F^2}}_{\gamma_5}$$

$$\cdot \underbrace{\csc \frac{\bar{R}}{r_e}}_{\gamma_6} \cdot \underbrace{\frac{\partial \beta_R}{\partial R_R}}_{\gamma_7} \cdot \underbrace{K\left(\frac{\bar{\psi}_T + \bar{\psi}_R}{2}\right)}_{\gamma_8} \cdot \underbrace{\rho_T e^{\alpha_T}}_{\gamma_9} \cdot \underbrace{\rho_R e^{\alpha_R}}_{\gamma_{10}} \cdot \underbrace{\Delta \beta_T}_{\gamma_{11}}$$

Here a prime superscript (e.g., R') means that the parameter is selected from the neighboring rayset with a next higher value of β. The bar above a symbol, as in $\bar{\beta}_R$, means that it is the average angle from a particular flux tube; that is,

$$\bar{\beta}_R = \frac{1}{2}(\beta_R + \beta_R')$$

Notice that the original raysets described single raypaths which could not carry energy because they had no cross-sectional area. However, in these calculations, each rayset is compared to another which pertains to the neighboring ray with the next higher β. The paired rays are considered to bound a flux tube so that $\bar{\beta}$ is the elevation angle of the flux-tube centerline. Then, it can be seen that

$$\gamma_7 = \frac{\partial \beta_R}{\partial R_R} \cong \frac{\beta_R - \beta'_R}{R_R - R'_R} = 2\,\frac{\beta_R - \bar{\beta}_R}{R_R - R'_R}$$

For purposes of summation, the ground will be considered to consist of concentric rings, each of which will be used in sequence as a source of backscatter. Each flux tube defined by a pair of rays will arrive at the backscattering ground to strike a ring which includes all the area between range R_T and R'_T. This annular section of ground will be denoted by the expression (R_T, R'_T). The terrain which is used for a single summation may, or may not, be identical to (R_T, R'_T) but the computer logic will be such that the ground annulus under consideration always lies within the boundaries of (R_T, R'_T). Suppose the ring being calculated is (R_1, R_2). Then, γ_{11} is the increment of takeoff angle which describes a flux tube that leads <u>only</u> to (R_1, R_2). Consequently, γ_{11} can be calculated by the following relation:

$$\gamma_{11} = \frac{\beta_T - \beta'_T}{R_T - R'_T}\,(R_2 - R_1) = 2\,\frac{\beta_T - \bar{\beta}_T}{R_T - R'_T}\,(R_2 - R_1)$$

Using this notation, it is seen that the range $\bar{R}$ which appears in γ_6 is related to γ_{11} in the following manner:

$$\bar{R} = \frac{R_1 + R_2}{2}$$

Since R_1 and R_2 are known prior to the selection of the transmitted raypath, the synthesis is speeded if the second factor in γ_{11} is transferred to γ_6.

Except for frequency, all of the factors in γ_5 will be constant in every backscatter calculation. The power P_T is chosen as 1 kw and the "infinitesimal" pulse direction ϵ is chosen as 0.1 msec. Calculation, in an appropriate system of units, then shows that if γ_5 equals $710/F^2$, the power will come out in milliwatts. Rewriting P_Δ incorporating the above operations yields

$$P_\Delta = \underbrace{\frac{1}{T_H - T_L}}_{\gamma_1} \cdot \underbrace{\cos \beta_T}_{\gamma_{2T}} \cdot \underbrace{\frac{\cos \beta_R}{\cos \psi_R}}_{\gamma_{3R}} \cdot \underbrace{g_i^2 g(\bar{\beta}_T) g(\bar{\beta}_R)}_{\gamma_4} \cdot \underbrace{\frac{710}{F^2}}_{\gamma_5}$$

$$\cdot \underbrace{\left(\csc \frac{R_1 + R_2}{2r_e}\right)(R_2 - R_1)}_{\gamma_6} \cdot \underbrace{2\frac{\beta_R - \bar{\beta}_R}{R_R - R'_R}}_{\gamma_7} \cdot \underbrace{K\left(\frac{\bar{\psi}_T + \bar{\psi}_R}{2}\right)}_{\gamma_8} \cdot \underbrace{\rho_T e^{\alpha_T}}_{\gamma_9}$$

$$\cdot \underbrace{\rho_R e^{\alpha_R}}_{\gamma_{10}} \cdot \underbrace{2\frac{\beta_T - \bar{\beta}_T}{R_T - R'_T}}_{\gamma_{11}}$$

There are some interesting symmetries in the foregoing equation. Notice that γ_7 and γ_{11} are the same except that one is selected from the transmitted rayset and one is selected from the received rayset; γ_9 and γ_{10} are similarly related. Also, γ_4 contains one factor from each of the two raysets, and the cosine terms in γ_2 and γ_3 follow the pattern. Thus, each of these can be calculated as soon as the raysets are read in by the computer, since their values depend on no other parameters. Therefore, they will be combined to speed the process.

Finally the power can be written in an expression which is the most convenient form for digital synthesis.

$$P_\Delta = \Bigg| \underbrace{\csc \psi_R}_{\gamma_{3R}} \cdot \underbrace{\frac{710}{F^2}}_{\gamma_5} \cdot \underbrace{\left(\csc \frac{R_1 + R_2}{2r_e}\right)(R_2 - R_1)}_{\gamma_6} \cdot \underbrace{\frac{K(\bar{\psi}_T/2 + \bar{\psi}_R/2)}{T_H - T_L}}_{\gamma_8}$$

$$\cdot \underbrace{\cos \beta_T \, g_i g(\bar{\beta}_T) \rho_T e^{\alpha_T 2\left(\frac{\beta_T - \bar{\beta}_T}{R_T - R'_T}\right)}}_{\xi_T} \cdot \underbrace{\cos \beta_R \, g_i g(\bar{\beta}_R) \rho_R e^{\alpha_R 2\left(\frac{\beta_R - \bar{\beta}_R}{R_R - R'_R}\right)}}_{\xi_R} \Bigg|$$

This equation looks wrong because the presence of γ_{3R} implies that P_Δ depends on <u>which</u> of the flux tubes is chosen to be the transmission path. Time-reversal invariance tells that the choice should not matter; the flow of energy should look the same when time runs backwards, as it will appear to do when the transmit and receive raysets are interchanged.

The source of this asymmetry is the absorption of a $\csc \psi_T$ term into $K(\psi)$ because of the definition of backscatter coefficient which was used in Ref. 33. There it is noted on page 43 that $K(\psi) = \sigma_o(\psi)/2 \sin \psi_T$, where σ_o is the standard radar cross section per unit area. This seems to imply that σ_o is a more fundamental measure than $K(\psi)$.

In the last equation for P_Δ, absolute values are taken because some of the factors have been allowed to become negative in the expression. Notice that ξ_T, ξ_R, γ_2, and γ_3 can be calculated as soon as the raysets are read into the computer. Also, γ_5 is evaluated only once in the entire program since it depends only on frequency. When the annulus of terrain has been selected for calculation, it is possible to calculate γ_6.

The operation which is carried out most often is the selection of specific transmit and receive raypaths. When this is done, it is only necessary to calculate γ_8, as all the other factors in P_Δ are already evaluated and stored in registers of the computer. The three parameters, P_Δ, T_H, and T_L, then constitute one modeset which might be thought

of as one element in an integration. Because of the streamlining of this operation the most frequent calculation is very short. Synthetic backscatter calculations in which there are 6000 or more modesets take less than 60 sec on an IBM 7090, despite the formidable appearance of the P_{Δ} equations. Thus, careful tailoring leads to a procedure which is very fast and consequently practical for synthesis of ground backscatter.

C. DETAILS OF THE SYNTHETIC PROCESS

When backscatter is to be synthesized, the digital computer is given a deck of cards which consists of three groups: (a) the program deck, written in accordance with the description which is now to be given; (b) a number of raysets which describe propagation through a specified ionosphere at a specified frequency; (c) a set of propagation parameters, which consists of the constants which the operator can choose at will to describe the ground backscatter and reflection characteristics, the absorption, antenna gain, pulse length, etc.

A good deal of the logic inside the program will depend on the sequence in which the raysets are read. This sequence is established prior to the operation of the computer when the rayset cards are shuffled in an automatic sorting machine. All of the cards must have the same F and the same IID. Next, the cards appear in major groups determined in the order of increasing B; that is, the first cards all describe the first hop, the second group of cards describe the second hop, and so forth. Within these groups, the cards must appear in order of increasing β. In operation, the program will read the first rayset card to obtain the values of IID and F to be used throughout the calculation. The rayset parameters T_{ϕ} and H are never used in this particular application.

The characteristics of the terrain are described to the computer by the following set of 14 constants:

$$
\begin{array}{lcccc}
 & {}^{1}\rho & {}^{1}K_1 & {}^{1}K_2 & {}^{1}K_3 \\
{}^{1}R & \multicolumn{4}{c}{\text{---------------------------------}} \\
 & {}^{2}\rho & {}^{2}K_1 & {}^{2}K_2 & {}^{2}K_3 \\
{}^{2}R & \multicolumn{4}{c}{\text{---------------------------------}} \\
 & {}^{3}\rho & {}^{3}K_1 & {}^{3}K_2 & {}^{3}K_3
\end{array}
$$

In this list, R signifies ground range, ρ symbolizes reflection coefficient, and K symbolizes ground-backscatter coefficient. As the layout of these constants would imply, they are interpreted according to the following logic: the ground range radially measured from the radar is divided into three sections. At all ranges less than ${}^{1}R$, the constants with a corresponding presuperscript of value 1 will be selected. At ground ranges between ${}^{1}R$ and ${}^{2}R$, the reflection and backscatter constants with a presuperscript of 2 will be selected. Beyond range ${}^{2}R$, the constants with a presuperscript of 3 will be selected. This system could easily be extended to include higher numbers, but so far added versatility has not been desired.

The constants are applied in the following manner. If radio energy strikes the earth at oblique incidence, some of it reflects as it might off a mirror, and some of it is scattered in all directions. The amount reflected is then ρ times the incident power. The scattering calculation is more complex and has been described previously. It is characterized by the backscatter coefficient $K(\psi)$, which is calculated according to the formula

$$K(\psi) = K_1 \sin^4\psi + K_2 \sin^2\psi + K_3$$

Generally, the user of this program will have some maximum time delay beyond which results are not desired. In order to take advantage of this limit, the maximum time delay T_p is given to the computer so that it will not wastefully calculate power which would appear at longer time delays. Associated with this parameter is a corresponding maximum

ground range which is also given to the computer. This is symbolized R_p, and is generally calculated as the round-trip range which could be reached by light in time T_p.

In this particular program, the decision was taken to make $\epsilon = 0.1$ msec. Any function of time is sampled at increments of ϵ and may be described either as a function or as a sequence of numbers which represent sampled-data points. The particular value chosen for ϵ could easily be changed, but 0.1 msec appears to be reasonable for two reasons. First, the bandwidth of a backscatter radar seldom exceeds 10^4 cps, and consequently the information which can be received is fully represented without any approximation by samples taken at increments of 10^{-4} sec. This result follows directly from the sampling theorem of information theory [Ref. 47]. Thus, ϵ can be taken as 0.1 msec and the resulting record will contain as much or more detail than actual experimental records obtained by radars of bandwidth 10 kc or less.

Another reason for this selection is that the final result, a drawing of power as a function of time, is made with a pen in an automatic plotting machine. With the largest practical scale and smallest pen available, the line width is about 0.1 msec.

It is considered that the maximum transmitted power is 1 kw, but this is not very significant because the results can be multiplied or divided by any factor to represent a corresponding higher or lower transmitted power. The nature of the transmitted pulse is described in two ways. First, the pulse shape is considered in some cases to be square. This approximation permits easier running of the program if one is willing to accept the corresponding assumption of excessive receiver bandwidth, as is often the case when interest is centered on other aspects of the backscatter phenomenon. The square pulse is fully described by the selection of a single parameter, pulse duration, which is measured in milliseconds and symbolized τ.

However, if the pulse shape as modified by the receiver bandpass characteristic is known, it is sampled at intervals ϵ and the resulting array of numbers is given to the computer. In subsequent operation these data points are considered to be sample points of the function $f(\tau)$ previously mentioned in the description of the effect of pulse shape.

The necessary convolution is carried out in the discrete number system where it appears in the more simple form of a weighted summation.

The two methods by which the gain (as a function of β) is given to the computer were discussed in the preceding chapter. When using the analytical form of input, the computer evaluates the expression (previously given) at each particular value of β where it needs a value of gain. Sometimes, the actual gain of an experimental antenna is available in graphical or tabular form. In this case it is easier to use the "itemized gain" approach where the curve showing gain plotted against β is approximated by a connected group of straight-line segments. The connection points are listed as a series of pairs of values of gain and β; then each is multiplied by g_i which is determined by planimeter integration. These sequences of paired values are given to the computer in digital form. The straight-line segments are reconstructed when the computer carries out a linear interpolation to find a value of gain for some value of β between two of the given pairs.

The amount of nondeviative absorption in the ionosphere is established by the selection of four constants: E_α, e_1, e_2, and e_3. These are used in the cubic equation,

$$E(R) = E_\alpha\left(1 + e_1R + e_2R^2 + e_3R^3\right)$$

which establishes the value of E to be used in evaluating the absorption for some particular pass of a ray through the D region at range R. Appropriate corrections are made for the angle at which the ray penetrates the D region and also for the effect of radio frequency.

D. PROGRAMMED STEPS

After the computer reads in the raysets, it changes all angles to radians. Then, after the last rayset, it makes an artificial rayset with the following values:

$$B = \text{previous } B + 1$$

$$T = T_p$$

$$R = R_p$$

$$\beta = \text{previous } \beta + 0.01$$

$$\Psi = \text{previous } \Psi + 0.01$$

This procedure facilitates the logic which will follow, and serves to shut off the calculation at the proper point without special tests.

The only rays which reach the ground will have $I = 0$, and they will be the only ones which account for any backscattered energy. To simplify the logic, the computer takes the raysets with $I \neq 0$ and modifies them as follows. In the first rayset of each hop, it replaces T, R, and Ψ with the values BT_p, BR_p, and β. In all other cases, it replaces T with the previous T plus 3 msec and it replaces R with the previous R plus 1000 km.

Next, the computer calculates $\gamma_5 = 710/F^2$. This is merely an intermediate product, and it contains the implicit assumption that peak transmitted power is 1 kw. Then, the computer processes the raysets, adding and deleting values, so that each will contain information which describes the flux tube bounded by itself and the next rayset.

To simplify language, the following description will make use of the symbol $(\cdot)$ which means "to be replaced by." Thus, $B \leftarrow B + 1$ means the same as the command, "Increase B by unity."

In each rayset, compare R and R'.

$$\text{If } |R - R'| < 1.0, \text{ then } T' \leftarrow T' \left(\frac{R - 1.0}{R'}\right) \text{ and } R' \leftarrow R - 1.0$$

This step is necessary because the array of R represents sample points from the function $R(\beta)$ and, on occasion, two successive sample points will be very close to one another. The result would imply an unreasonably high energy density striking the ground between the two R's. In some cases, further raytracing would resolve the problem because a ray with an intermediate value of β might fall at some range outside of

the interval spanned by the two R's. This would mean that the flux-tube approximation broke down, and that the energy which started out between the two rays underwent a folding operation and now lay partly outside the interval spanned by the rays.

However, raytracing will not always correct this situation because the corresponding continuous function, $R(\beta)$, may have an infinite derivative, $d\beta/dR$. This is a very common phenomenon and occurs at the skip distance of every layer. Ray theory in the continuous number system indicates that energy density is infinite at the skip distance. This obviously false result is resolved by wave theory which shows that the energy distribution at the skip distance is somewhat complicated but not infinite [Ref. 48]. The computer operation resolved the problem by the artificial spreading of this energy over a 1-km range with a corresponding time spread.

If ^1R lies in an interval whose end points are the R's of two successive raysets, and if each rayset has $I = 0$ and the same B, then manufacture a new rayset with $R \leftarrow {}^1R$. The new rayset should be placed between the two original raysets and should have values of T, β, and ψ which are calculated by interpolating between the values in the existing raysets in a manner which is linear with respect to the parameter range.

If ^2R lies in the range interval between any two successive raysets, make new raysets again according to the criteria described above for ^1R.

This operation makes an artificial ray land precisely at the range which separates various types of terrain. It results in a simplification in the logic because only a single scatter or reflection coefficient will now be needed in the calculation of a single modeset.

In each rayset, store R_L and R_H which are, respectively, the lowest and the highest of R and R'. If B is not equal to B', set $R_L \leftarrow R_p + 1$ and $R_H \leftarrow R_p + 2$. If $B = B'$ and $I = 0$, set $\xi \leftarrow G(\bar{\beta})$. Otherwise, set $\xi = 0$. In each rayset, store $\bar{\beta} = (\beta + \beta')/2$; $\bar{\psi} = (\psi + \psi')/2$; erase ψ if desired. The following definitions are made:

$$\zeta = \arccos\left(\frac{r_e}{r_e + 80}\cos\bar{\beta}\right)$$

$$R_D = r_e\,(\zeta - \bar{\beta})$$

$$\bar{R} = \frac{R_L + R_H}{2}$$

In each rayset, multiply ξ by ξ_1 as follows:

If B = 1, go to Instruction 1.
If B = 2, go to Instruction 2.
If B = 3, go to Instruction 3.

Instruction 1

$$\xi_1 \cdot \exp\left[-\frac{\csc\zeta}{F^2}\right]\left[E(R_D) + E(\bar{R} - R_D)\right]$$

Go to Instruction 4.

Instruction 2

$$\xi_1 \cdot \rho \exp\left[-\frac{\csc\zeta}{F^2}\right]\left[E(R_D) + E\left(\frac{\bar{R}}{2} - R_D\right) + E\left(\frac{\bar{R}}{2} + R_D\right) + E(\bar{R} - R_D)\right]$$

If $\bar{R}/2 \leq {}^1R$, $\rho \cdot {}^1\rho$

If ${}^1R < \bar{R}/2 \leq {}^2R$, $\rho \cdot {}^2\rho$

If ${}^2R < \bar{R}/2$, $\rho \cdot {}^3\rho$

Go to Instruction 4.

Instruction 3

$$\xi_1 \leftarrow \rho_1\rho_2 \exp\left[-\frac{\csc\zeta}{F^2}\right]\left[E(R_D) + E\left(\frac{\bar{R}}{3} - R_D\right) + E\left(\frac{\bar{R}}{3} + R_D\right) + E\left(\frac{2\bar{R}}{3} - R_D\right) + E\left(\frac{2\bar{R}}{3} + R_D\right) + E(\bar{R} - R_D)\right]$$

If $\bar{R}/3 \leq R_1$,	$\rho_1 \leftarrow {}^1\rho$	If $2\bar{R}/3 \leq R_1$,	$\rho_2 \leftarrow {}^1\rho$
If $R_1 < \bar{R}/3 \leq R_2$,	$\rho_1 \leftarrow {}^2\rho$	If $R_1 < 2\bar{R}/3 \leq R_2$,	$\rho_2 \leftarrow {}^2\rho$
If $R_2 < \bar{R}/3$,	$\rho_1 \leftarrow {}^3\rho$	If $R_2 < 2\bar{R}/3$,	$\rho_2 \leftarrow {}^3\rho$

Go to Instruction 4.

Instruction 4

In each rayset,

$$\xi \leftarrow 2\xi\left(\frac{\beta - \bar{\beta}}{R_H - R_L}\right)\cos\bar{\beta}$$

Store in each rayset $\gamma_3 = \csc\bar{\psi}$.
Notice that each rayset has a value for each of the following:

$$B\ \beta\ \bar{\beta}\ \psi\ T\ R\ R_L\ R_H\ \xi\ \gamma_3$$

Now begins the creation of perhaps several thousand modesets. Examine all the raysets and find the lowest R_L.
Call it R_1, and go to Instruction 5.

Instruction 5

Find the lowest $R > R_1$ and call it R_2.
If $R_2 > R_p$, go to Instruction 6. Otherwise calculate

$$\gamma_6 = (R_2 - R_1)\left(\csc\frac{R_1 + R_2}{2r_e}\right)$$

Now select the constants for use in calculating $K(\psi)$ according to the following criteria:

$$\text{If } \frac{R_1 + R_2}{2} \leq {}^1R, \qquad (K_1, K_2, K_3) \leftarrow \left({}^1K_1, {}^1K_2, {}^1K_3\right)$$

$$\text{If } {}^1R < \frac{R_1 + R_2}{2} \leq {}^2R, \qquad (K_1, K_2, K_3) \leftarrow \left({}^2K_1, {}^2K_2, {}^2K_3\right)$$

$$\text{If } {}^2R < \frac{R_1 + R_2}{2}, \qquad (K_1, K_2, K_3) \leftarrow \left({}^3K_1, {}^3K_2, {}^3K_3\right)$$

Select for processing all raysets which satisfy both of the following relations:

$$0 \leq R_1 - R_L < 200 \text{ km}$$

$$R_2 \leq R_H$$

This procedure selects for processing only those raysets which describe energy that propagates to or from the range interval of interest, (R_1, R_2). Semibounded flux tubes are included only for the first 200 km beyond R_L. (In the computer, it is necessary to establish a maximum number of such raysets, and thus far, after a year and a half of operation, the number has never exceeded 20. Usually, there are 2 to 4.)

If no such raysets are found, go to Instruction 5.

In each of the selected raysets, store T_1 and T_2 calculated as follows:

$$T_1 = T + (T - T^1)\frac{R_1 - R}{R - R^1}$$

$$T_2 = T + (T - T^1)\frac{R_2 - R}{R - R^1}$$

It automatically follows that $T_1 < T_2$. To understand this operation, it must be appreciated that we are now processing the energy that lands within the range interval, (R_1, R_2). The raysets will commonly be describing energy flux tubes that land on the ground in a range interval which is larger than and includes (R_1, R_2). It is then necessary to calculate the time of flight to the near and far edges of the range interval under consideration. These times of flight are T_1 and T_2 under the assumption that the energy is distributed uniformly in space and time within a flux tube.

For this particular range increment, the processing of the raysets is now complete. Each rayset under consideration identifies a propagation mode which leads to the strip of terrain under consideration, and thus each such mode can be either a route from the transmitter to the ground or a return route from the ground to the receiver. If there is just one rayset, the situation is trivial and the energy goes out and back along the same path. Suppose that there are two raysets: let us call them A and B. The energy can go out on A and return on A. It can go out on A and return on B. It can go out on B and return on A. It can go out on B and return on B. Thus, there are four propagation modes and the computer must calculate four modesets for this particular range interval. If there were three raysets, there would be $(3^2 = 9)$ modesets. Similarly, if there were n raysets, there would be n^2 modesets for this range increment. One of the novel features of this form of analysis is that the resulting complicated energy distribution in space and time can be simulated by a simple accounting procedure within the computer. This procedure is described as follows.

From among the selected raysets, pick one and call it the transmit rayset (abbreviated T/R). Elements selected from this rayset will be given an additional T subscript. Select another rayset, which can be the same as the T/R; it will be the receive rayset, symbolized R/R, and its elements will receive an R subscript. This procedure must be carried out for each of the possible combinations of T/R and R/R which can be found from among the raysets available.

Define $T^1 = T_{1T} + T_{1R}$ and $T^2 = T_{2T} + T_{2R}$. Pick the lowest of these, round off to the nearest multiple of ϵ, and call it T_L. Similarly, round off the highest of the numbers and call it T_H. If the roundoff process has caused them to be equal, set $T_H = T_L + \epsilon$. Also, if $T^2 - T^1 < \epsilon$, set $T_2 = T_1 + \epsilon$. Now calculate γ_8 according to the following:

$$\gamma_8 = \left[K\left(\frac{\psi_R + \psi_T}{2}\right)\right] \frac{1}{T^2 - T^1}$$

(Recall that K is a function.) Now

$$P_\Delta = |\gamma_6\ \gamma_8\ \gamma_{3R}\ \xi_R\ \xi_T\ \gamma_5|$$

This corresponds to the last P_Δ equation in Sec. B, thus "closing the loop" with the analysis previously given.

Now create 1100 storage registers, each identified by a whole number n where $0 < n < 1101$. These registers will be filled with the numbers which constitute a timeset. Define a parameter j which equals the width of the transmitted pulse measured in tenths of milliseconds (for $\epsilon = 0.1$ msec). In the case of a square pulse, $j = 10\tau$. Then, add P_Δ to each element of the timeset in which $10T_L + j \leq n < 10T_H + j$. Now go back and select a new T/R and a new R/R from among the raysets which reach this range increment, and start a new P_Δ calculation. If all combinations have been selected, set $R_1 = R_2$. Repeat Instruction 5.

Instruction 6

The timeset registers now contain $P_\epsilon(t)$.

If the transmitted pulse is square, such that $j = 10\tau$, find the sum of the first j timeset elements and substitute this sum for the first element. Starting at the second element, sum the first j elements and substitute the sum for the second element. Starting at the third element, sum the first j elements and substitute the sum for

the third element. Continue this operation until it has been carried out $20T_p$ times.

If a shaped pulse is used, substitute the following procedure. Pair up the first j timeset elements with the j elements in the transmitted pulse description, in reverse order. Multiply each pair together and take the sum. Substitute this sum for the value in the first timeset element. Starting at the second element, pair up the first j elements with the j factors in the (reversed) pulse description. Again, sum the product of the pairs and this time put the result in the second timeset element. Repeat this process $20T_p$ times. The timeset register now contains the final answer, ready for plotting.

Add a very small number to each element. This number should be small enough to be negligible and yet large enough to permit calculation of the logarithm of the number if the prior entry in the register was 0. Now find the $\log_{10}$ of each element and substitute it for the element. Plot the logs on a linear graph as a function of n for all values of n up to $20T_p$. The result is then a semilogarithmic representation of the received power as a function of time.

Figure 21 shows a typical result. Although 100 db of amplitude and 100 msec of time are plotted, the useful part is usually about 30 db × 50 msec. The rest of the plot, particularly the bottom portion, serves mainly to provide insight in case of computer, plotter, or program error. The labels shown were also automatically drawn. The first shape shows $f(t)$, the transmitted pulse as modified by the receiver bandpass characteristic. The next shape plotted is the resulting backscatter from three hops. The background noise level would be near 10^{-14} mw.

E. ADDITION OF THE THIRD DIMENSION--FREQUENCY

So far this analysis has taken place only at a single frequency. Now, the results from a number of frequencies will be combined to produce a single synthetic "sweep-frequency backscatter record." The method of doing this is a straightforward simulation of the natural process and is carried out manually using a rather simple graphic technique. The technique will be illustrated by an example.

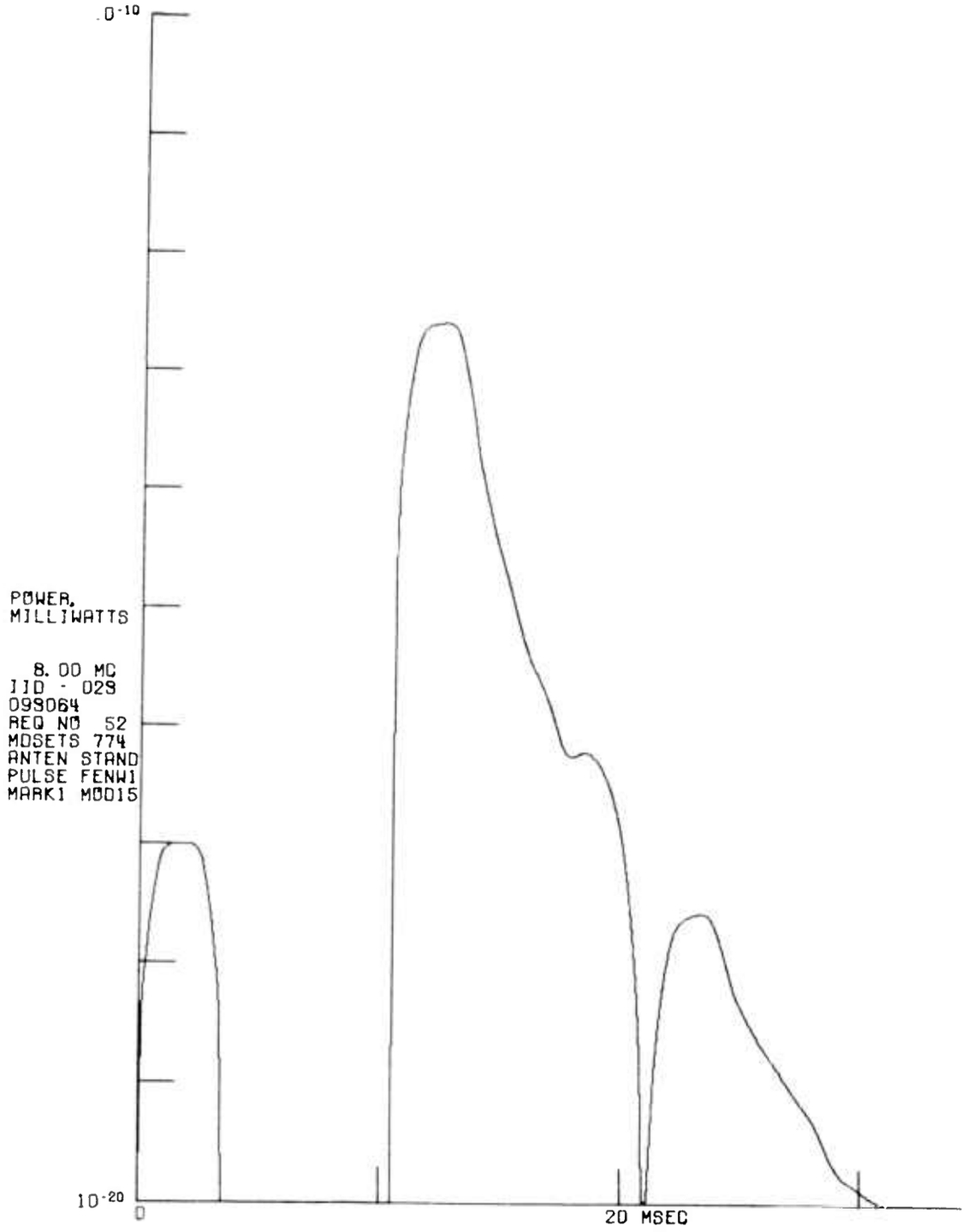

FIG. 21. THE FINAL RESULT: A COMPUTER PLOT OF THE TIME VARIATION OF AVERAGE BACKSCATTER AMPLITUDE.

Figure 22 shows a group of fixed-frequency backscatter records obtained for a single ionosphere under a set of fixed circumstances. The only thing that changes from record to record is the antenna gain pattern, which is varied in accordance with its known functional relationship to frequency.

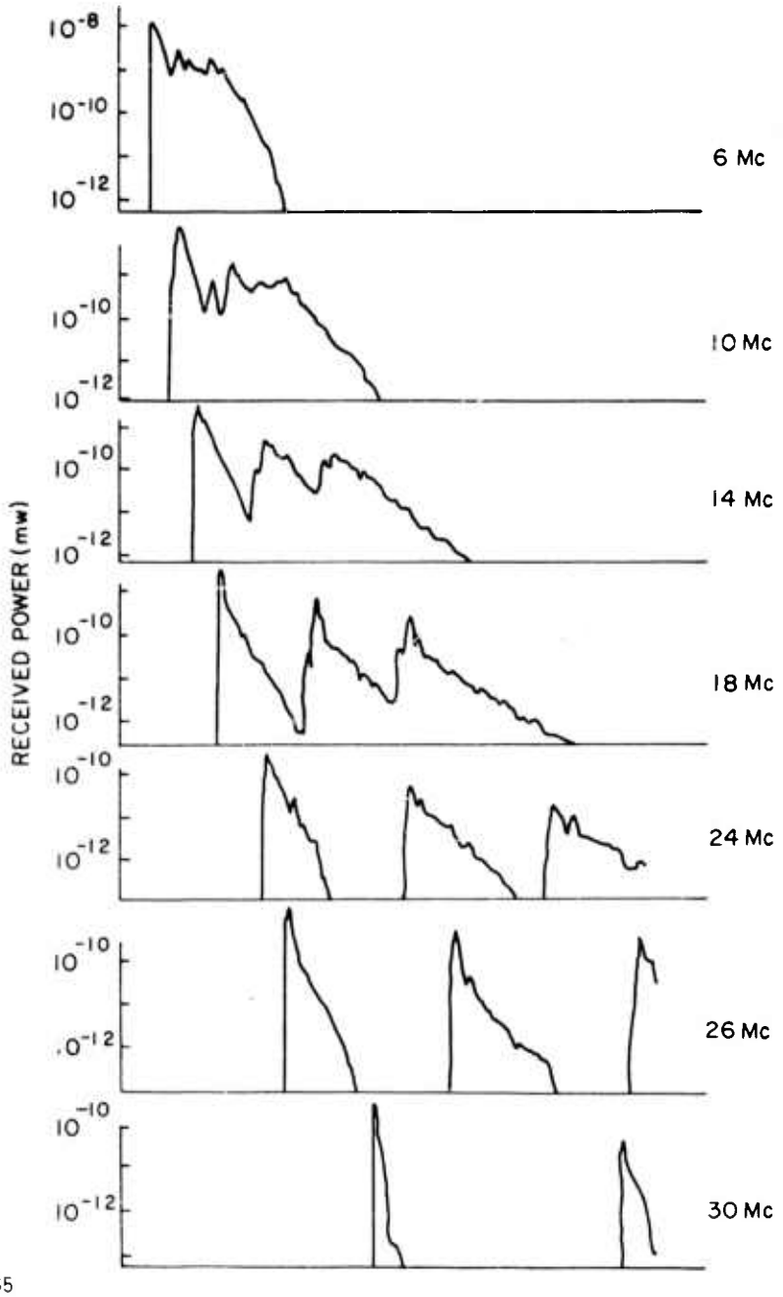

FIG. 22. SYNTHETIC BACKSCATTER OBTAINED AT SEVEN DIFFERENT FREQUENCIES.

One other parameter varies with frequency and that is the received noise, which is known to change in the upper high-frequency band in proportion to the radio wavelength raised to a power which is near 2.3. In a previous report, the author consulted a number of sources in the literature and concluded that noise power can realistically be simulated by the expression $P_n = 90kB\lambda^{2.3}$ [Ref. 49]. In this expression, P_n is received noise power, k is Boltzmann's constant, B is the receiver bandwidth, and λ is the radio wavelength; all units are mks. This expression gives the average noise power with the understanding that actual measurements can vary from this value by quite large amounts. In the lower half of the 3- to 30-Mc band, where man-made noise is the primary source, the day-to-day and band-to-band variation can be orders of magnitude [Ref. 50]. Consequently, the expression for P_n should be considered as an indication of order of magnitude and, in this report, it serves the very useful function of providing a reference level for power measurements which behaves in a manner consistent with the known variation of the received noise levels when frequency or bandwidth are changed.

Since it will be desirable to assign a noise power level to each synthetic backscatter record, the receiver bandwidth must be specified. It has been found that for the purpose of obtaining sweep-frequency backscatter records experimentally, the optimum bandwidth is very near the theoretical minimum value of 1.2 divided by the pulse duration, τ [Ref. 23]. Therefore, unless otherwise stated in reference to a specific synthetic record, the assumption will be made that $B = 1.2/\tau$. Using this relation, the noise can be expressed in terms of frequency and pulse duration only. When evaluated throughout the range of values which are useful here, the received noise power may thus be represented by the two-dimensional graph given on Fig. 23.

Now at last it is possible to synthesize a single sweep-frequency backscatter record. Power will be measured in decibels above the noise, using data from Fig. 23. The method of putting together several fixed-frequency synthetic records to produce a single sweep-frequency record is illustrated by the three-dimensional model which is shown on Fig. 24.

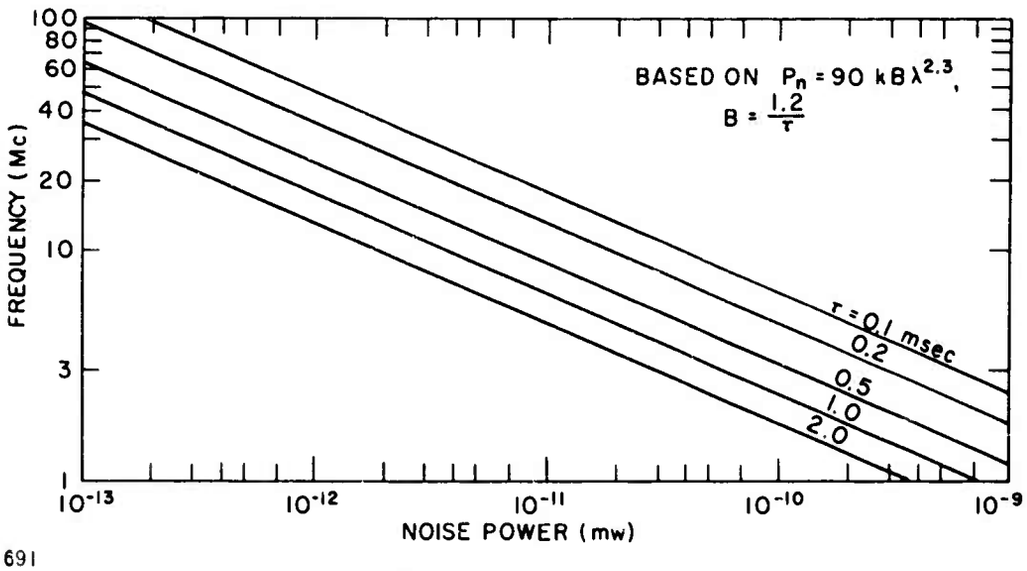

32691

FIG. 23. THE CALCULATED NOISE LEVEL FOR GIVEN FREQUENCIES AND PULSE DURATIONS.

Here, each of the shaded vertical planes represents a single fixed-frequency synthesis, taken from Fig. 22. The gradually descending plane which cuts through these vertical ones then represents noise power taken from Fig. 23. The gray shades painted on the vertical planes represent bands 10 db wide measured upward from the noise level.

Of course, in actual practice the cardboard model is not made, but rather a tracing process is used to produce what might be called a "paint-by-number" pattern. This pattern is then painted in shades of gray watercolor to produce the result given on Fig. 24. When accompanied by proper frequency and time scales and a description of the ionosphere, terrain, and radar parameters, such a painting is a synthetic sweep-frequency backscatter record.

In some work, however, the 10-db increment of power level is too coarse, so that other representations of the sweep-frequency records are occasionally necessary. For example, when a strip of mountainous terrain is simulated, it is more convenient to show the difference that this simulation causes in the sweep-frequency record as compared to a similar record synthesized without the mountain range.

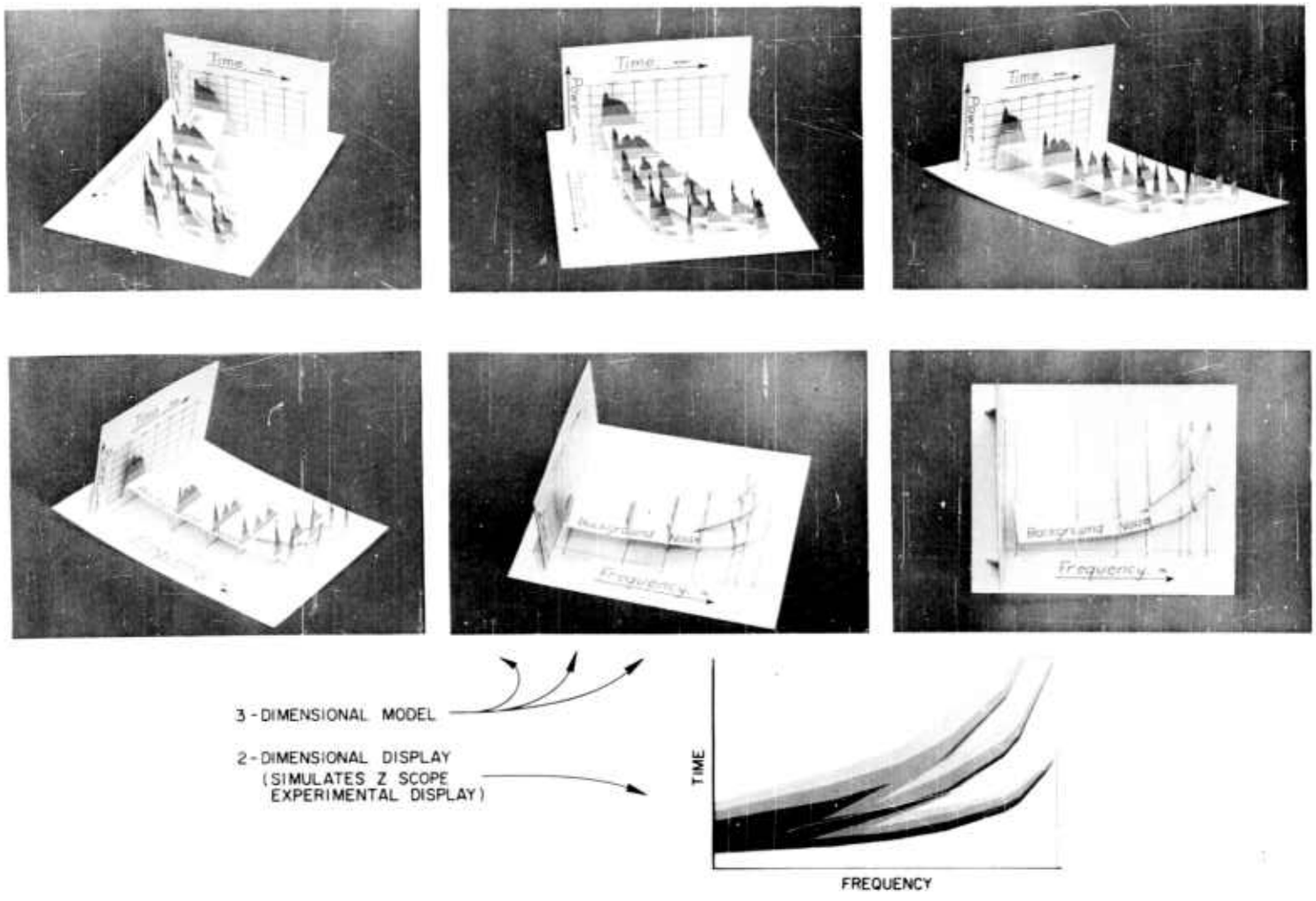

FIG. 24. A MODEL SHOWING THE ADDITION OF THE FREQUENCY DIMENSION.

The particular backscatter record illustrated on Fig. 24 shows little similarity to actual backscatter because, among other things, there is no absorption. Other unrealistic parameters are used in this particular model and so it is seen that the third-hop echo is almost as strong as the first-hop echo, whereas the natural backscatter dies off rapidly with an increase in the hop number. Figure 24 was generated as part of a study in which the effect of the ionospheric structure was isolated.

F. A COMPARISON OF SYNTHETIC AND EXPERIMENTAL RECORDS

The acid test of the complicated technique which is presented here is comparison between synthetic and experimental records taken under identical conditions. Previously it has not been possible to do this under well-controlled circumstances because a properly instrumented backscatter radar did not exist. Thus, the direct comparison was prevented by limitations in the experimental technique used in the past. The limitation is understandable when it is considered that it has not been possible before to make use of all the information which is now found to be necessary.

In order to permit such a study, a well-calibrated sweep-frequency backscatter radar has been assembled by the Radioscience Laboratory for the specific purpose of permitting the comparison to be made. The radar operates into an antenna whose pattern has been flown and the resulting reduced data published [Ref. 45]. The use of this antenna, kindly made available by the Stanford Research Institute, eliminates one of the major uncertainties which would usually limit the validity of a direct comparison between synthetic and experimental records. Also, this radar has good calibration in power, frequency, and group time delay. Vertical ionograms, also provided by SRI, are obtained to maximize the information available concerning the ionosphere. The effort appears worthwhile because it shows a promise of producing information about such things as the scattering characteristics of the ground as a function of frequency, terrain type, and incidence angle. An example of such a comparison is given here to show that the computer technique is capable of producing a match.

Figure 25 shows a synthetic record and a corresponding experimental record which was obtained by a Granger Associates sounder located at Stanford. The striking resemblance between the structures is readily apparent. Notice in particular that the shape and location of the two-hop echo is closely simulated.

Figure 26 shows a corresponding experimental and synthetic one-hop record. For synthesis, it was necessary to use horizontal electron-density gradients in order to simulate the sharply upturned tail at the high-frequency end. The experimental record is one of the early practice scans taken with the calibrated radar when it was being prepared. Here again it can be seen that the correspondence between synthesis and experiment is quite close. The experimental record does show an additional echo on the near side of the main trace; this is probably due to an antenna side lobe which looks in a different azimuth at a slightly different ionosphere; however, these two records have not been fully investigated, and they are presented here only to show that there actually is some correlation between synthetic and experimental backscatter.

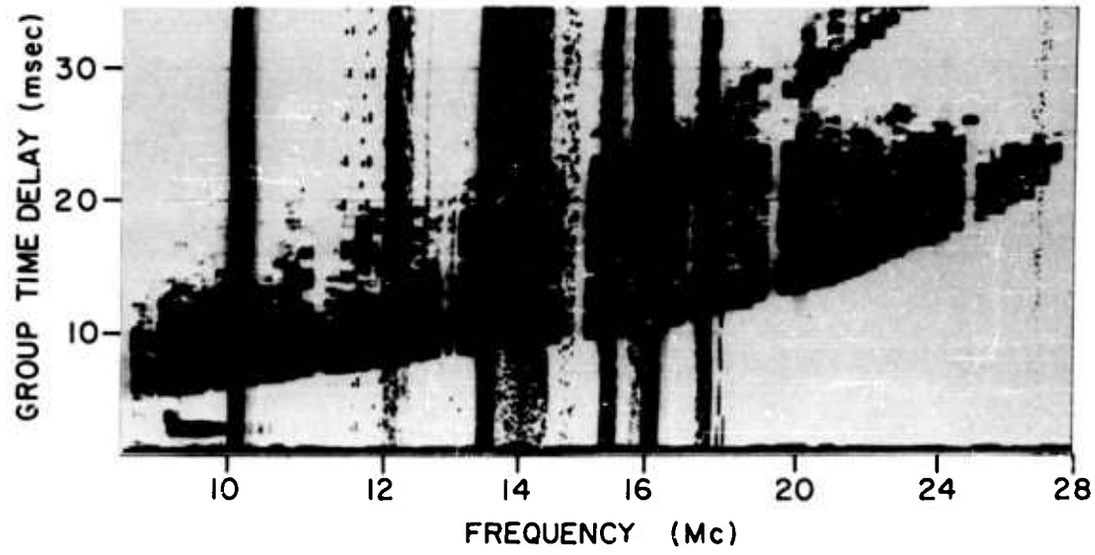

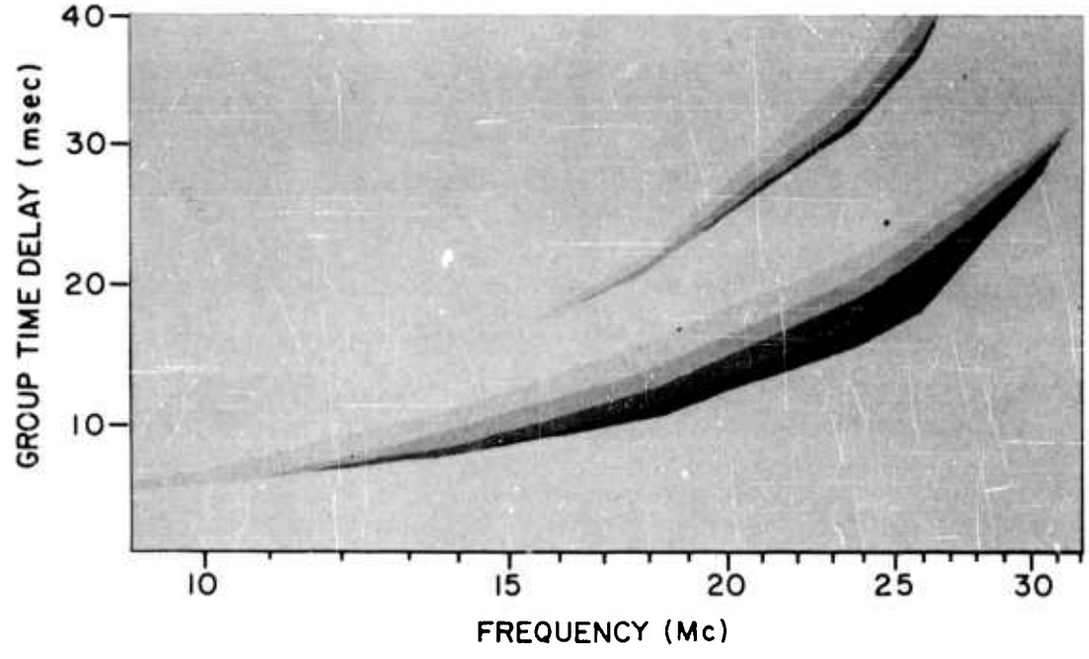

b. Synthetic record

FIG. 25. EXPERIMENTAL AND SYNTHETIC RECORDS OF TWO-HOP BACKSCATTER.

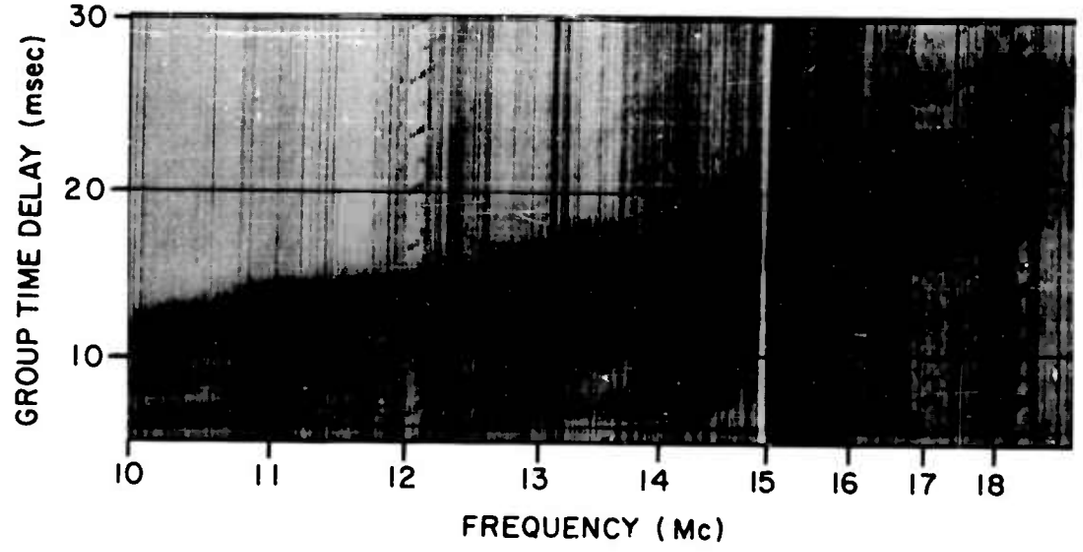

a. Experimental record

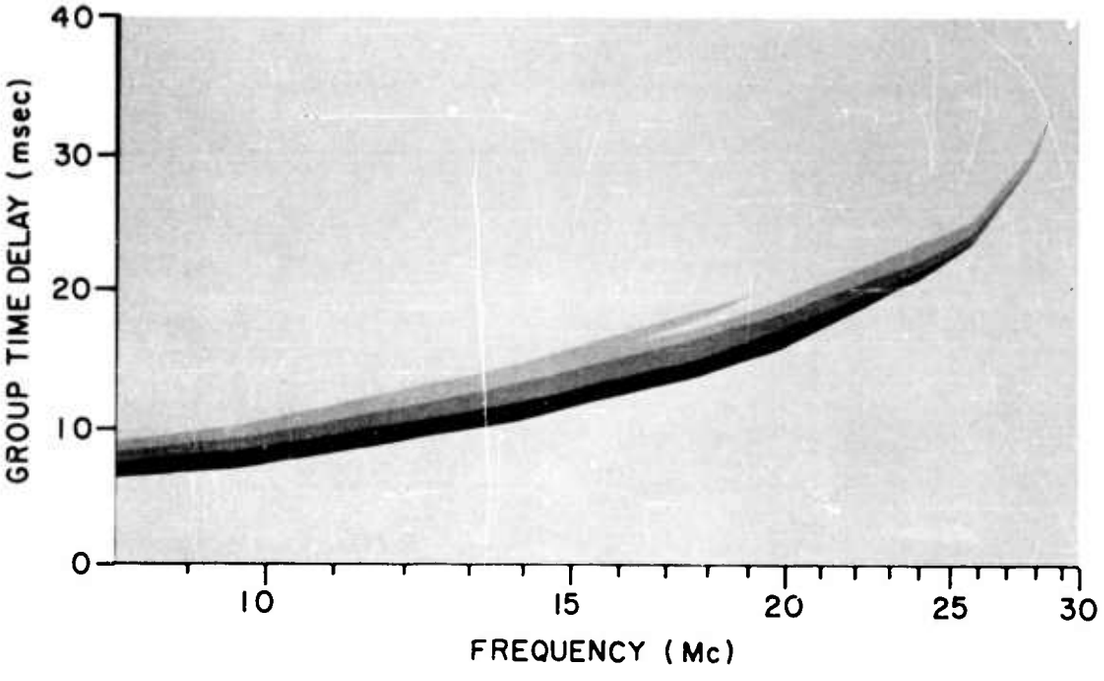

b. Synthetic record

FIG. 26. EXPERIMENTAL AND SYNTHETIC BACKSCATTER WITH A TILTED IONOSPHERE.

VI. ILLUSTRATION OF THE SYNTHESIS OF A SPECIFIC EXPERIMENTAL RECORD

There are two primary uses for the digital computer technique described in the preceding chapters. First, it can be used to investigate the effect on backscatter of changes in only one of the various factors which influence the record. For example, it is possible to change only the antenna pattern and hold all other factors unchanged to determine the effect which the antenna has on backscatter. Similarly, the absorption may be changed in some predetermined way, while all other things are held constant; an isolated irregularity could be inserted in the ionosphere at a distance, and the resulting backscatter perturbation could clearly be illustrated in a quantitative manner.

The second potential use for the digital technique is in the synthesis of specific experimental records which are acquired by a well-calibrated backscatter radar. Prior to this time, there has been to the author's knowledge no backscatter radar which was adequately calibrated to support comparison studies of this type. The lack is understandable, because there has never been any prior need for such precise quantitative data. However, now it will be necessary to know the transmitted power, the pulse shape, the effect of the receiver on the pulse shape, the antenna pattern, the absolute power level of the received signal, and the precise frequency scale of any sweep-frequency records, to mention a few examples. Also, it will be very convenient to have nearly simultaneous "A" and "Z" records of the same backscatter. (An A record shows backscatter amplitude as a function of group time delay at a fixed frequency, while a Z record shows frequency and group time delay on the X and Y axes of an oscilloscope, while backscatter signal amplitude modulates the Z intensity axis.)

One of the major problems has been the need for a well-calibrated antenna suitable for operation in the frequency interval of approximately 7 to 30 Mc. Fortunately, the Stanford Research Institute had recently measured the radiation pattern of a rhombic antenna [Ref. 45], and they kindly made the antenna available for this experiment.

In mid-1964, Radioscience Laboratory personnel began the assembly and calibration of a sweep-frequency backscatter radar to operate into the SRI antenna. It has proven possible to build a radar which is satisfactory for these purposes by using equipment already on hand. The basic item was a near-prototype version of a sweep-frequency pulse radar, built by Applied Technology, Inc. of Palo Alto, Calif., and designated the ES-1A. This device consists of a transmitter which is servo-tuned so that it tracks the frequency tuning of a modified SP-600 receiver. The ES-1A transmits approximately 1 kw in pulses of variable duration and, in the most common situation, this energy is used to drive a PA-1A power amplifier made by the same manufacturer and similarly servo-tuned. The peak transmitted power is on the order of 5 kw, although the exact value is a function of frequency due to the interaction of a large number of circuit elements which have frequency-sensitive impedances.

The first calibrated record suitable for synthesis was made between 1032 and 1042 Pacific Daylight Time on 20 October 1964 (PDT is GMT minus 7 hr). This record is shown as Fig. 27. The array of dots is placed on the record by a system which provides precise quantitative indicators of the frequency and the group time delay of the record. It can be seen that there was some jitter in the time marks toward the high-frequency end of the record, but stability at the low frequencies provides an unambiguous indication of the group time delay.

Figure 28 shows calibrated A records which were acquired shortly before the Z record. These will provide the quartitative measure of backscatter signal strength for use in the synthesis. However, it will be seen that the high-frequency records were acquired as much as 1 hr 20 min prior to the Z record, and, since this was in the morning, adjustments have to be made to allow for the changes in the ionosphere which took place between acquisition of the A and Z records.

The remainder of this chapter deals with the use of the digital-synthesis technique for the simulation of frequency-time data of Fig. 27 together with the amplitude information from Fig. 28.

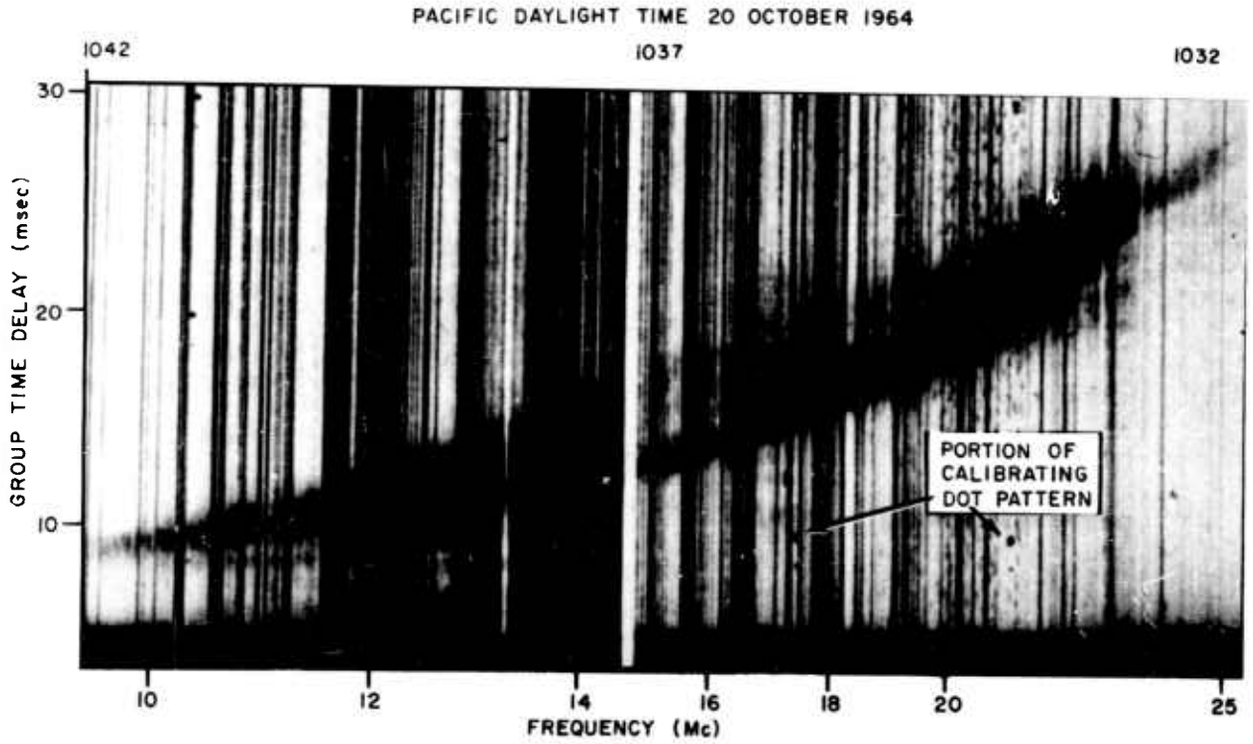

FIG. 27. THE FIRST CALIBRATED SWEEP-FREQUENCY RECORD FOR SYNTHESIS.

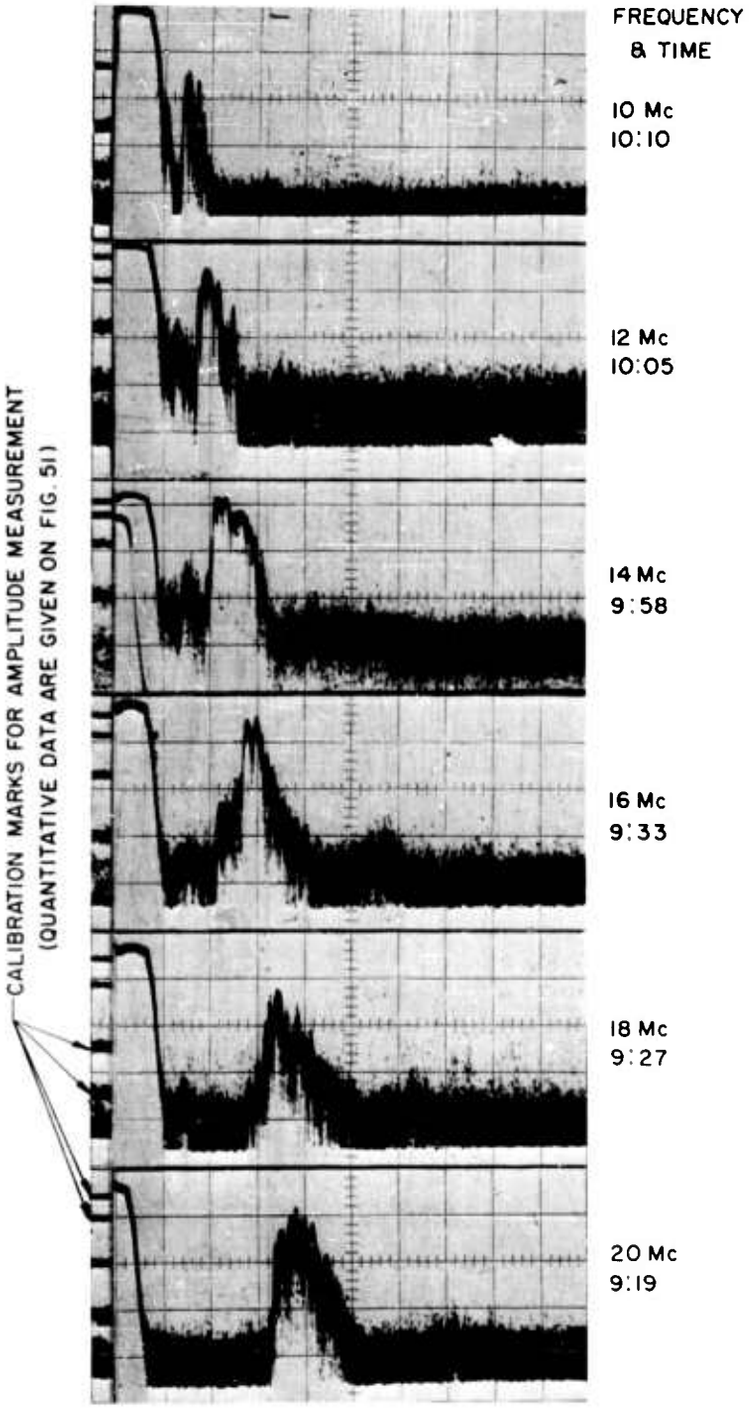

FIG. 28. CALIBRATED "A" RECORDS FOR MEASURE OF SIGNAL STRENGTH ON FIG. 27.

A. DESCRIPTION OF THE CALIBRATED RADAR

Figure 29 shows the equipment which has been assembled to gather calibrated backscatter records. In the rack nearest the camera are the exciter-sounder and the power amplifier previously mentioned. In the other two racks are the modified SP-600 receiver, linear detectors, logarithmic detectors, oscilloscopes for data monitoring and recording,

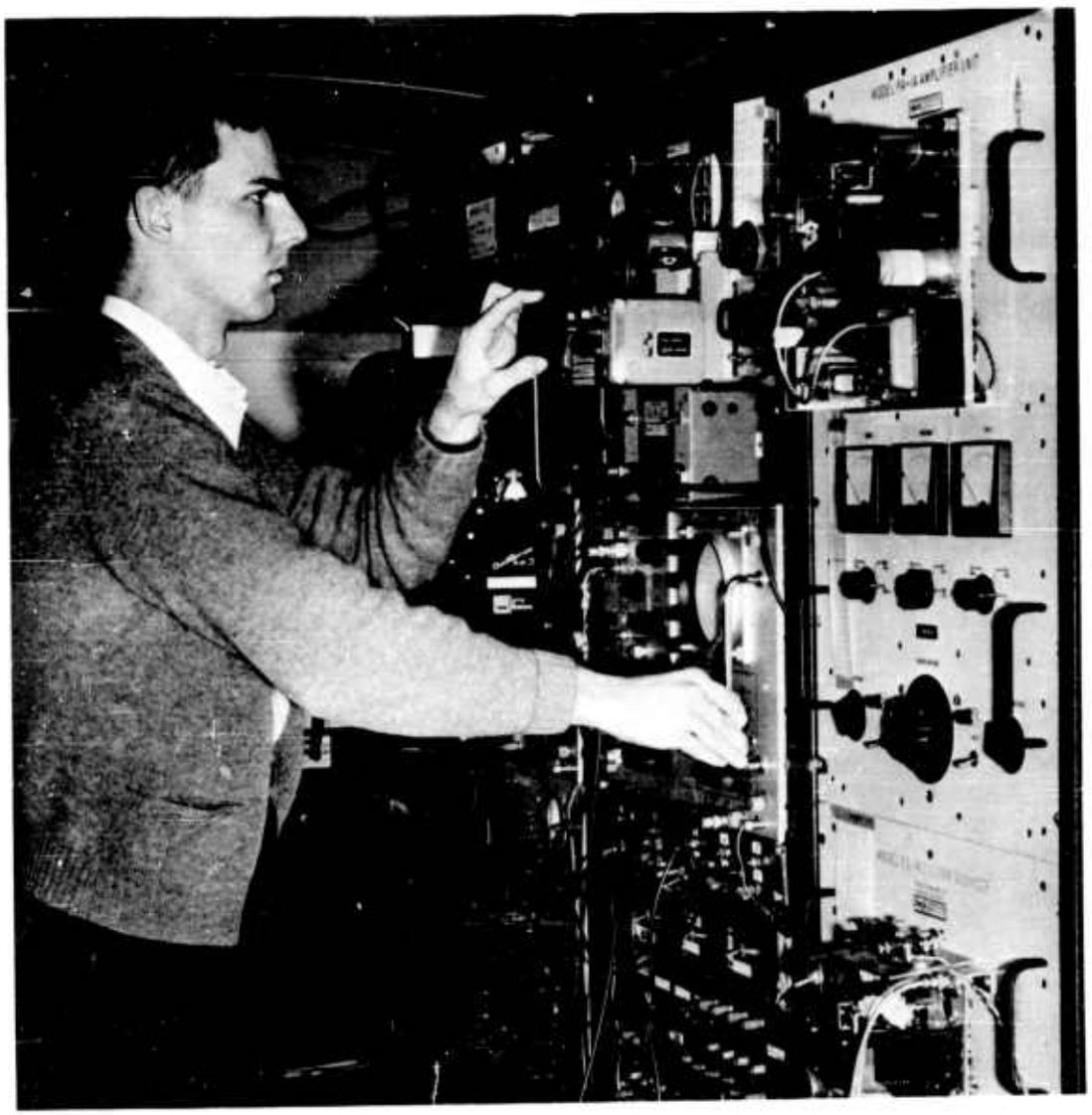

FIG. 29. PHOTOGRAPH OF THE CALIBRATED RADAR EQUIPMENT.

a polaroid camera for A-scope records, and a strip-film camera for Z-scope records.

The equipment is located in a bus which is temporarily stationed at one end of the rhombic antenna. This antenna has a gain pattern which has been measured by aircraft. The azimuthal gain integration, described in Sec. IVB, can be done quite accurately on this antenna because the patterns are precisely known. The result of the calculation is given on Fig. 30 which shows the scalar multiplier of the backscatter amplitude as a function of frequency.

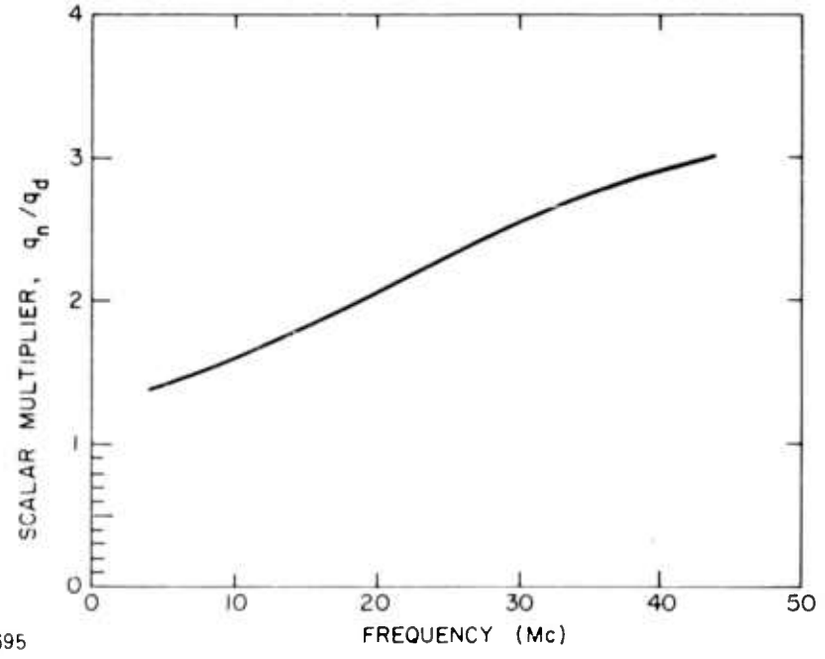

FIG. 30. SCALAR MULTIPLIER REPRESENTING THE EFFECT OF AZIMUTHAL GAIN.

The variation of gain with respect to elevation angle involves a good deal more work. Reference 45 shows the shape of a number of gain functions in a typical polar plot. These are transferred by a simple coordinate transformation to the chart which has been devised for the integration of itemized gain (Fig. 19). The result is shown on Fig. 31 for the frequencies which were plotted by Barnes. It should be mentioned that these curves, shown on Fig. 31, are the theoretical curves given in Ref. 45, and that

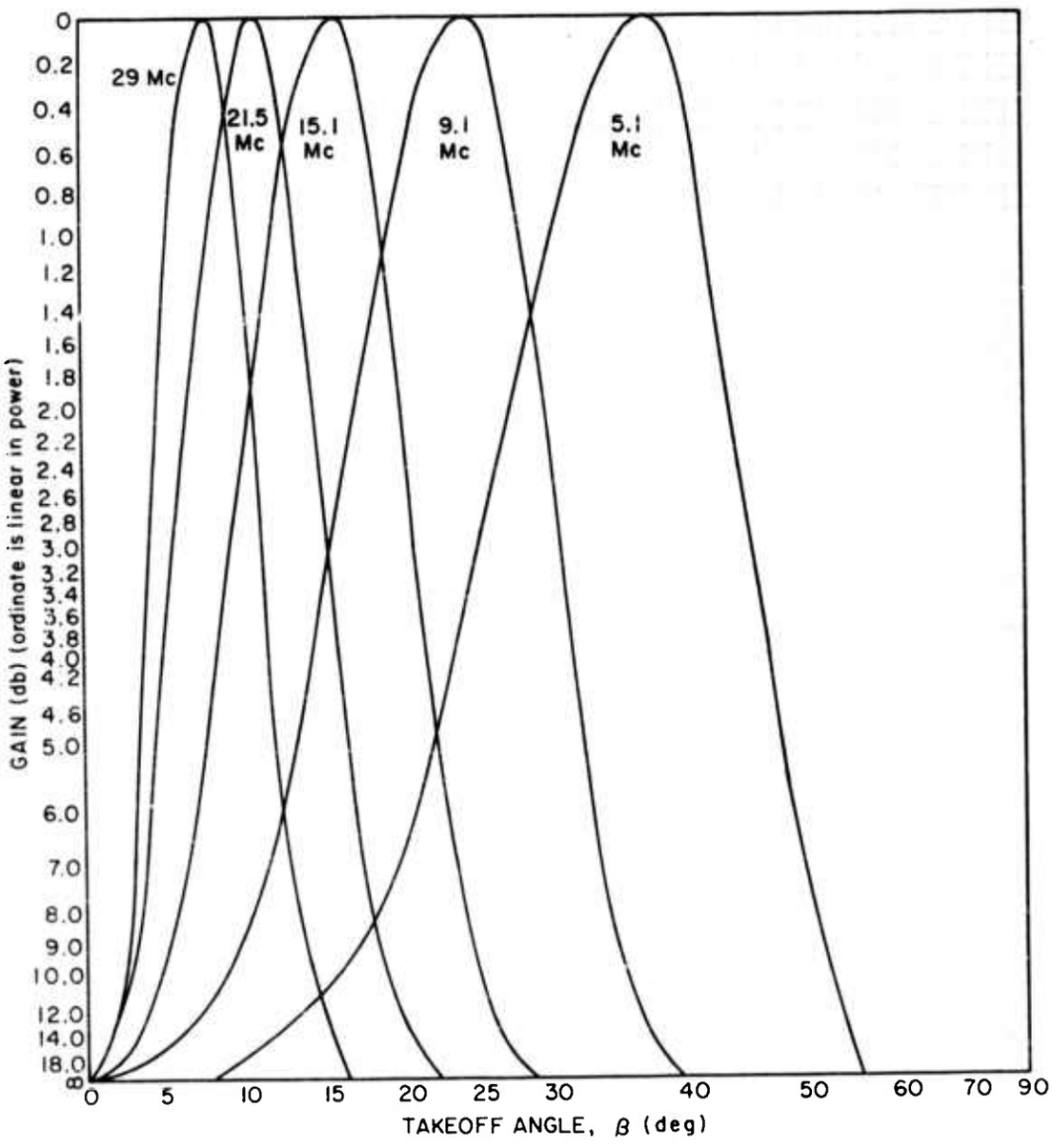

FIG. 31. VARIATION OF GAIN WITH RESPECT TO ELEVATION ANGLE.

there are some data points along some of these curves which differ measurably in a few cases. When these data are used for the synthesis of backscatter, it will be shown that the gain patterns lead to a better match between synthetic and experimental backscatter records when they are corrected for the actual gain measurements acquired by Barnes' aircraft.

It is necessary to be able to interpolate between the curves given on Fig. 31 in order to arrive at a gain pattern for any frequency desired. Since almost nothing involved is linear, a graphical interpolation technique is used, as shown on Fig. 32. If one visualizes a three-dimensional array of gain functions, with the absolute value of gain being displayed normal to the plane of the paper, then the various curves on this chart represent the intersections of the gain surface with a series of ten planes which are equally spaced in amplitude between zero and maximum gain. Notice that maximum gain is normalized to be 1.0, since the gain function $g(\beta)$ can have any amplitude so long as it has the correct shape. It is thus possible to select any frequency and to read from this chart a series of 21 points along the curve of $g(\beta)$.

Next a series of measurements was conducted to determine the shape of the transmitted pulse and also to determine the shape of this pulse after it is received and detected. To this end, three measurements were made, as shown on Fig. 33. The top part shows a direct measurement of the transmitted pulse which was obtained simply by holding an oscilloscope probe in the vicinity of the antenna lead wires. The vertical axis is thus uncalibrated, but the relative proportions are correct. It can be seen that the transmitted power level decreased during the half-millisecond pulse. This situation will be corrected, but it was occurring at the time when the calibrated record of 20 October was made. Careful measurements show that the transmitted power level actually decreased 17 percent from the leading to the trailing edge of the pulse.

The second picture on Fig. 33 shows the received pulse which was acquired by removing the receiver and detector about 5 miles to a partially shielded site located in rolling terrain. It is seen that the pulse shape deteriorates even further after it is received by this method. The third picture on Fig. 33 shows the received pulse displayed after detection by the same logarithmic-response detector which was used for the measurement of the backscatter. Careful measurements show an extremely close agreement between the linear and logarithmic records of the received pulse shown here. As a consequence of these measurements, the pulse shape is represented in the computer by a series of numbers between 0 and 1 which

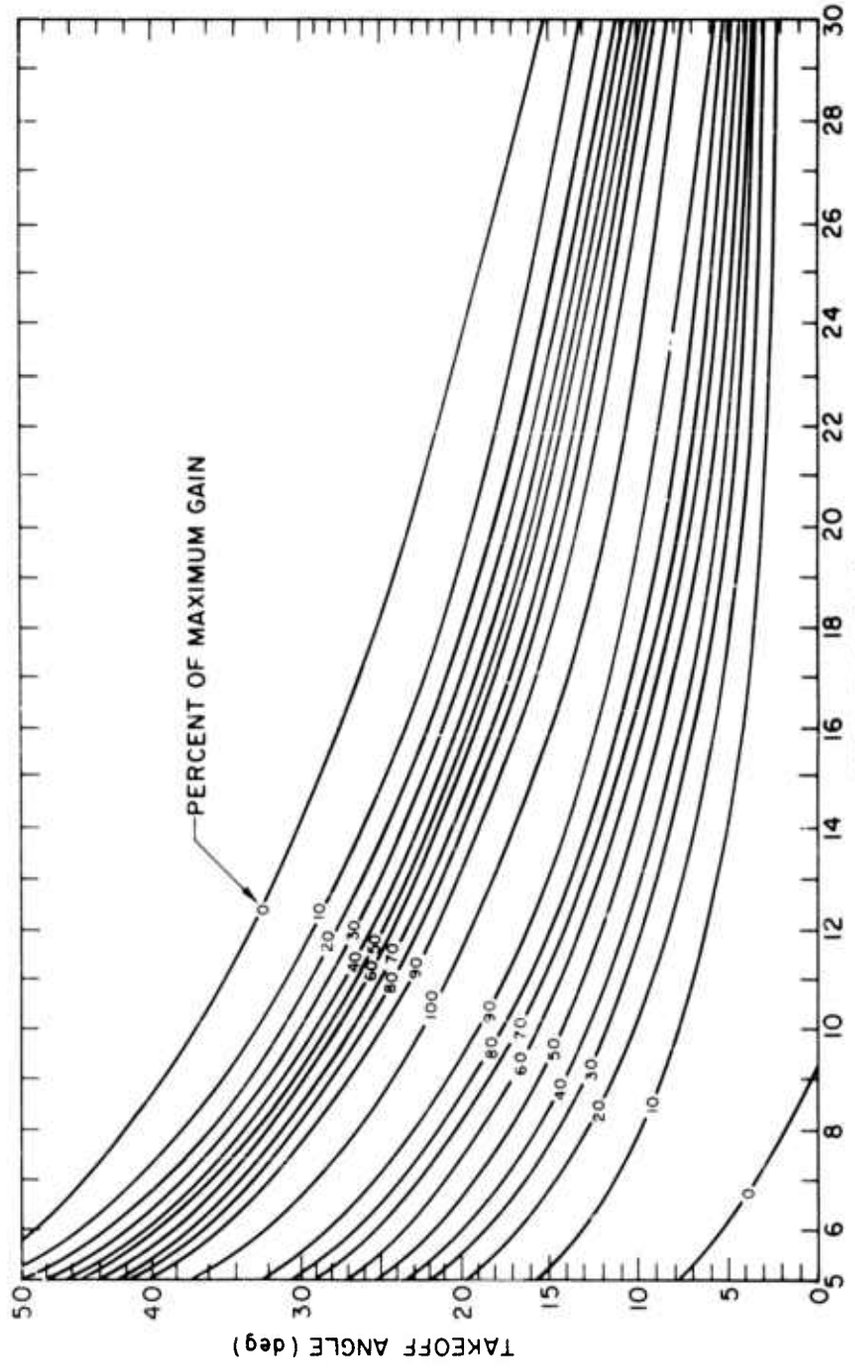

FIG. 32. CHART USED FOR DETERMINATION OF GAIN AT ALL FREQUENCIES.

32692

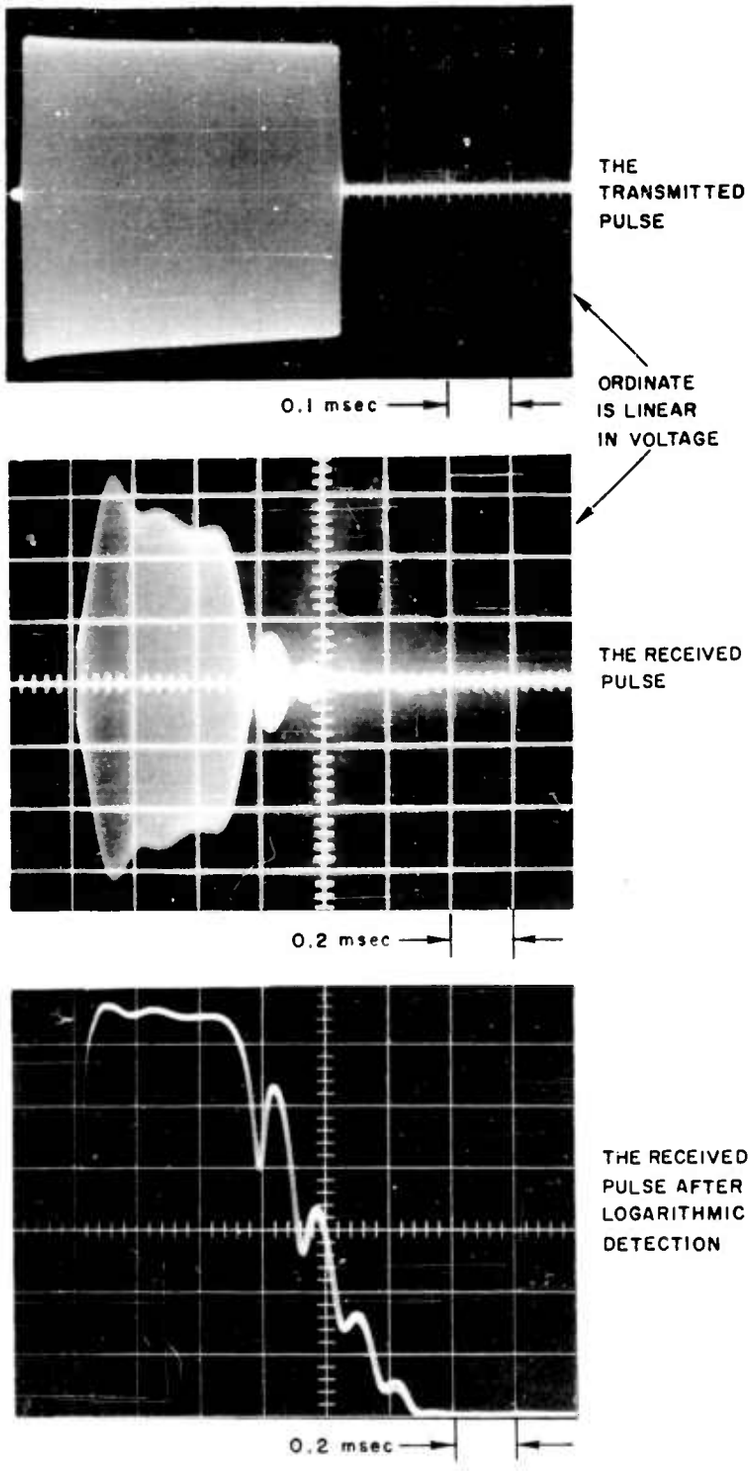

FIG. 33. MEASUREMENTS OF THE TRANSMITTED, RECEIVED, AND DETECTED PULSE SHAPE.

simulate the shape. They have been determined to be the following: 0.177, 1.000, 0.762, 0.691, 0.623, 0.177, 0.036, 0.001. When synthetic backscatter is shown later in this chapter, the reader will be able to see a plot of this synthetic pulse shape and compare it to the bottom picture on Fig. 33.

The receiver passband is 3 kc wide. Since the sweep rate is approximately 3 kc per 100 msec, it can be seen that detuning is negligible for the under-30-msec time delays of one-hop backscatter. The A records were generated at fixed frequencies, so no detuning was involved.

The exact shape of the frequency scale on the figures is a function of the tuning scale on an SP-600 receiver. The sweep is accomplished by turning the receiver knob at a constant angular rate through the 7-15 and 15-30 Mc bands of the receiver. Within these bands, the frequency variation is neither linear nor logarithmic, but is actually somewhere in between. At the junction of the bands, a series of switchings is accomplished manually while the strip-film camera is off, and the junction is not generally noticeable on the records. However, on Fig. 27, the junction can clearly be seen at 14.5 Mc because an automatic camera switch had not yet been installed; also the gain changed considerably during the band switch. Figure 34 shows the variation of frequency as a function of time during the sweep. Since the strip-film camera moves at a constant rate, the horizontal axis may be interpreted as a direct indication of the horizontal axis on the backscatter records. The plotted points in the figure show the variation of the radar, and the straight line through these points shows what the ideal track would be if the frequency sweep were logarithmic. It can be seen that this radar is nearly logarithmic, and for most purposes in this study the straight line is used as a substitute for the measured values. This leads at most to an error of perhaps 1/3 Mc, and even this small error can be taken out through the use of the calibration marks on the films. However, the reader will see that great advantages follow from the use of a logarithmic scale because it enables the use of transparent overlays which can be slid along the horizontal axis to accomplish what is, in effect, a multiplication of plasma frequency. This will become clear later.

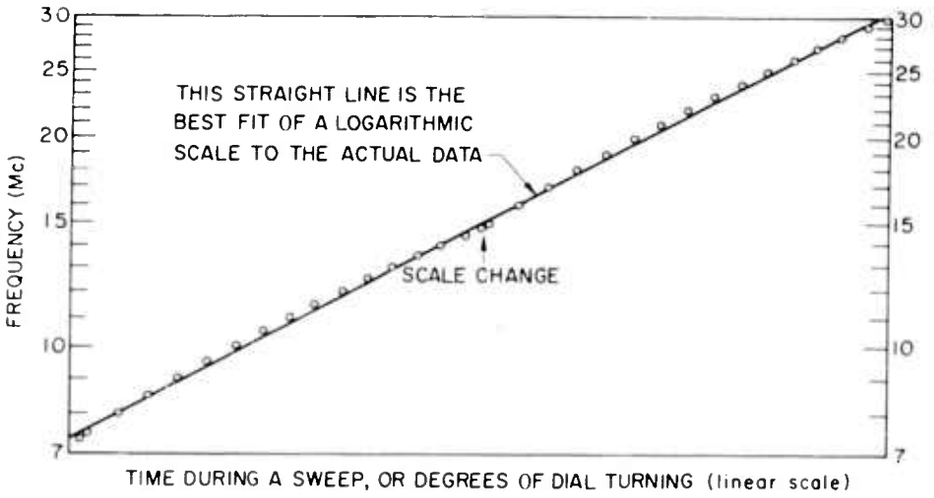

FIG. 34. SCALE COMPRESSION FACTOR OF THE CALIBRATED RADAR.

B. EXPERIMENTAL CONDITIONS FOR THE 20 OCTOBER RUN

Figure 35 is an equidistant azimuthal projection centered on San Francisco. Consequently, all straight lines through the origin are great circles, and all distances measured from San Francisco are great-circle distances. The concentric rings drawn around San Francisco define ground ranges of 1000, 2000, 3000, and 4000 km. Since backscatter time delay is approximately 6.7 msec per 1000 km, it can be seen that the backscatter on Fig. 27 came from ranges not exceeding 4000 km, approximately. The antenna azimuth is 122 deg true, as shown on the figure. Also shown are the subsolar points at various times of day. These are computed from data given in Ref. 51, where the declination of the sun is given as slightly more than 10 deg south. The subsolar point had recently crossed the west coast of Peru at the time of the calibrated radar record. Since the antenna was looking almost directly toward the sun, the electron density along the path probably increased with radar range. Similarly, the absorption should increase with range away from the radar. Throughout the path, as time increases, the sun approaches nearer the radar and consequently the electron density and absorption will be expected to increase along the entire length of the path during the progress of this particular experiment. The A-scope records which

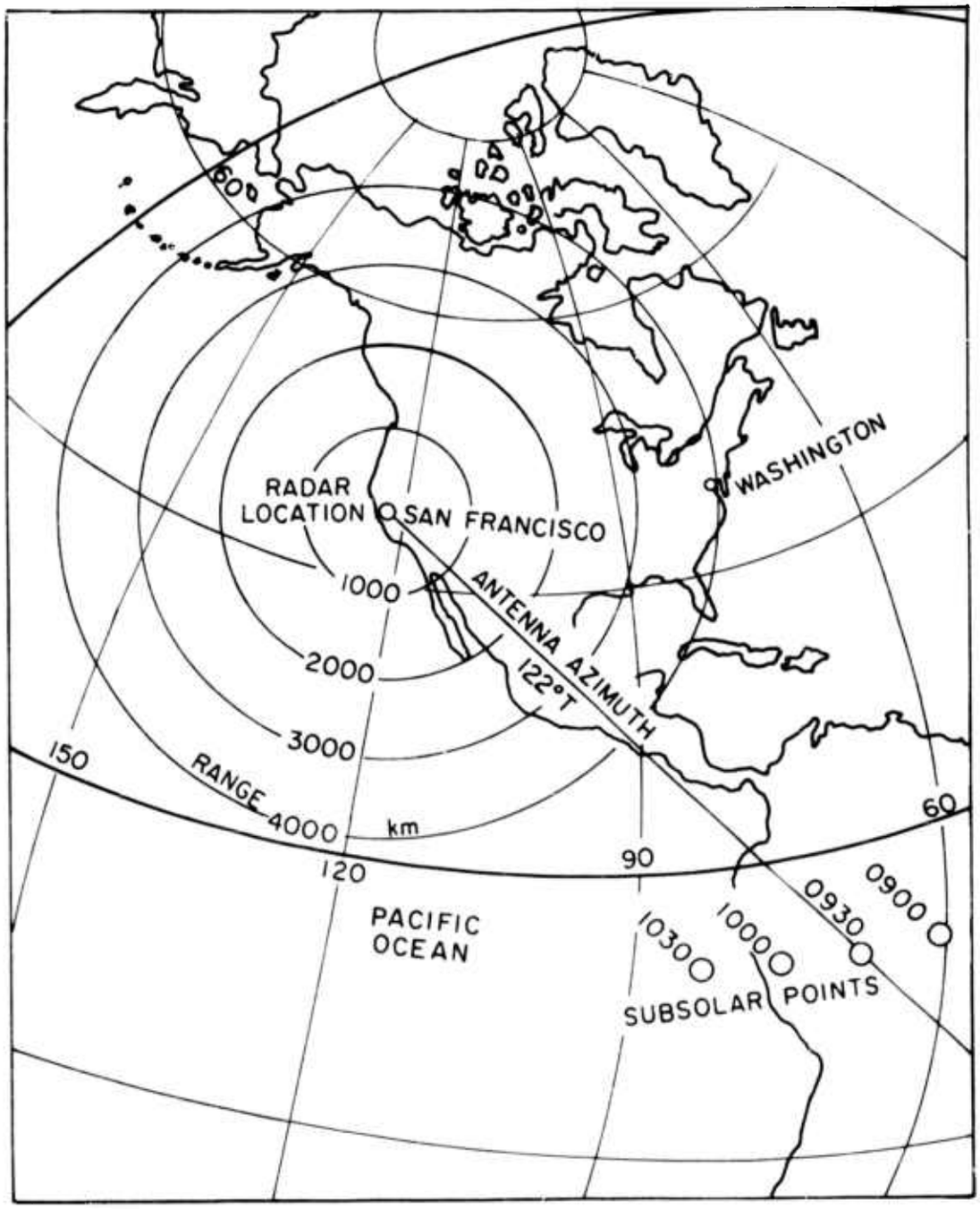

FIG. 35. MAP OF THE AMERICAS SHOWING RADAR CONDITIONS ON 20 OCTOBER. (Subsolar points reflect various times of the morning.)

were taken earlier than the Z-scope record should reflect fewer electrons and less absorption.

The timing of the various events is given on Fig. 36. As shown, two other Z-scope records were obtained prior to the one shown on Fig. 27. These are shown on Fig. 37; both were obtained prior to the final adjustments on the radar, and consequently they have a flattened shape due to a different camera film speed. They will be useful here in the interpretation of the A-scope records given on Fig. 28.

Also shown on Fig. 36 are the times at which a large number of vertical-incidence ionosonde sweeps were obtained by a C-2 sounder operated by the Stanford Research Institute. This sounder is located near the calibrated radar, and consequently its measurements can be used to determine the state of the ionosphere over the radar. A sequence of ten sweeps was obtained during the experiment. These traces have been

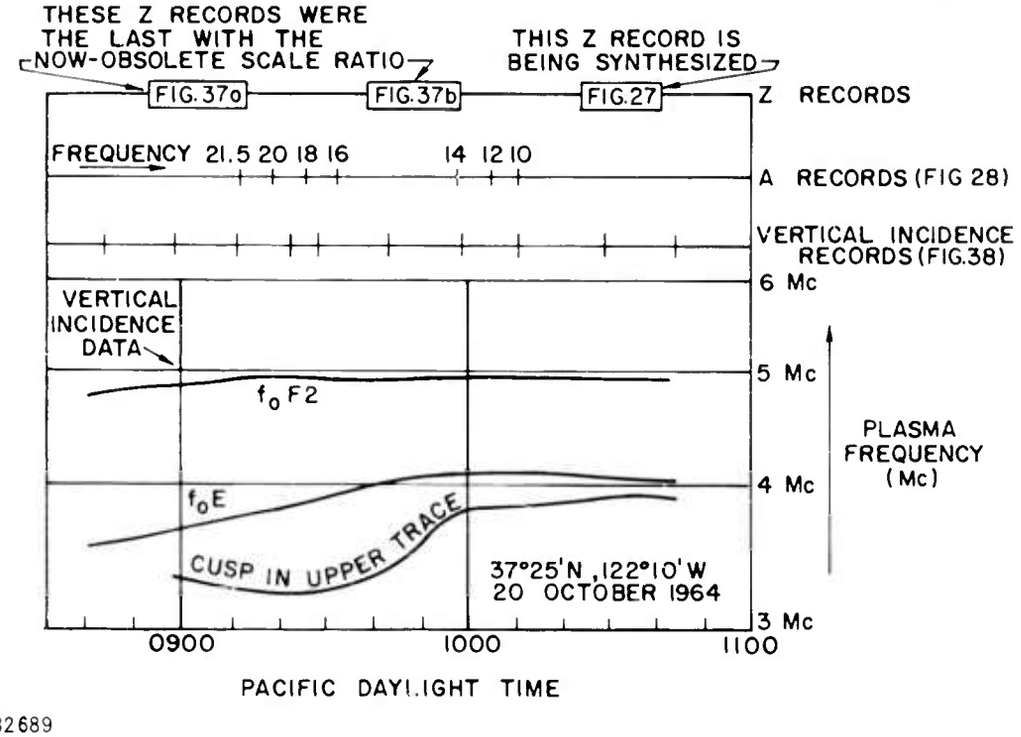

FIG. 36. TIMING OF EVENTS ON 20 OCTOBER.

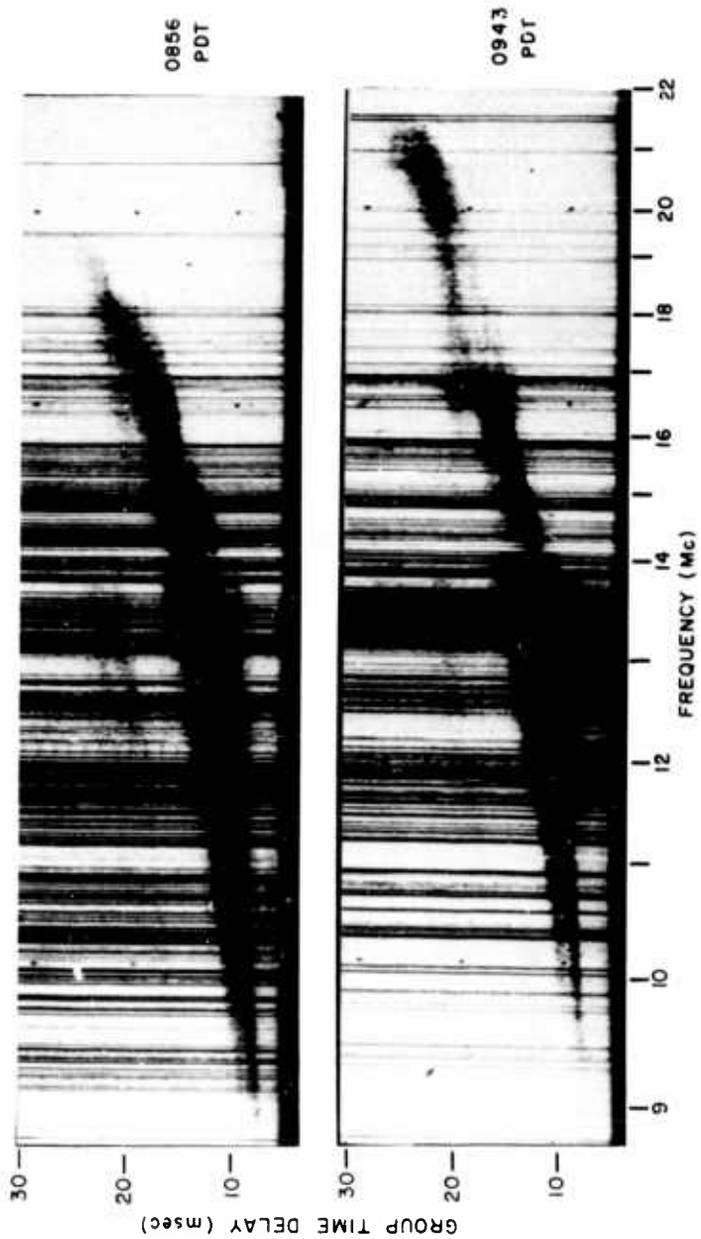

FIG. 37. OTHER SWEEP-FREQUENCY RECORDS WHICH PRECEDED FIG. 27.

copied directly from the experimental films by the author, and they are presented on Fig. 38. A number of interesting changes can be seen, but in particular notice the fortunate circumstance that the vertical-incidence critical frequency remains relatively stable over an hour-and-a-half period at a value near 5 Mc. This stability proves useful in the synthesis of the ionosphere as it varies along the path. Lower layers were present, and it appears that they increased in density during the advance of the morning hours. Three of the most interesting frequencies were transferred to Fig. 36 which shows the time variation in the vertical-incidence critical frequency, the cusp in the upper trace, and the E layer.

The staff of the Stanford Research Institute has reduced by computer techniques, the ionogram for 0859 PDT, and the results of their calculations are given on Fig. 39. This reduction indicates the presence of a main layer of critical frequency of 5 Mc at an altitude near 250 km. Also, there appear to be hints of layers at 120 and 160 km with critical frequencies of approximately 2.8 and 3.4 Mc. The ionogram itself is shown in Fig. 40, and it can be seen that the traces are not sufficiently complete to be unambiguously interpreted. Consequently, the layer structure given in Fig. 39 can only be considered as a good estimate of the state of the upper atmosphere.

Since the experimental record was obtained at a time when the radar antenna was directed toward the subsolar point, there was a considerable range dependence of the sun's zenith angle, χ. In Sec. IIC it was explained how absorption is accounted for with a function $E(R)$ whose magnitude and shape are determined by the selection of the four parameters in the equation

$$E(R) = E_{\alpha}\left(1 + e_1 R + e_2 R^2 + e_3 R^3\right)$$

with power loss represented by the factors of the form

$$e^{\alpha} = \exp\left[-\frac{E(R)\ \csc\ \zeta}{F^2}\right]$$

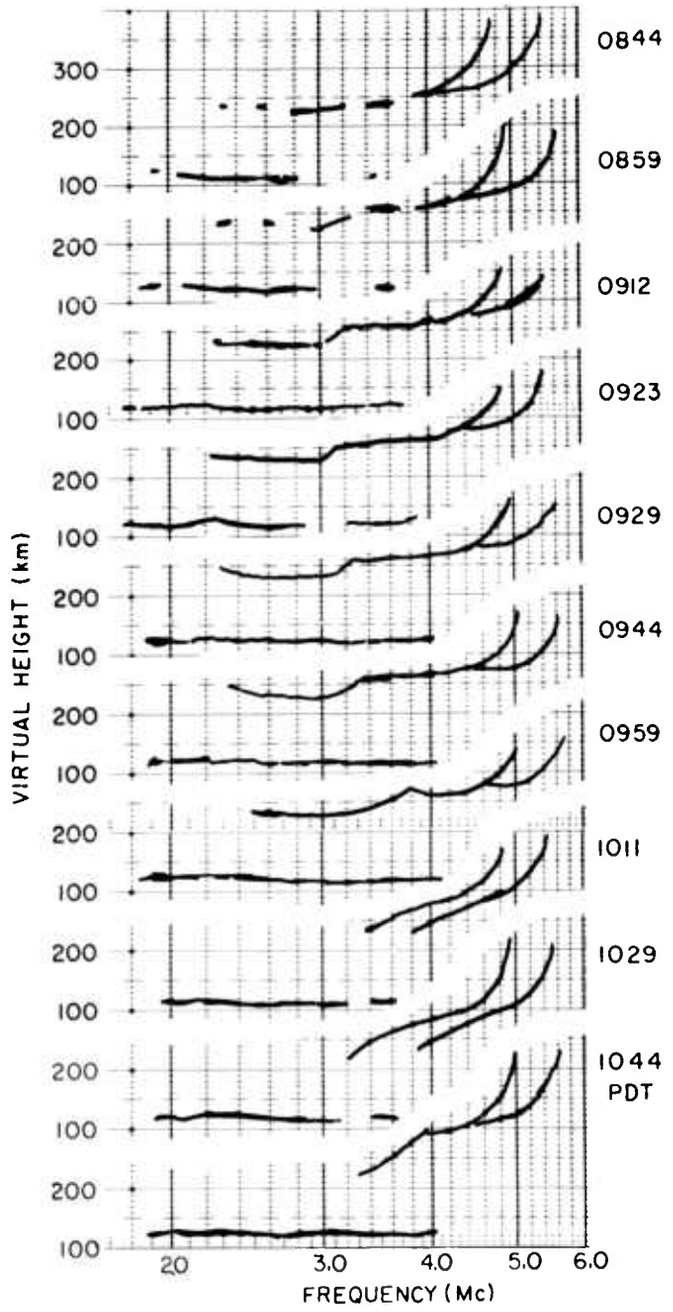

FIG. 38. VERTICAL-INCIDENCE TRACES OBTAINED DURING THE MORNING OF 20 OCTOBER.

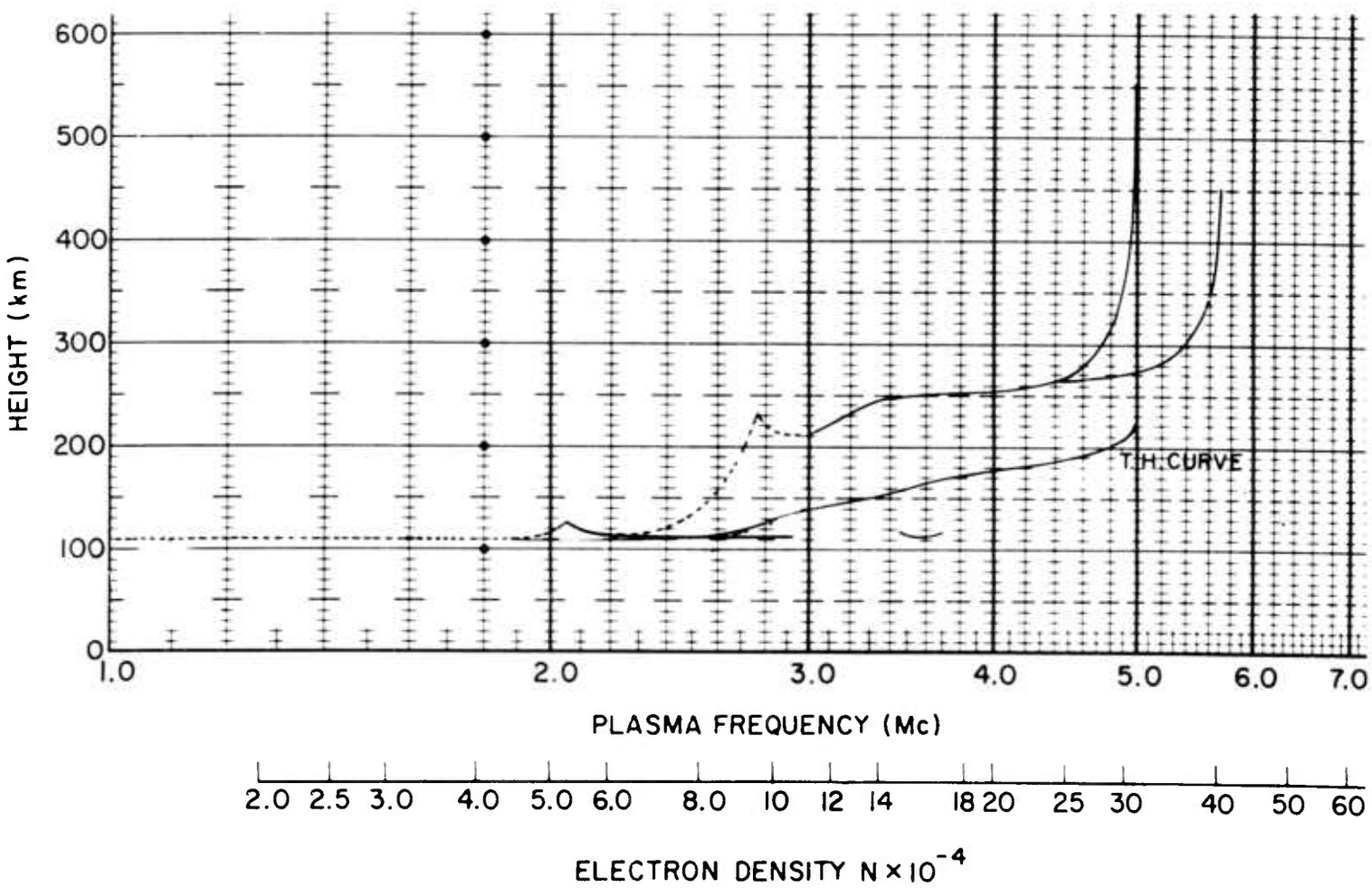

FIG. 39. THE 0859 IONOGRAM REDUCED TO INDICATE TRUE HEIGHTS.

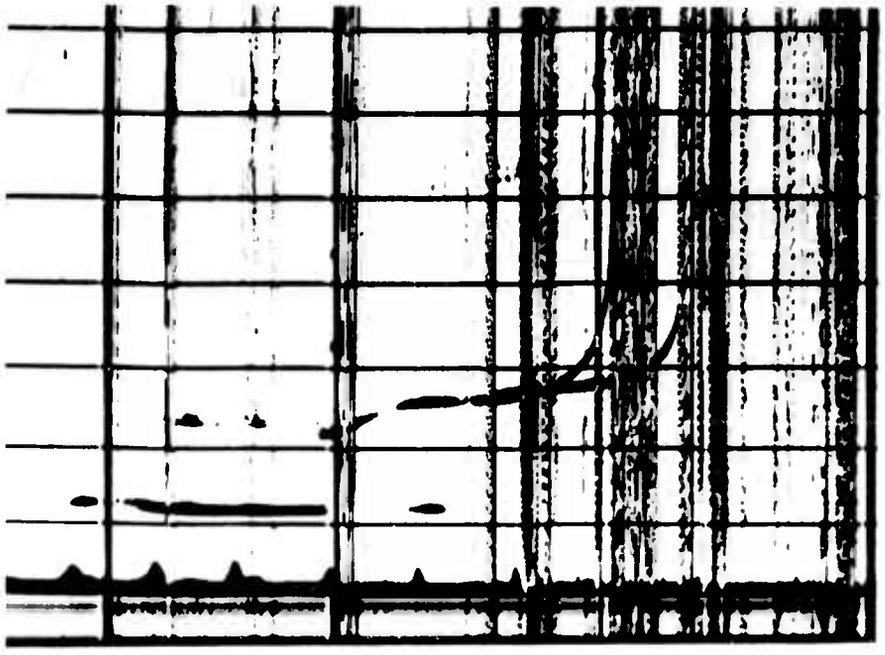

FIG. 40. PHOTOGRAPH OF THE TRACE USED IN FIG. 39.

The magnitude of the numbers which can be inserted in these equations can be obtained from a comprehensive study of skywave field intensities published by Laitinen and Haydon in Ref. 52. There, analysis of a great deal of experimental data led to the conclusion that absorption could be simulated by a function of two variables: the solar zenith angle χ and the Zurich sunspot number S. In Ref. 53 it was predicted that the value of S at the time of the 20 October experiment should have been approximately 17. The accuracy of such a prediction is certainly adequate for these purposes, because the expression for E will be seen to depend only slightly on the exact value of S during these times of weak solar activity.

From Fig. 88 of Ref. 52 it is found that for S = 0, χ = 0, and F = 7 Mc, the vertical-incidence absorption is approximately 10.5 db. At vertical incidence, csc χ = 1.0, and calculation yields a value of $E = 5.93 \times 10^{7}$. This establishes the maximum value of E anywhere on the surface of the earth for S = 0. Then, use of Eq. 15 from Ref. 52 gives a value of E as follows:

$$E(\chi, S) = (5.93 \times 10^7)\ (\cos^{1.3} 0.881\chi)\ (1 + 0.0037S)$$

Inserting $S = 17$,

$$E(\chi) = 6.3 \times 10^7\ \cos^{1.3} (0.881\chi)$$

The final step is the expression of this function in terms of the variable R through use of the cubic equation which is built into the program. This task is carried out on Fig. 41 which shows two families of curves, one of which gives the zenith angle as a function of range. The families of curves are unfortunately necessary because of the long time interval during which the records were gathered on 20 October. In the ideal situation, the experimental A and Z records might all be obtained within a time span of perhaps 15 min, and in such a case it would be necessary to calculate only one function $E(R)$.

The zenith-angle curves on Fig. 41 were calculated simply by laying out the radar azimuth and the subsolar point on a globe. Measurements were then directly made of the geocentric angle between the subsolar point and points along the antenna azimuth at the desired ranges. This is a quick procedure, and yet it yields data of adequate accuracy. The values of χ (= geocentric angle) thus derived were inserted in the equation for $E(\chi)$, yielding points along the curve that defines $E(R)$. The final step was the selection of the parameters in the cubic equation. This is done as follows: the value of E_α is simply the value of $E(0)$ and thus it can be directly read off the graph. Next, a straightedge is laid over each curve of $E(R)$ so that it passes through $E(0)$ and lies along the approximate place where the user desires to have the straight-line function, $E_\alpha(1 + e_1 R)$. Using this technique, it is assumed at the outset that e_3 will be zero, so that only the second-order term will be used as a correction to the straight line. It is then possible to lay the straightedge in such a position that some multiple of R^2 will provide a good final correction. The selected multiplier is then e_2, and the value of e_1 is found from the slope of the straight line.

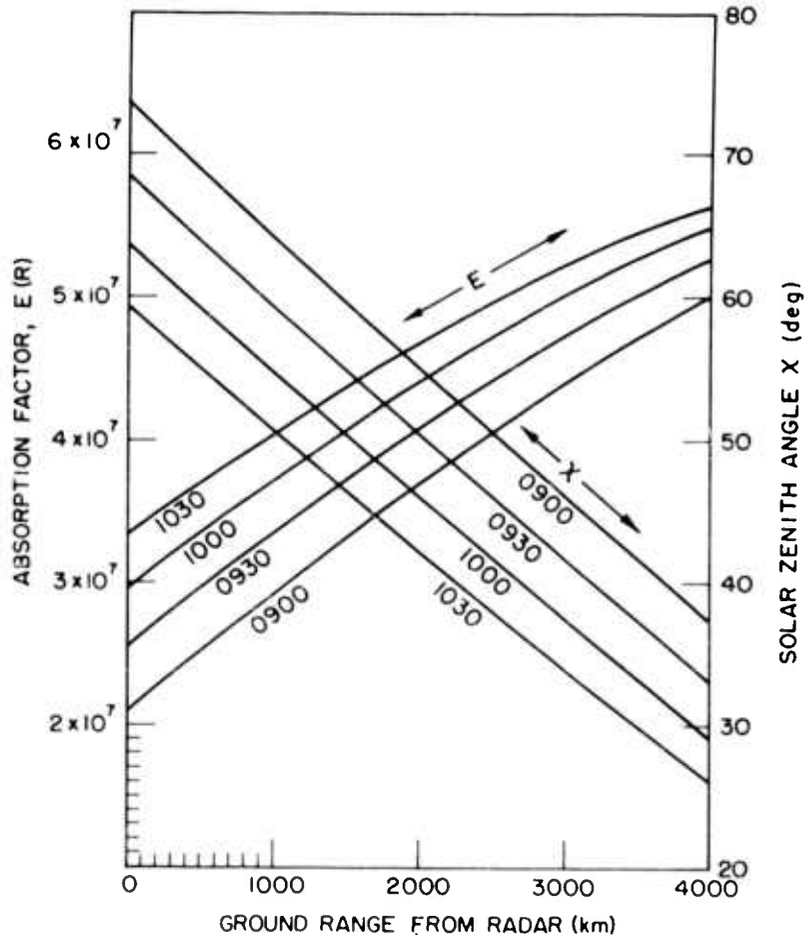

32697

FIG. 41. GRAPHICAL DERIVATION OF THE CUBIC EXPRESSION FOR ABSORPTION.

Using this technique, the constants were selected, and they are given in Table 2.

In order to show the quality of the simulation, Fig. 42 shows E(R) calculated from the values given in Table 2, and it should be compared to Fig. 41. In this regard, note that very little of the energy involved in the calculation of backscatter will undergo absorption at ranges in excess of 3000 km, so a slight mismatch at the upper ranges is tolerable.

TABLE 2. CONSTANTS SELECTED FOR SIMULATION OF ABSORPTION VARIATION VS RANGE AND TIME OF DAY

Time of Morning (PDT)	E_0	e_1	e_2
0900	2.10×10^{7}	4.07×10^{-4}	-1.52×10^{-8}
0930	2.55×10^{7}	3.26×10^{-4}	-1.25×10^{-8}
1000	2.95×10^{7}	2.63×10^{-4}	-1.08×10^{-8}
1030	3.32×10^{7}	2.23×10^{-4}	-1.00×10^{-8}

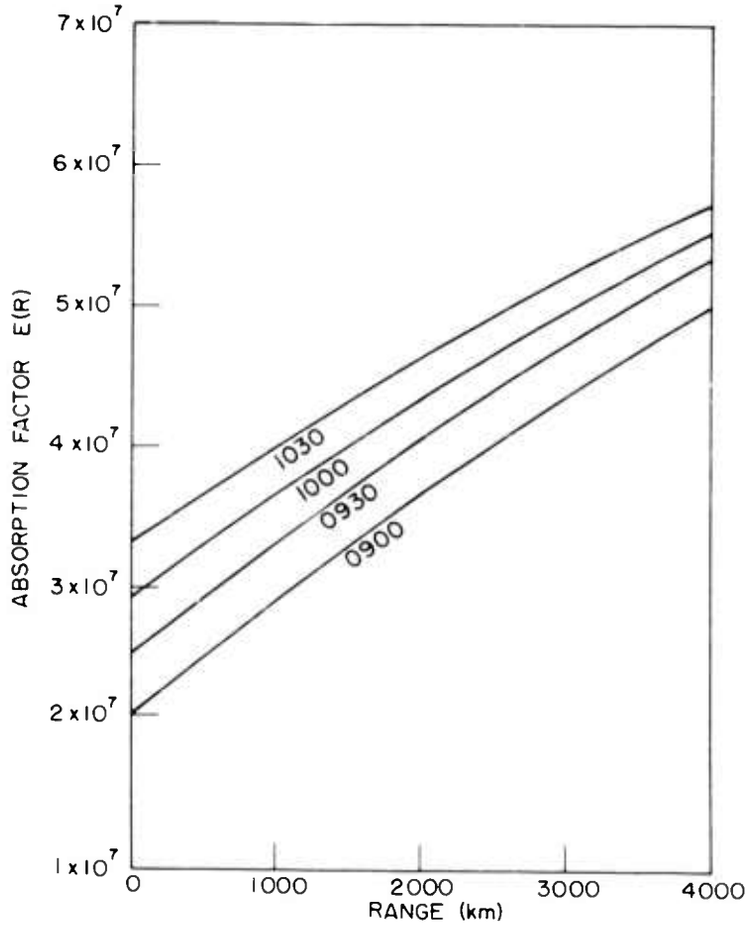

32694

FIG. 42. COMPUTER DATA FOR SIMULATION OF ABSORPTION CURVES OF FIG. 41.

C. LOGARITHMIC SLIDERS SHOWING BACKSCATTER SHAPE FOR TYPICAL ION LAYERS

A major factor in the synthesis of backscatter is the generation of a correct ionosphere so that the sweep-frequency backscatter echo will have the correct shape. The electron density will vary as a function of altitude, radial range, transverse distance, and time of day. It will probably never be possible to simulate the structure of an entire ionosphere over a backscatter path, although some success has been attained in measuring the variation of the ionosphere as a function of height and radial range through the use of a series of spaced sounders along a great circle [Ref. 54].

One of the best ways for determination of the variations in the ionosphere is through the use of sweep-frequency backscatter records such as the one being synthesized. The shape and appearance of such backscatter can yield a great deal of information about the ionosphere if it can be properly interpreted. It does appear that the use of a digital-synthesis technique will lead to a better understanding of the ways in which ionospheric variations affect backscatter so that eventually records themselves can be used for a quantitative study of upper atmospheric conditions.

In order to simulate the 20 October record, it was necessary to generate a large number of synthetic backscatter records with various ionospheres in order to determine the nature of the horizontal gradients and the vertical layer structures which were present. The first requirement was a quantitative guide to the shape of the leading edge of backscatter which results when the ionosphere is composed of a single Chapman layer without horizontal gradients. In order to determine this shape, 24 Chapman layers with various heights and thicknesses were synthesized, and rays were calculated through them at a large number of frequencies. A subsequent computer program operated on the raysets to determine the frequency variation of the minimum group time delay for any given ionosphere. Each set of such data yields a curve which is one of the most important characteristic parameters for the particular ionosphere. The 24 resulting curves are presented on Fig. 43 which is a reduced photograph of transparent plastic overlays generated from the data.

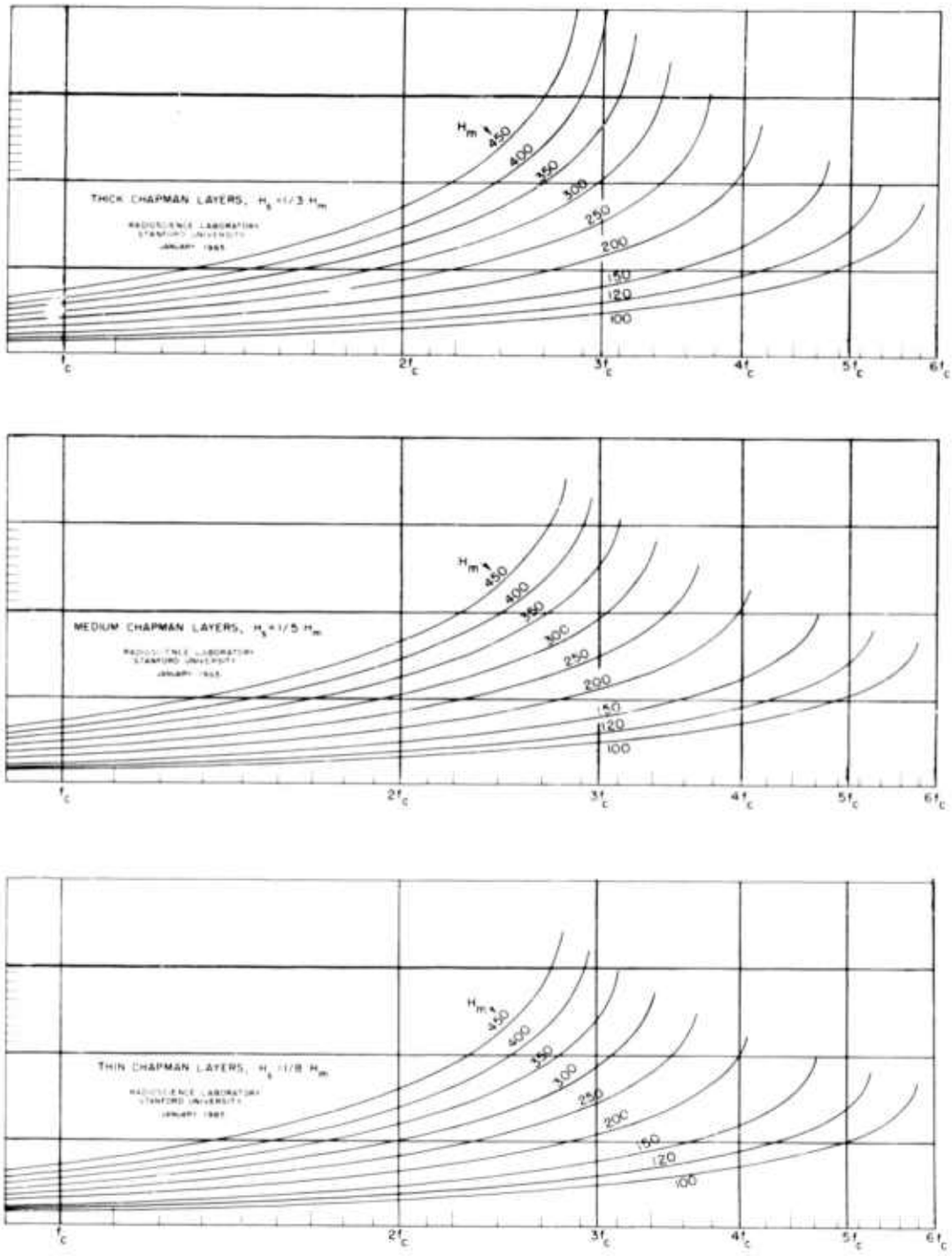

32505

FIG. 43. LOGARITHMIC SLIDERS SHOWING MINIMUM T_g VS F FOR ALL CHAPMAN IONOSPHERES.

The three overlays on Fig. 43, which are termed "sliders," contain a sufficient amount of information to completely describe the leading edge of backscatter which will result from Chapman layers of any realistic height, thickness, or critical frequency. Because of this, the sliders represent a very powerful tool for the interpretation of sweep-frequency backscatter records. They can be placed over the experimental records and slid parallel to the frequency axis in an attempt to find a match between the theoretical and experimental backscatter edges. If a vertical-incidence trace is available, as it is here, then the critical frequency f_c is a known parameter, and the slider can be placed in a specific location. This general procedure is possible only because the frequency scale is logarithmic, and it should be emphasized that such a convenient technique could not be developed without a log scale.

For calculation, Chapman layers were formulated as follows:

N = electron density, cm^{-3}

N_m = maximum electron density = 10^6 always, although it does not matter ($F_c \approx 9$ Mc)

H_m = height at which N_m occurs

H_s = scale height

$N = N_m \exp(1 - z - e^{-z})$ where $z = (\text{height} - H_m)/H_s$

Note that there are three variables: N_m, H_m, and H_s. On each slider, only one of these can be varied to generate a family of curves. On Fig. 43 it was decided to vary the parameter H_m because it has a very strong effect on the shape of the curves. For different sliders, different values can be used for another parameter. It was decided to make one slider for each value of H_s because this has only a weak effect on backscatter, as examination of the curves will show. The third variable, N_m, is taken care of without further calculation by virtue of the log scale. Notice that the index of refraction is calculated from the relation

$$n = \sqrt{1 - F_p^2/F^2}$$

so that all work is parametric in the ratio F_p/F, not in F. Also, F_p is related to N by the relation

$$F_p = \sqrt{80.6N}$$

The fortunate result is that any calculation for a Chapman layer with a particular N_m will yield results which are directly applicable for other values of N_m provided the operating frequencies are adjusted to maintain a constant value of the parameter F_p/F. (On the sliders, f is used to denote frequency.)

Usually, the ionosphere has horizontal gradients. In particular during the 20 October run when the antenna was directed toward the subsolar point, the electron density must have increased with increasing range. As an initial study to determine the effect of horizontal gradients on the shape of the slider curves, four tilted ionospheres were generated and their corresponding minimum-time-delay curves have been calculated. The results are presented on Fig. 44, together with a curve from one of the nontilted ionospheres which is most similar to the tilted examples given. For this set of figures, the layer scale height, a measure of thickness, was fixed at 100 km. Throughout the range of heights, the electron density was programmed to be a linear function of ground range, either increasing or decreasing. In the strongest tilts, the vertical-incidence critical frequency was allowed to double in a distance of 4000 km; in the weakest tilts, the critical frequency doubled in 8000 km. Rays were traced in both directions through these tilted ionospheres, so it is possible to see also the effect when the critical frequency decreases by a factor of 2 in these distances. In each case, f_c is measured over the radar.

Ideally, as a method of searching for the shape of a given ionosphere, one should have a complete set of curves such as is given on Fig. 44 for each of the 24 individual situations depicted on Fig. 43. This would require a total of 24 sliders so that the user could interpolate between the various situations. Although the work has not yet been done, it is possible to use the tilted slider curves of Fig. 44 as a guide for the

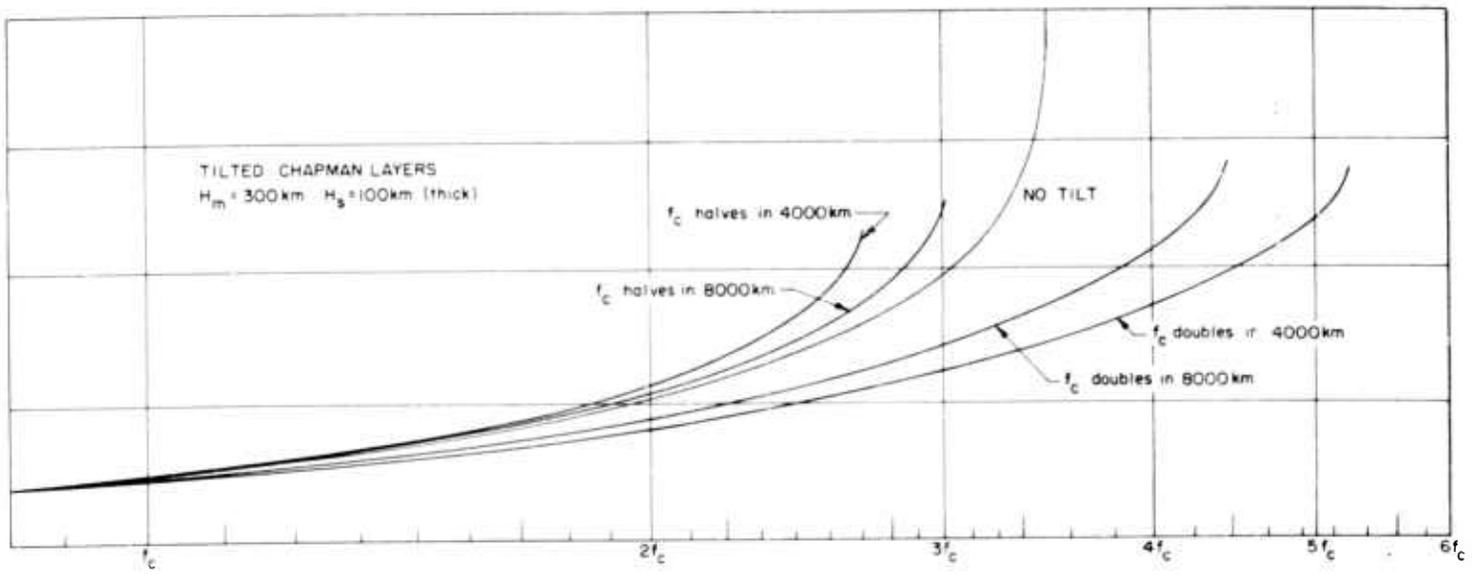

32532

FIG. 44. THE EFFECT OF IONOSPHERIC TILTS ON THE T_g VS F SLIDER CURVES.

interpretation of the nontilted curves so that one can guess fairly closely the nature of the ionosphere from an observation of the shape of the experimental minimum-T_g curve. This procedure was used for the synthesis which follows, and it will be illustrated by a sequence of studies wherein the author has estimated the shape of the ionosphere, synthesized and raytraced through it, and then produced the corresponding slider to see if further corrections are needed to match the shape of the 20 October experimental curve. It will be seen that an extremely close match is obtained in only two iterations by this method.

D. MATCHING THE LEADING EDGE OF THE 20 OCTOBER BACKSCATTER

The first step in matching an ionosphere to the experimental record consisted of a comparison between the shape of the leading edge of the backscatter and the shape of the various curves on the transparent sliders when f_c was set on the 5-Mc mark. As an initial step, it was decided to try to match the shape of the backscatter by a linear variation of electron density vs range at every height within the layer. Study of the curves indicated that the ionosphere contained a layer which was somewhat like one of those described in Table 3.

TABLE 3. FIRST ESTIMATE OF ION-LAYER PARAMETERS FOR 20 OCTOBER

Ionosphere Identification Number (IID)	N_m	H_m	H_s	Critical-Frequency Doubles (km)
789	3.1×10^5	250	83.3	6370
790	3.1×10^5	230	76.7	6370
791	3.1×10^5	270	90.0	6370
792	3.1×10^5	250	83.3	8000
793	3.1×10^5	230	76.7	8000

In this table the first column contains the three-digit IID which is a convenience and serves as a name for the layer during its study. Notice that all these layers have an N_m of 3.1×10^5, so that all f_c = 5 Mc. This group of ionospheres was selected to permit a comparison in the following manner. Ionospheres 789, 790, and 791 all have the common property that $H_s = 1/3\ H_m$. Thus, each ionosphere would be classed as "thick" in the terminology of Fig. 43. In other words, the first three ionospheres in Table 3 are thick ionospheres with the same amount of tilt, and the only thing that is different is the layer height. The results of ray calculations through these ionospheres are shown in Fig. 45a. The effect of the layer height can clearly be seen and, when the curves are compared to the experimental data, it is evident that the horizontal gradient is too strong.

Also shown on Fig. 45a is another curve which might be thought of as the trailing edge of the backscatter; that is, it is a group time delay of the ray which takes off at zero degrees tangent to the earth. If one considers only the lower rays, then this curve represents the longest time delay that can be generated with the particular ionosphere. However, it will be shown later that in the higher frequency portion of the curves, the upper (Pederson) rays play a major role in the structure of backscatter.

In Fig. 45b are shown the ionospheres 790 and 793. Both are thick Chapman layers at an altitude of 230 km, and they differ only in the severity of the horizontal gradient present. Figure 45c shows a similar comparison between thick layers which are 250 km high. When these overlays were compared to the experimental data, it could be seen that the layer height was slightly in excess of 250 km, and that the horizontal gradient must have had a value somewhere between the two values which were computed. Ionosphere 792 is quite close to the right answer, and consequently another iteration was tried with smaller variations in the parameters. The new ionospheres selected for trial are described in Table 4.

The results of this calculation are given in Fig. 46. In part (a) are shown the comparisons between the results for IID 797, 798, and

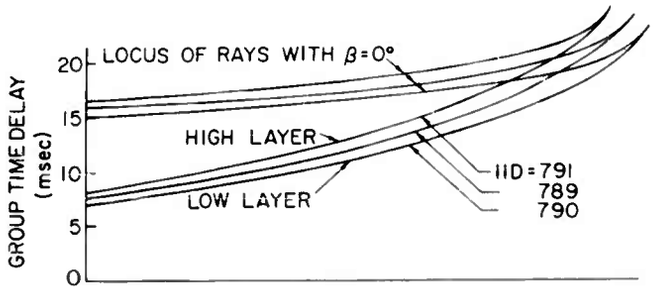

a. Thick layers at various heights

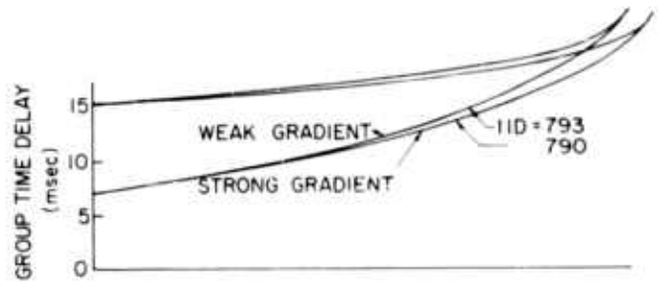

b. Layers 230 km high

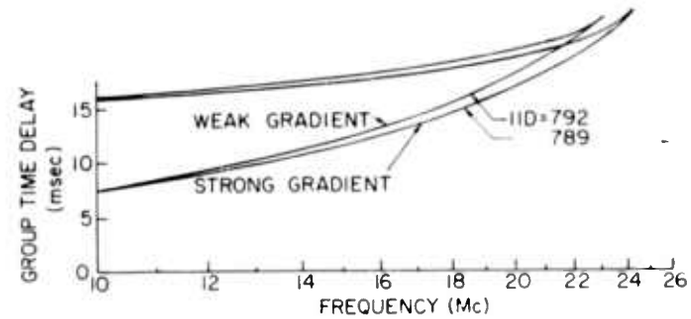

c. Layers 250 km high

FIG. 45. BACKSCATTER OUTLINE FOR TILTED IONOSPHERES OF VARYING HEIGHTS AND GRADIENTS.

TABLE 4. SECOND ESTIMATE OF LAYER PARAMETERS

IID	N_m	H_m	H_s	Distance to Double f_c
795	3.1×10^5	260	60.0	7650
796	3.1×10^5	260	40.0	7650
797	3.1×10^5	260	86.7	9560
798	3.1×10^5	260	86.7	7650
799	3.1×10^5	260	86.7	6370

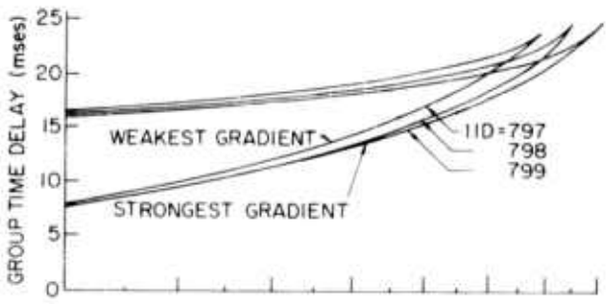

a. Thick layers 260 km high

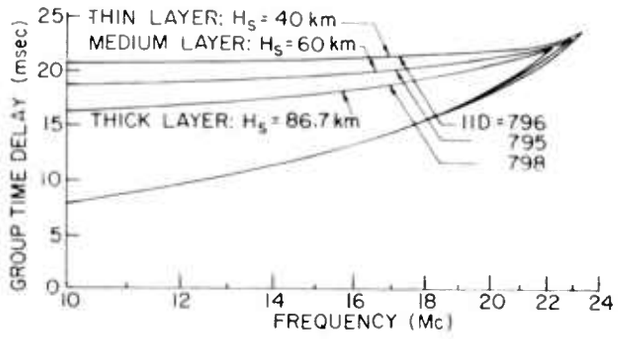

b. Layers of various thicknesses (H_s varies)

FIG. 46. BACKSCATTER OUTLINE FOR VARYING THICKNESSES AND GRADIENTS.

799 which are all thick Chapman layers. Comparison of these three curves with the experimental record shows that the center one, No. 798, has the same shape as the experimental record. However, the trailing edge of this echo does not have a sufficient time delay to permit simulation of the record because the low-takeoff-angle rays do not have a sufficiently great time delay. This effect is shown more clearly in part (b) in which all three ionospheres have the same height and horizontal gradient as the matching one, except that their thickness (H_s) varies.

It can clearly be seen that the thinner the layer, the "thicker" the backscatter. This should prove to be a very handy rule of thumb for future backscatter simulation. There is another effect which must be taken into account, and that is the presence at high frequencies of an upper-ray structure in the backscatter trace only when the layer is relatively thick. This effect is shown very clearly in the next illustration, Fig. 47. The two arrays of horizontal lines on this figure were drawn by a plotter which is associated with the IBM 7090 used for calculations. Each horizontal line on this drawing shows the group time delay and frequency of a raypath which has been computed through the ionospheres. Figure 47a shows the results for ionosphere 798, which is thick. The second part shows the exact same calculation when the ionosphere is thin, that is, H_s is 33.75 km instead of 86.7. Notice how thick the backscatter trace would be at the lower frequencies for a thin layer, while at the high frequencies the upper-ray structure gives a rounded shape to the terminus of the backscatter from a thick layer. The thin layer, on the other hand, ends in a sharply pointed structure. A comparison of these records with the experimental one shown on Fig. 27 gives a clear indication that the ionosphere was behaving like a "thick" layer at the time of the 20 October experiment.

In an effort to make the backscatter "thicker" without creating a sharply pointed structure at the high-frequency end, it was decided to insert an E layer beneath the layers shown on Fig. 47. This effort was only partly successful in accomplishing the desired effect, but it unexpectedly provided an explanation for a number of commonly encountered structures of sweep-frequency backscatter.

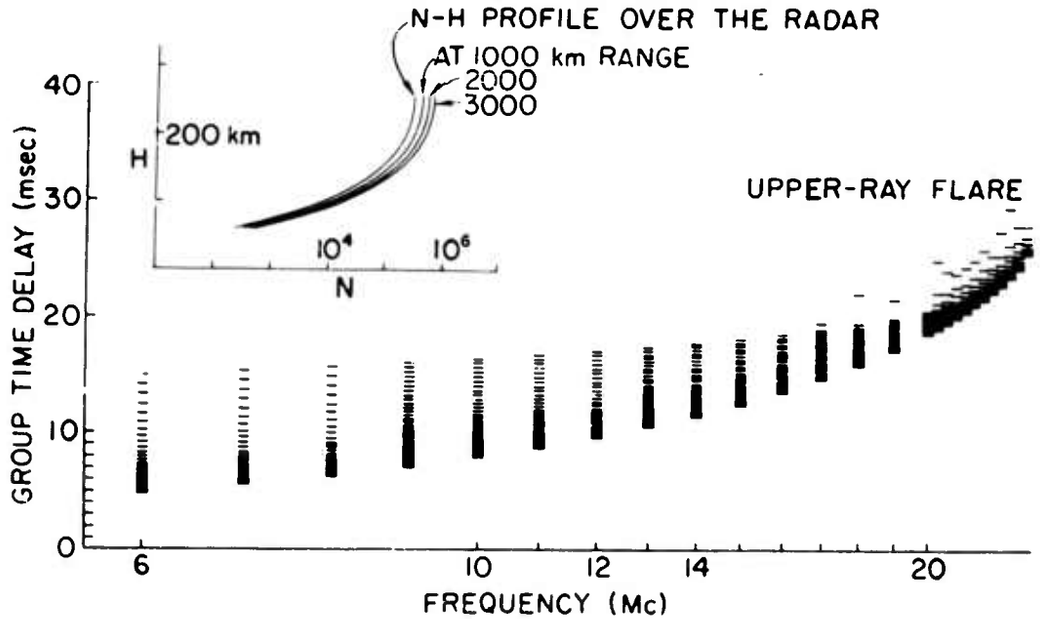

a. Thick Chapman layer

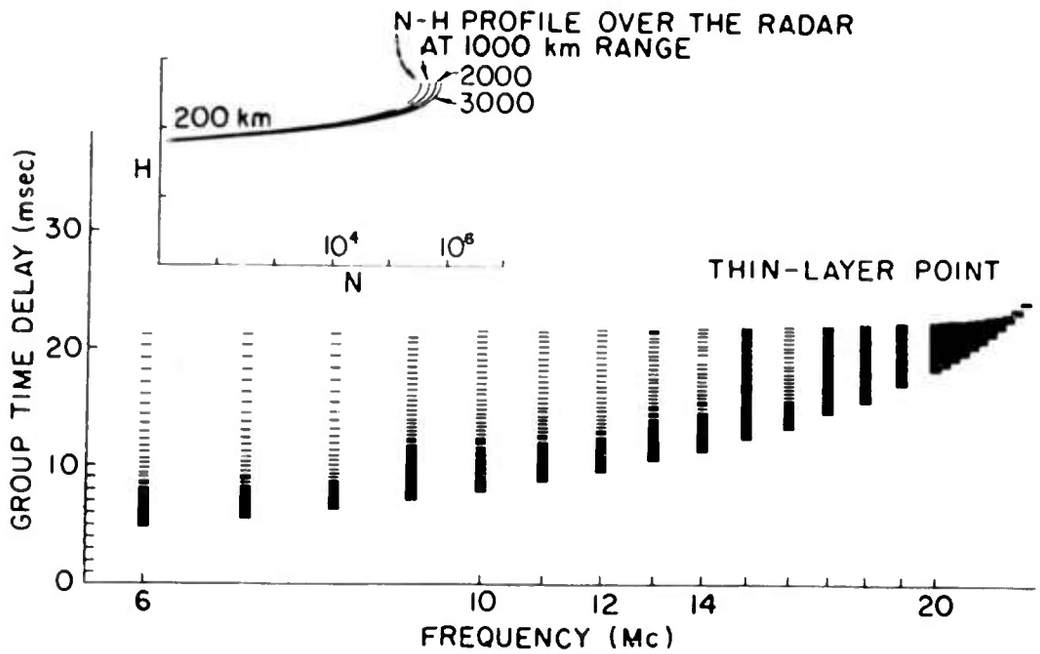

b. Thin Chapman layer

FIG. 47. COMPUTER-DRAWN PLOT OF RAYPATH TIME DELAY VS FREQUENCY.

A study of the experimental records using the slider technique of Sec. VIC indicated the possibility that there might exist an E layer with a critical frequency of 2.84 Mc at an altitude of 120 km. A medium thickness (Chapman) layer according to these specifications was then inserted underneath each of the two ionospheres shown on Fig. 47. In both cases, the E layer has a horizontal gradient of lesser intensity than the gradient in the F layer; the critical frequency doubles in a distance of 9560 km at all heights below 120 km. When this E layer was inserted under the ionosphere shown in Fig. 47a, calculations yielded the results which are shown on Fig. 48. Careful examination of part (a) of the figure reveals the leading edge of the E and F echoes as discrete curves similar to those which would be expected from the data previously given on sliders. The intersection of these two curves appears as a slight concavity on the near edge of the echo which has been labeled the "E-F inflection." The high-frequency terminus of the echo still has the rounded appearance characteristic of the F layer alone, as shown on Fig. 47a. This structure has been termed the "upper-ray flare." An unexpected result was the appearance of the feature called a "low-angle flare." Examination of the numerical data which accompanies these calculations shows that the latter feature is composed primarily of energy which propagates at extremely low takeoff angles. The peak of this flare occurs at exactly the frequency of the terminus of the E-layer backscatter. The E-F inflection point is at a slightly lower frequency.

Figure 48b is an experimental record acquired by the same calibrated radar using the same antenna at approximately the same time of day as the record which is being synthesized. The only significant difference is that this record was acquired two days after the one shown on Fig. 27. The E-F inflection is visible and the upper-ray flare is clear. The low-angle flare is faintly visible on the original record but was too weak to show in the reproduced version of Fig. 48. It was doubtlessly very weak because of the combined action of the low antenna gain and heavy absorption at low takeoff angles.

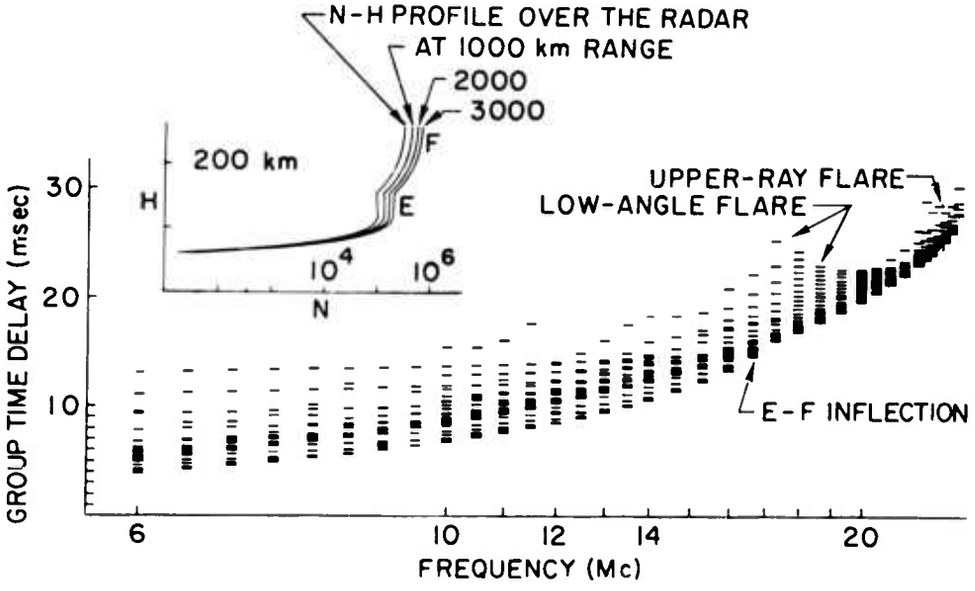

a. Computer plot

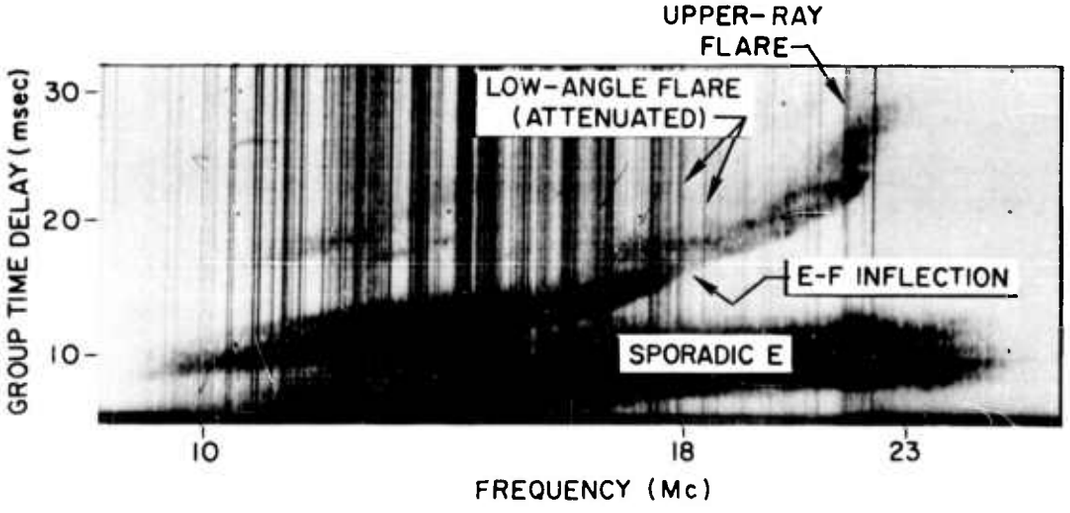

b. Experimental record: 0855, 22 October 1964; same radar and antenna as produced Fig. 27

FIG. 48. EFFECTS OF AN E LAYER AND A "THICK" F LAYER.

The broad, nearly horizontal swath across the lower side of Fig. 48b is caused by sporadic E. On Fig. 49 is shown the result of raytracing through an E_s layer and it can clearly be seen that the presence of such a low thin layer, which has a generally "patchy" structure, would account for the simultaneous presence of both the echoes seen on Fig. 48b.

When the same normal E layer as described above was inserted under the thin ionosphere shown in Fig. 47b, rayset calculations produced the result shown on Fig. 50a. Here it can be seen that the sharply pointed high-frequency terminus of the thin F layer is preserved, while at the same time the E-F inflection and the low-angle flare have appeared on the record. This combination of features produces a sweep-frequency backscatter record which seems to have an abrupt cutoff at a fixed ground range. Such backscatter records are very common and a good example was acquired 5 days prior to the 20th of October, again using the same radar and the same antenna at approximately the same time of day. This record is shown in Fig. 50b where all of the features can be seen. Again, however, the low-angle flare is almost invisible, probably because of the combination of low antenna gain and high absorption. To the author's knowledge, these commonly encountered structures have never been explained before.

E. THE FINAL STEP: MATCHING THE AMPLITUDE RECORDS

The object of this report has been the development of a method for the study of the amplitude of backscatter signals. Consequently, it is of interest to synthesize the A records of Fig. 28. The first step in such a matching process is the conversion of these data to the standardized format of Fig. 51. In part (a) of this figure are shown the estimated time histories of the average value of the backscattered signal derived from the data of Fig. 28 after all corrections have been made for measurements on the calibrated radar parameters. Great care has been exercised in the acquisition of these quantitative data; a number of the calibration instruments were even returned to their original manufacturers to permit final small corrections to the numbers given on Fig. 51. The peak amplitudes are within 3 db of similar measurements published by Shearman [Ref. 20].

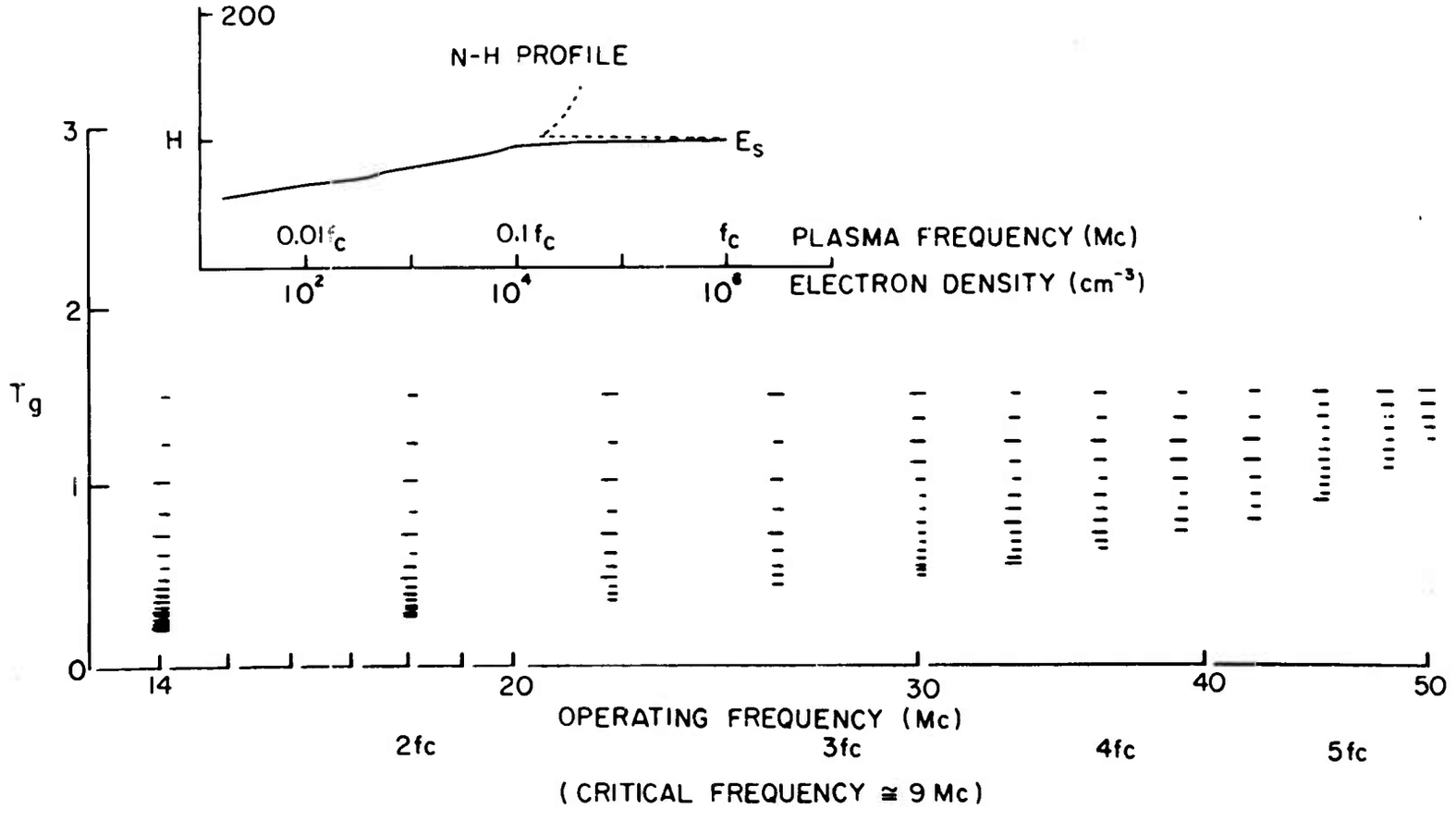

FIG. 49. THE SHAPE OF SPORADIC-E BACKSCATTER.

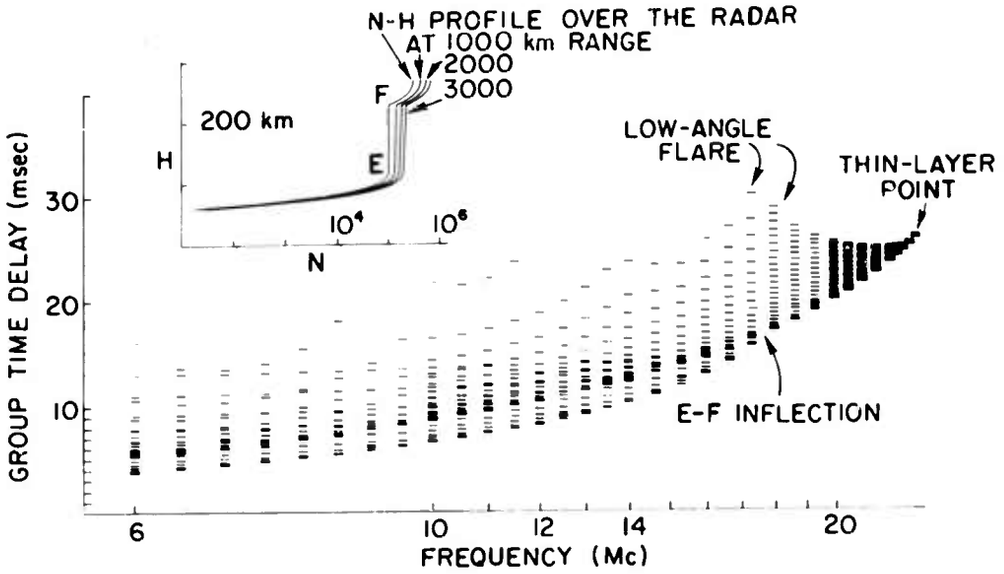

a. Computer plot

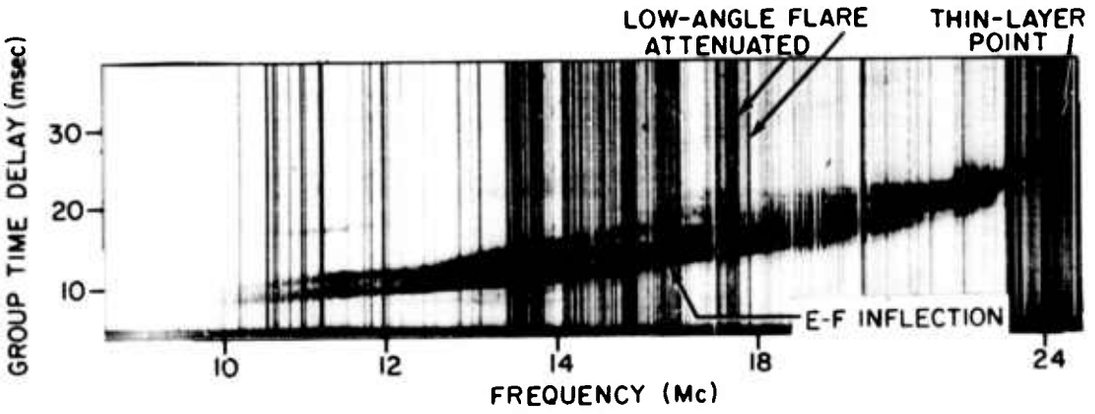

b. Experimental record: 0929, 15 October 1964; same radar and antenna as produced Fig. 27. (Note the apparent shape change due to ordinate compression.)

FIG. 50. EFFECTS OF AN E LAYER AND A "THIN" F LAYER.

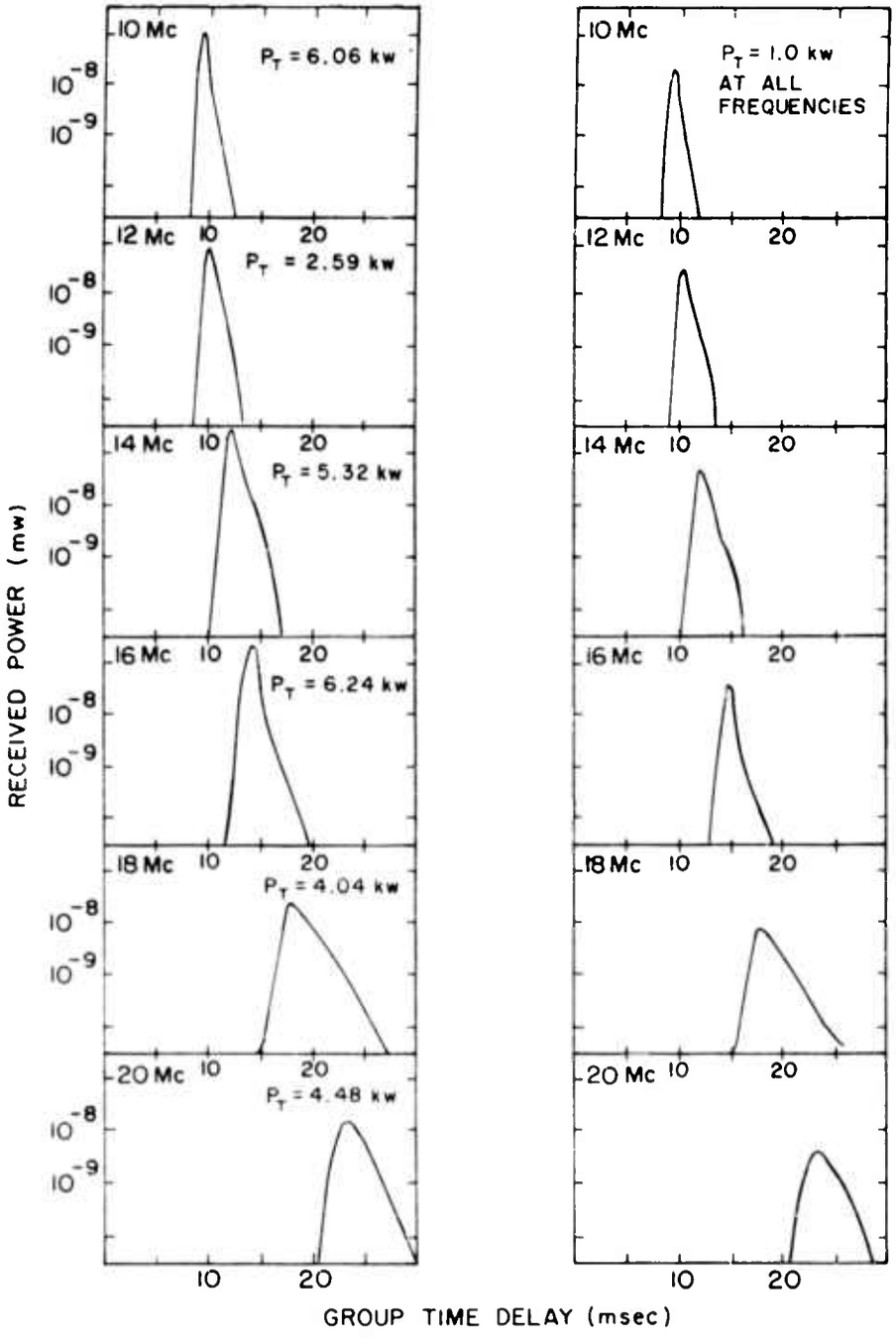

a. Experimental A records scaled from data on Fig. 28

b. The same data, but adjusted for P_T = 1 kw

FIG. 51. EXPERIMENTAL "A" RECORDS IN A STANDARDIZED FORMAT.

In part (b) of Fig. 51, the same data are presented but the vertical scale is slightly adjusted so that the effective transmitted power is 1 kw at each of the six calibrated frequencies. A seventh record was acquired, at 21.5 Mc, but it was so far removed from the other records in time that it was not possible to calibrate the group time delay. Consequently, it was not included in this analysis.

The rest of this chapter is devoted to the synthesis of backscatter records which match the amplitudes given on Fig. 51b. As a basis of calculation, the ionospheres of the preceding section will be used even though they were synthesized to match the record of 1030 PDT. Consequently, there will be small errors in the group time delays of the records which follow but these could be removed by small changes in the ionosphere and subsequent re-raytracing. However, it will be seen that the timing error inserted through the use of the same ionosphere for all A records is acceptable and the added expenses of raytracing through six new and different ionospheres would doubtless cause an insignificant change in the conclusions which follow.

Figure 52 illustrates a number of things: in the lower left corner of part (a), note the synthetic received pulse which is drawn by the computer in order to show the calculated shape of the echo from a single scatterer. It is a direct plot of the sequence of numbers which were chosen to describe the received pulse. (The absolute values plotted are not significant.) This shape is identical to the bottom picture on Fig. 33 except for the obvious compression of the horizontal scale and smoothing over 0.1-msec time intervals.

Also shown on Fig. 52a is a dotted outline showing what might be considered as the "useful portion" of the plot. Since this figure is supposed to show a synthetic version of the record which might be acquired by a real backscatter radar, there should be some noise level below which echoes cannot be received. In the computer there is no noise level but, because of the discrete integration steps used, the quality of this synthetic record deteriorates at the lower signal levels. In fact, it was through trial and error with different integration steps that the author determined which values yield good results on signals

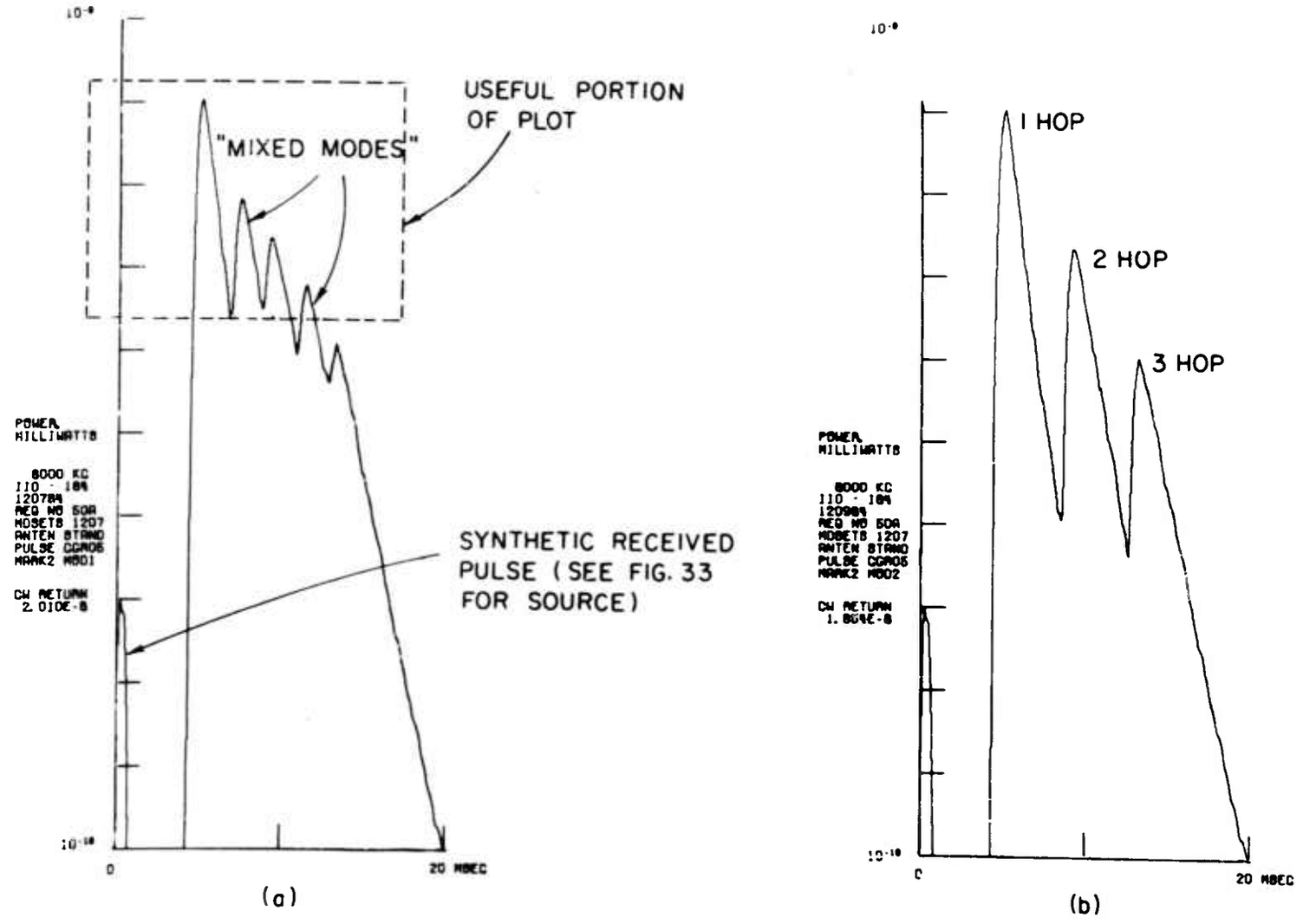

FIG. 52. FEATURES OF THE SYNTHETIC RECORDS.

strong enough to be received experimentally. It would be wasteful to use smaller integration steps since this would increase the cost without increasing the useful quality of the product. For the analysis which follows, a large number of backscatter records have been run and in each case, only the "useful portion" will be presented.

The backscatter record of Fig. 52a has been selected because it is an exceptionally good illustration of the strength of "mixed mode" echoes. These are the echoes composed of energy which travels out to the ground and then returns by a different mode. For example, the energy may go out by two hops and return by one hop. Such energy accounts for the peak in the received signal between the one- and two-hop peaks on Fig. 52a. Similarly, energy which goes out by two hops and returns by three (or vice versa) accounts for the peak which is located approximately midway between the two- and three-hop echoes on Fig. 52a.

The fact that these peaks are indeed due to energy which is propagated by mixed modes is graphically shown in part (b) of the figure where the same calculation is carried out by the synthesis program after it has been modified so that it cannot calculate mixed modes. It can thus be seen that in some circumstances the mixed-mode echoes may account for a considerable amount of the received energy. At the time of this writing, the author had not yet demonstrated the existence of such echoes on experimental records, but it is hoped that this will be possible through use of the calibrated radar.

The first attempt to match experimental A records resulted in Fig. 53 which shows a dozen calculations using the antenna patterns derived from Fig. 32. The absorption values are approximately equal to the 0900 data given in Table 2. Part (a) of the figure shows the situation when the backscatter coefficient, K, is a multiplier of $\sin^4\psi$. Part (b) of the figure shows the identical situation when the backscatter coefficient is independent of ψ. Notice that both sets of data produce spikes which are too thin (not sufficiently spread in group time delay) but which have amplitudes approximately correct. However, in Fig. 53a the multiplier of $\sin^4\psi$ had to be increased by nearly an order of magnitude for each 2-Mc increase in frequency. At 20 Mc, it reached a value of 100 which is unrealistic because values much in excess of 1

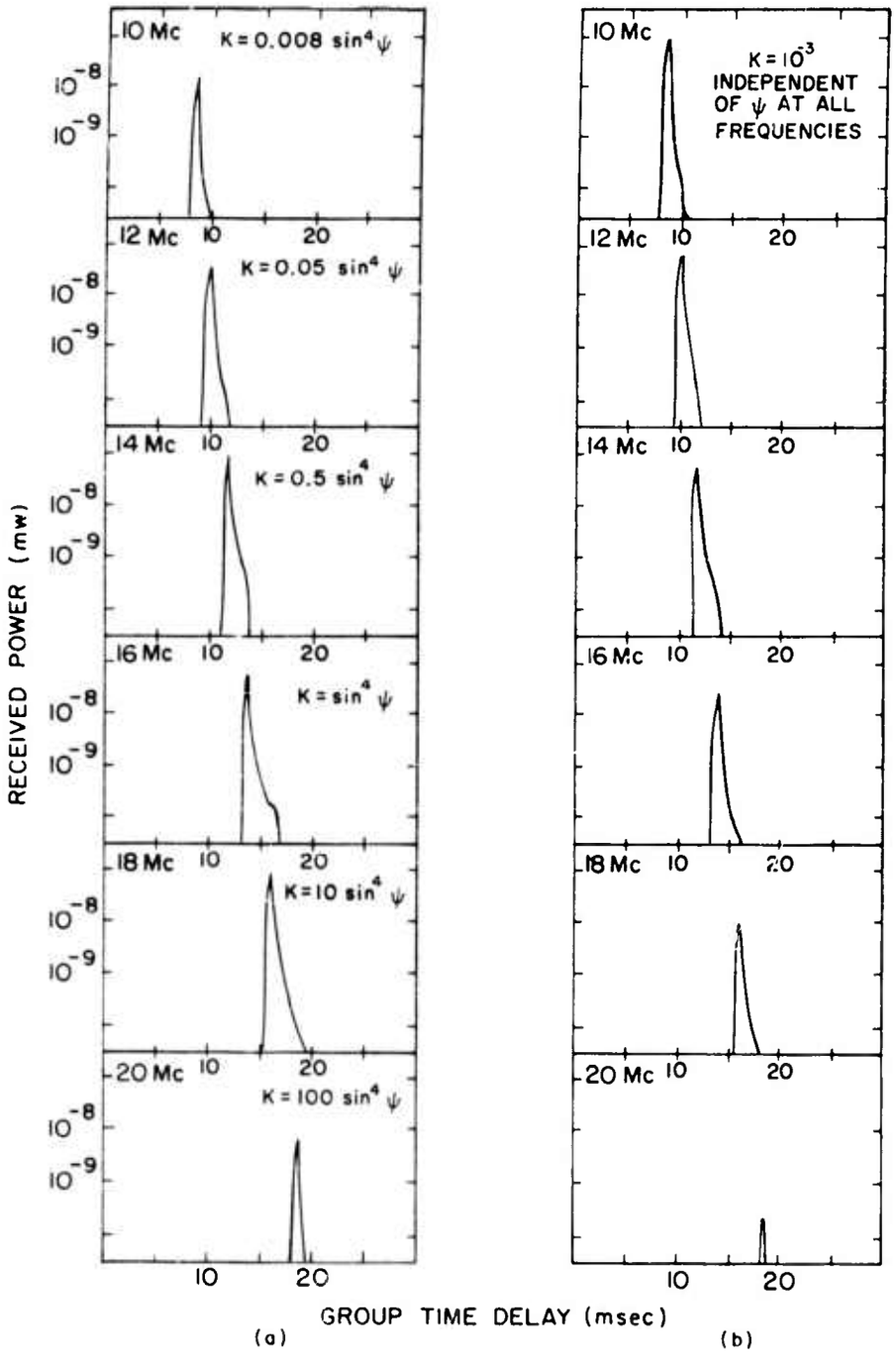

FIG. 53. FIRST ATTEMPT AT "A" RECORD SYNTHESIS.

violate the principle of conservation of energy (e.g., see the definition of $K(\psi)$ in Sec. IIB). To receive echoes that large would require a source on the ground. Not all synthetic backscatter is shown here, but a number of other calculations similar to Fig. 53a produced the same indication that the predominant source of backscatter could not be proportional to $\sin^4\psi$.

Figure 53b is an excellent match for the experimental data except for the narrowness of the spikes, as has been mentioned. Notice that the backscatter coefficient K is a function of neither frequency nor angle of incidence. It is merely a constant. Both portions of Fig. 53 were calculated using the "thick" ionosphere shown on Fig. 47a.

Figure 54 shows two more sets of calculations, each of which should be compared to Fig. 53b. Figure 54a shows the situation when the backscatter coefficient varies as $\sin^2\psi$. Here, the situation is similar to that encountered when $\sin^4\psi$ was used; that is, the multiplier of the sine function increases with frequency and gets quite large. In fact, at 20 Mc, the multiplier is almost large enough to violate the energy-conservation principle. It can be concluded that a $\sin^2\psi$ dependence of the backscattering coefficient, although not impossible, appears to be much less likely than a simple constant.

The major objection to the synthetic backscatter calculated thus far has been its insufficient spread in time delay. An examination of Fig. 47 indicates that better results would be obtained with the "thin" ionosphere of part (b). The result of this substitution is shown in Fig. 54b. Here, and in all the calculations which follow, the 10 AM absorption values are used.

It can be seen that Fig. 54b is considerably better as a match of the experimental data than were any of the previous calculations. Nevertheless, the returns are still too thin and a study of the numerical data which accompany these plots indicated that the energy along the trailing edge of the echoes was being severely attenuated by the very low antenna gain at low angles. The experimental antenna measurements were again examined and it appeared advisable to increase the assumed gain of the antenna at low angles by a small amount. Figure 55 shows the

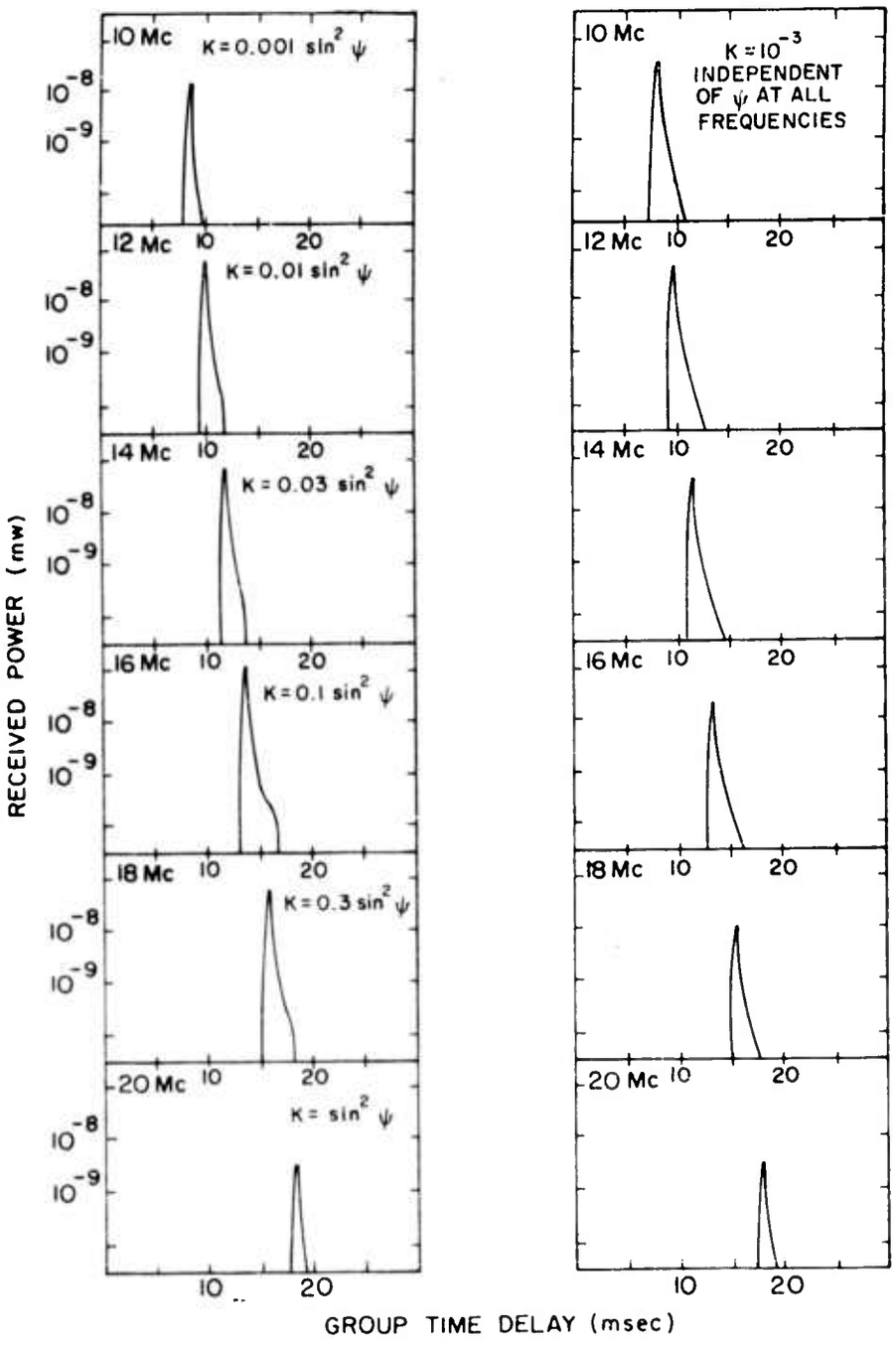

a. Thick Chapman layer

b. Thin Chapman layer

FIG. 54. SECOND ATTEMPT AT SYNTHESIS.

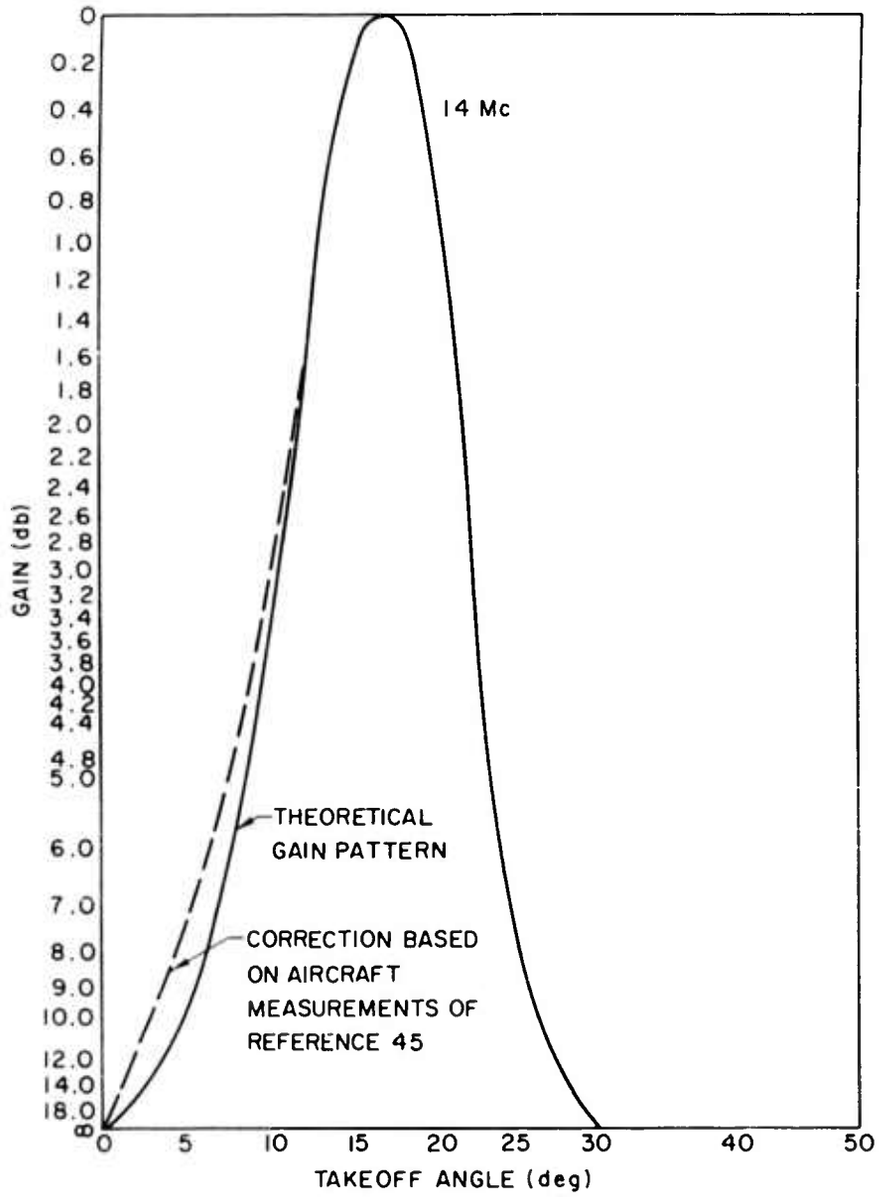

FIG. 55. SYNTHETIC ANTENNA-PATTERN CHANGE BASED ON AIRCRAFT MEASUREMENTS.

synthetic gain pattern at 14 Mc before and after this change was accomplished. At other frequencies, the situation was similar. Barnes [Ref. 45] made no measurement of the antenna at the frequencies used for this synthesis, but his measurements at nearby frequencies indicated that the gain at low angles was in many cases considerably higher than indicated by the theoretical curves which have been used until now.

Figure 56 shows the new calculations with the thin ionosphere (178) and the modified antenna patterns. Two cases are shown: a constant backscatter coefficient and a $\sin^2\psi$ backscatter coefficient. A calculation was also carried out for $\sin^4\psi$ and again the result was found to be unrealistic.

It can be seen that Fig. 56a would be a good match for the experimental record except for the presence of a very strong leading edge on the echoes. Examination of the printed data showed that all of this energy came from rays which had apogees in excess of 253 km. If the actual ionospheric electron-density profile on the 20th of October followed the general contour of the assumed ionosphere only up to 253 km and above that altitude the electron density decreased, then there would be no rays with apogees above 253 km. This is a reasonable assumption, since rocket measurements of the electron-density profiles usually show data curves which are not smooth like the Chapman layers used for synthesis here.

Using this assumption, final calculations were carried out and the results are shown on Fig. 57b. It can be seen that the match between the synthetic and experimental records is quite good at the four lower frequencies. At 18 and 20 Mc, the echoes are still too thin. Examination of Fig. 36 shows that these two records were acquired more than an hour prior to the time of the Z record which was matched by use of the thin ionosphere. Consequently, it is not surprising that the agreement is poor at the high frequencies and good at the low frequencies because the latter were measured last at a time not far removed from the Z record. Figure 57a shows the experimental data of Fig. 51b so that it may be directly compared to the final synthetic data.

From the amplitude-matching exercise, the following conclusions and comments can be made:

1. A ground reflection coefficient which is neither frequency nor angle sensitive can account for the experimental backscatter record. In terms of the more familiar radar parameter σ_o this implies a variation like $\sin\psi$. However, other variations are not ruled out. It can only be said at this time--in the light of the match between experimental and computed results--that if the coefficient is a function of angle, then it must be a function of frequency; if it is not a function of angle it is not a function of frequency within the 10-20 Mc band. Future work with different ionospheres and better records should permit a decisive resolution of this matter.

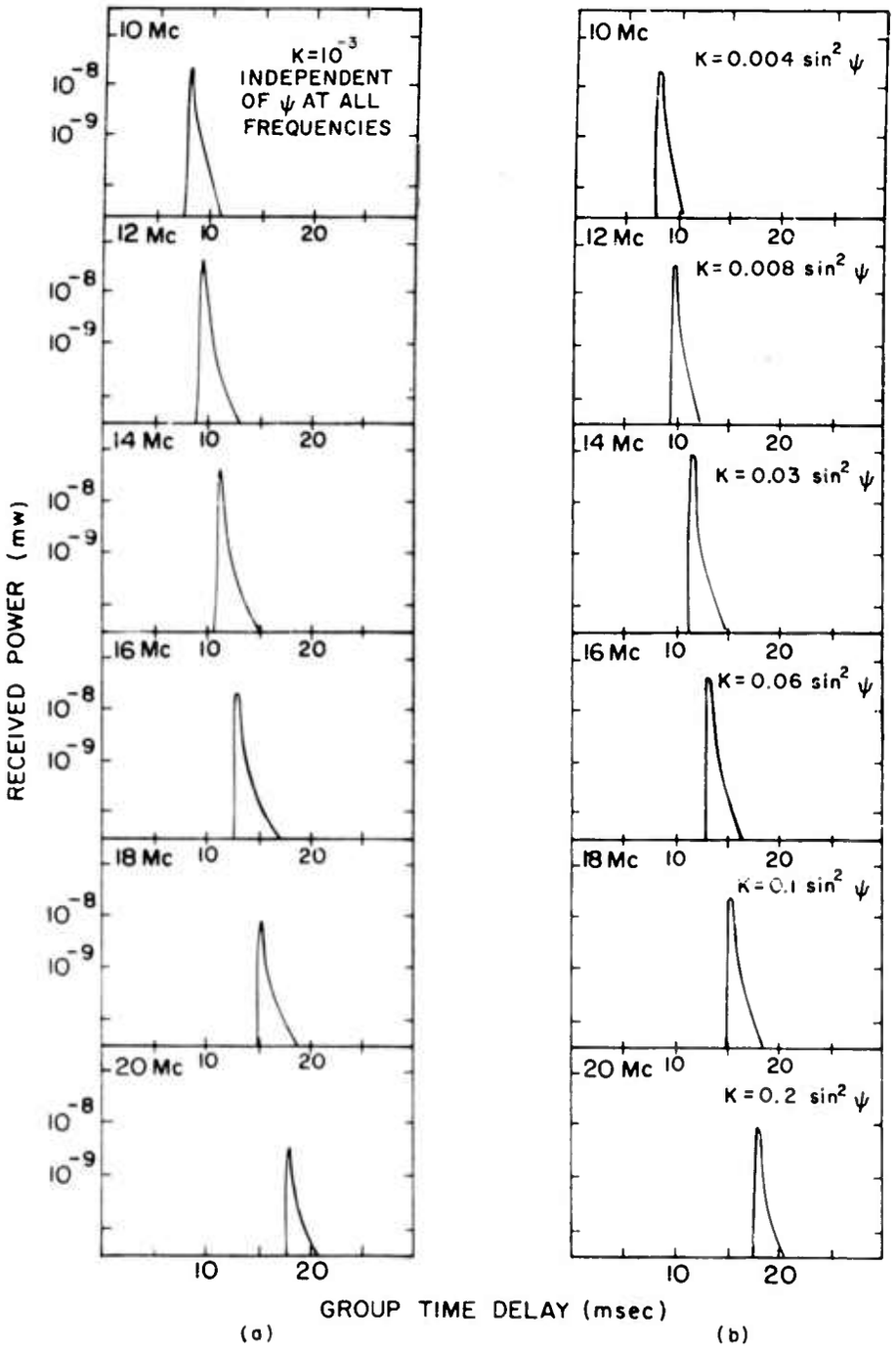

FIG. 56. FURTHER SYNTHESIS.

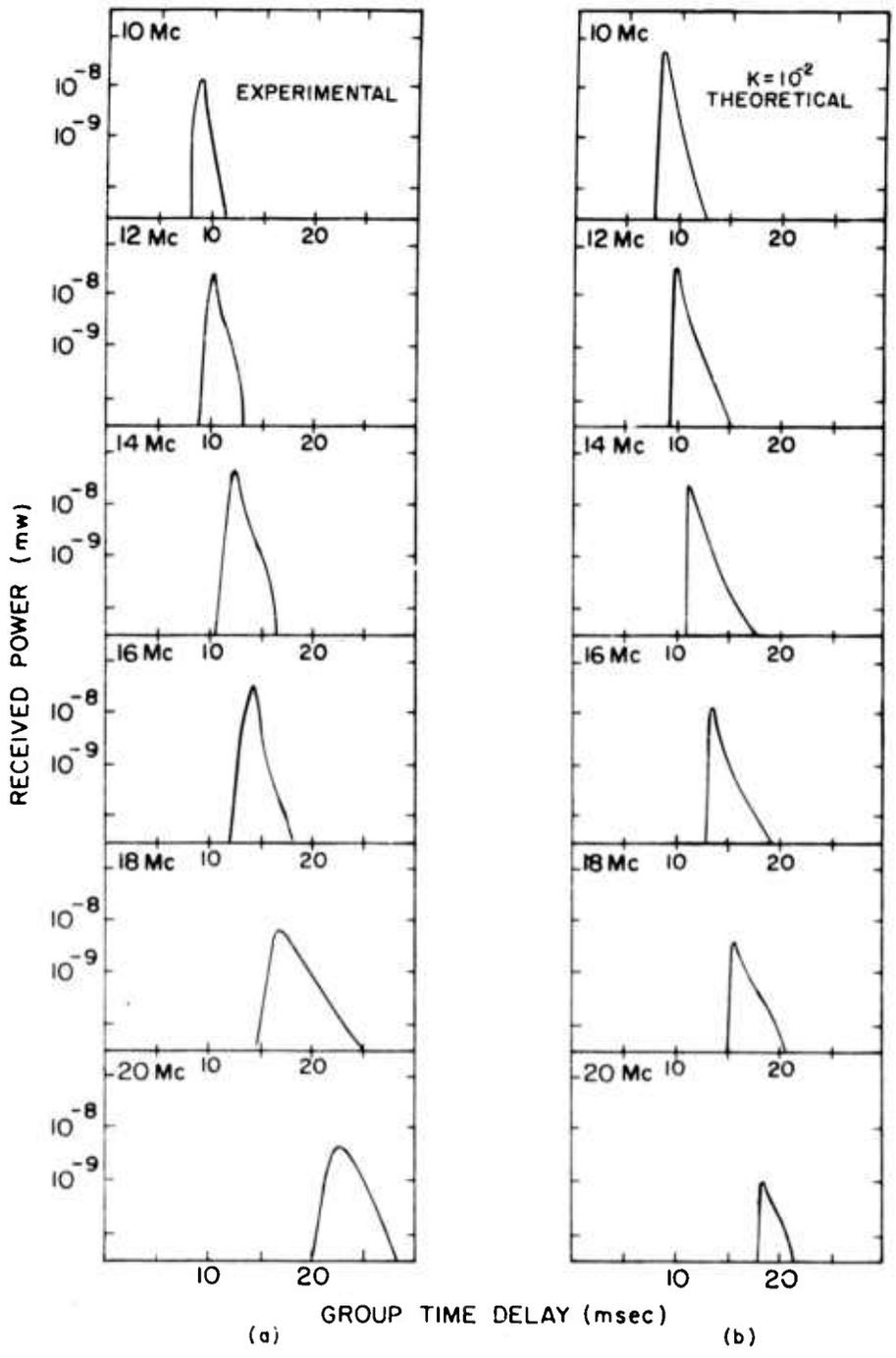

FIG. 57. COMPARISON OF EXPERIMENTAL AND SYNTHETIC RESULTS.

2. Comparison between synthetic and experimental backscatter has been severely hindered by the long time interval for acquisition of records. In future work, emphasis will be placed on the measurement of A and Z records in a short interval of time so that they can be used together as a set without inaccuracy due to changes in the ionosphere.

3. The antenna pattern has a major influence on the time distribution of received backscatter energy. The strength of this influence can be seen clearly by the program user because printed data which accompany the record break the calculation down into stages where each individual factor can be seen. On occasion, when the wrong synthetic antenna was accidentally used, the backscatter echo was severely distorted.

4. Future work of this nature will be greatly aided by a more thorough study of the effect of various ionospheric structures on the general shape of backscatter. A number of features are still not understood and the method given here seems to show promise of being able to answer many questions. The synthesis of an ionosphere to match the 20 October record would have been much easier if it could have followed a thorough study of the effect of ionospheric layer structures on sweep-frequency backscatter shapes.

REFERENCES

1. T. L. Eckersley, "Studies in Radio Transmission," Jour. IEE (London), 71, Sep 1932, pp. 405-459; in particular, Part (3) on Scattering, pp. 439-443.

2. A. M. Peterson, "The Interpretation of Long Scatter Echo Patterns," Proc. of Conference on Ionospheric Research, 1, Jun 1948, pp. 1F-11F.

3. W. Dieminger, "The Scattering of Radio Waves," Proc. Phys. Soc. (London), 64B, Feb 1951, pp. 142-159.

4. W. Dieminger, "Ground Scatter by Ionospheric Radar," in Avionics Research, papers presented at the AGARD Avionics Panel Meeting, Copenhagen, Oct 1958, Pergamon Press, New York, 1960, pp. 29-43.

5. A. M. Peterson, "Scatter-Sounding Ionosphere Investigations by Back-Scatter Techniques," Ph.D. Dissertation, Stanford University, Stanford, Calif., May 1952.

6. C. G. McCue, "High-Frequency Back-Scatter Observations at Salisbury, South Australia," Aust. J. Phys., 9, Dec 1956, pp. 454-70.

7. H. F. Bates, "Direct HF Backscatter from the F Region," J. Geophys. Res., 65, Jul 1960, pp. 1993-2002.

8. A. M. Peterson, O. G. Villard, Jr., R. L. Leadabrand, and P. B. Gallagher, "Regularly Observable Aspect-Sensitive Radio Reflections from Ionization Aligned with the Earth's Magnetic Field and Located Within the Ionospheric Layers at Middle Latitudes," TR No. 93, Contract N6onr 251(07), Radio Propagation Laboratory, Stanford University, Stanford, Calif., 30 Sep 1955.

9. P. B. Gallagher, "Analysis of a New Type of Radio Scattering from the Ionospheric E-Region," TR No. 107, Contract N6onr-251(07), Radio Propagation Laboratory, in cooperation with Electronics Laboratory, Stanford University, Stanford, Calif., 7 May 1956. AD-95 546.

10. R. D. Egan, "Anisotropic Field-Aligned Ionization Irregularities Within the Ionosphere Near the Magnetic Equator," TR No. 1, NSF Grant Y 22-10/309, Radio Propagation Laboratory, Stanford University, Stanford, Calif., 30 Dec 1959.

11. R. D. Egan and A. M. Peterson, "Backscatter Observations of Sporadic-E," TR No. 2, NSF Grant Y 22-10/309, Radioscience Laboratory, Stanford University, Stanford, Calif., 30 May 1961.

12. L. Owren and H. F. Bates, "Arctic Propagation Studies at Tropospheric and Ionospheric Modes of Propagation," Final Report, Contract AF 19(604)-1859, Geophysical Institute of the University of Alaska, College, Alaska, Oct 1959. "Task A. Ionospheric Backscatter," pp. 1-46. AFCRC-TR-59-366. AD-231 504.

13. P. B. Gallagher and O. G. Villard, Jr., "Radio Reflections from Artificially Produced Electron Clouds: Snowpuff II," Scientific Report 1, Contract AF-19(604)-2075, Stanford Electronics Laboratories, Stanford, Calif., 15 Dec 1958.

14. V. C. Pineo, L. C. Kraft, and H. W. Briscoe, "Ionospheric Backscatter Observation at 400 Mc/s," J. Geophys. Res., 65, May 1960, pp. 1620-21.

15. G. H. Hagn, D. L. Nielson, and F. H. Smith, Backscatter Literature Survey, Prepared for Office of the Secretary of Defense, Contract SD-66, SRI Project No. 3311, Stanford Research Institute, Menlo Park, Calif., Jun 1961.

16. A. K. Brown, "Abstracts of Articles on Ground Backscatter Propagated by the Ionosphere," TR No. 4, Contract Nonr 225(33), Stanford Electronics Laboratories, Stanford, Calif., 28 Jul 1959.

17. L. A. Manning, Bibliography of the Ionosphere (An Annotated Survey Through 1960), Rept. SEL-62-064, Stanford Electronics Laboratories, Stanford, Calif., May 1962. AFCRL-62 188.

18. W. Nupen, "Bibliography on Ionospheric Propagation of Radio Waves," Tech. Note No. 84, Nat. Bur. Std., Washington, D.C., Oct 1960.

19. R. F. Mlodnosky and R. A. Helliwell, "Graphic Data on the Earth's Main Magnetic Field in Space," Rept. SEL-62-026 (TR No. 1), Grant NsG-174-61, Stanford Electronics Laboratories, Stanford, Calif., Feb 1962.

20. E. D. R. Shearman, "The Technique of Ionospheric Investigation Using Ground Back-Scatter," Proc. IEE, 103B, 1956, pp. 210-221.

21. O. G. Villard, Jr. and A. M. Peterson, "Scattersounding: A Technique for Study of the Ionosphere at a Distance," TR No. 54, Contract N6onr-251, Electronics Research Laboratory, Stanford University, Stanford, Calif., Aug 1952.

22. L. P. Bolgiano, Jr., "Some Characteristics of Multiple-Hop Sweep-Frequency Backscatter Observations Between 15 and 54 Mc/s," TR No. 17, Contract Nonr 225(33), Stanford Electronics Laboratories, Stanford, Calif., 10 Oct 1960.

23. R. Silberstein, "Sweep Frequency Backscatter--Some Observations and Deductions," IRE Trans., AP-2, 2, Apr 1954.

24. A. M. Peterson, "The Mechanism of F-Layer Propagated Backscatter Echoes," J. Geophys. Res., 56, 2, Jun 1951.

25. R. Silberstein, "The Use of Sweep-Frequency Backscatter Data for Determining Oblique-Incidence Ionospheric Characteristics," J. Geophys. Res., 63, 2, Jun 1958.

26. M. L. Phillips, vols. I and II, 1 Aug 1958 [published Jun 1961 under Contract Nonr-2455(00)], ACF Industries Inc., Hyattsville, Md., pp. 180 and 220. (Title and report SECRET)

27. W. C. Hoffman, "A Theoretical Model for High-Frequency Backscatter from the Sea Surface via the Ionosphere," J. Atmos. Terr. Phys., 7, Nov 1955, pp. 278-284.

28. S. N. Denno and O. G. Villard, Jr., "Some Backscatter, Sweep-Frequency Observations," Rept. SEL-63-011 (TR No. 72), Stanford Electronics Laboratories, Stanford, Calif., Jan 1963.

29. J. W. Finney, "Ray Tracing Development for Propagation Studies," Tech. Note No. 7697, Nat. Bur. Std., Boulder Laboratories, Boulder, Colo., 4 Jun 1963.

30. T. A. Croft and L. Gregory, "A Fast, Versatile Ray-Tracing Program for IBM 7090 Digital Computers," Rept. SEL-63-108 (TR No. 82), Stanford Electronics Laboratories, Stanford, Calif., Oct 1963.

31. T. A. Croft, "The Synthesis of Oblique Ionograms by Digital Computer," Rept. SU-SEL-64-106 (TR No. 89), Stanford Electronics Laboratories, Stanford, Calif., Sep 1964.

32. D. Nielson, G. Hagn, L. Rorden, and N. Clark, "An Investigation of the Backscatter of High-Frequency Radio Waves from Land, Sea, Water, and Ice," Final Report, SRI Project 2909, Contract Nonr 2917(00), Stanford Research Institute, Menlo Park, Calif., May 1960.

33. G. Hagn, "An Investigation of the Direct Backscatter of High-Frequency Radio Waves from Land, Sea, Water, and Ice Surfaces," Final Report, SRI Project 2909, Contract Nonr 2917(00), Stanford Research Institute, Menlo Park, Calif., May 1962.

34. R. P. Ingalls and M. L. Stone, "Characteristics of Sea Clutter at HF," (Abstract from IRE-URSI Symposium), IRE Trans., AP-4, 164, Jan 1957.

35. I. Ranzi, "Radio Communication by Backscatter," Tech. Summary Report NR 1, 1 Jul 1958 to 30 Nov 1959, Contract NR AF 61(052)-139, Centro Radioelettrico Sperimentale, G. Marconi Lab., Rome, Italy, 31 Dec 1959. AFCRC-TN-60-154.

36. I. Ranzi, "Tropospheric Influence on H.F. Backscatter Near the Sea," Scientific Note 2 (research sponsored in part...under contract AF 61(052-139), Centro Radioelettrico Sperimentale, G. Marconi Lab., Rome, Italy, 30 Mar 1960. AFCRL-TN-60-953.

37. W. S. Ament, "Forward- and Back-Scattering from Certain Rough Surfaces," IRE Trans., PGAP-4, 1956, pp. 369-373.

38. T. Hagfors, "Backscattering from an Undulating Surface with Applications to Radar Returns from the Moon," J. Geophys. Res., 69, 18, 15 Sep 1964, pp. 3779-84.

39. "Ionospheric Radio Propagation," Nat. Bur. Std. Circ. 462, 25 Jun 1948

40. J. A. Ratcliffe, The Magneto-Ionic Theory and Its Applications to the Ionosphere, Cambridge University Press, Cambridge, Mass., 1959.

41. M. L. Phillips, "Theoretical Evaluation of HF-Backscatter Observations," Tech. Memo. No. E-13, Electro-Physics Laboratories, ACF Industries, Hyattsville, Md., 1 Dec 1960.

42. C. D. Hodgman, et al, Handbook of Chemistry and Physics, The Chemical Rubber Publishing Co., Cleveland, Ohio, May 1963.

43. F. E. Terman, et al, Electronic and Radio Engineering, McGraw-Hill Book Co., Inc., New York, 1955, p. 858.

44. J. A. Aseltine, Transform Method in Linear System Analysis, McGraw-Hill Book Co., Inc., New York, 1958, p. 114.

45. C. Barnes, "Antenna Pattern Measurements of a Full-Scale Rhombic Antenna," Supplement 2 to Research Memorandum 9, Contract DA 36-039 SC-87197, SRI Project No. 3670, Stanford Research Institute, Menlo Park, Calif., May 1963.

46. R. A. Smith, Aerials for Metre and Decimetre Wave-Lengths, Cambridge University Press, Cambridge, Mass., 1949, p. 19.

47. J. R. Ragazzini and G. F. Franklin, Sampled Data Control Systems, McGraw-Hill Book Co., Inc., New York, 1958.

48. K. G. Budden, Radio Waves in the Ionosphere, Cambridge University Press, Cambridge, Mass., 1961.

49. T. A. Croft, "An HF-Radar Search for the Effects of Earth Satellites upon the Ionosphere," TR No. 24, Contract Nonr 225(33), Stanford Electronics Laboratories, Stanford, Calif., 10 Mar 1961.

50. H. V. Cottony and J. R. Johler, "Cosmic Radio Noise in the VHF Band," Proc. IRE, 40, 9, 1952, p. 1058.

51. Nautical Almanac, 1964, Nautical Almanac Office, U.S. Naval Observatory, Washington, D.C.

52. P. O. Laitinen and G. W. Haydon, "Analysis and Prediction of Sky-Wave Field Intensities in the High Frequency Band," TR No. 9, Signal Corps Radio Propagation Agency, Fort Monmouth, N.J., Mar 1956.

53. Ionospheric Predictions, Central Radio Propagation Laboratory, U.S. Department of Commerce, Washington, D.C., Sep 1964.

54. J. W. Wright, "Note on Quiet-Day Vertical Cross Sections of the Ionosphere Along 75° West Geographic Meridian," J. Geophys. Res., 64, Oct 1959, pp. 1631-34.

ONR-ARPA UNCLASSIFIED DISTRIBUTION LIST
January 1965

No. of Copies

NAVY

Chief of Naval Res.
Dept. of the Navy
Washington, D.C. 20360
1 Attn: Code 402C
2 Attn: Code 418

Dir., Naval Res. Lab.
Washington 25, D.C.
1 Attn: Code 5320 (Mr. J. M. Headrick)
1 Attn: Code 2027
1 Attn: Code 5320 (Mr. E. Zettle)

Chief of Naval Operations
Dept. of the Navy
Washington 25, D.C.
1 Attn: OP-723E
1 Attn: OP-07TE

Dir., Special Projects Off.
Dept. of the Navy
Washington 25, D.C.
1 Attn: Code SP-204

Commander
Pacific Missile Range
Point Mugu, Calif.
1 Attn: Code 3215

Commander
Naval Missile Center
Point Mugu, Calif.
1 Attn: Code NO3022

Commanding Officer and Dir.
U.S. Navy Elec. Lab.
San Diego, Calif. 92152
1 Attn: Mr. H. J. Wirth
1 Attn: Library

Commanding Officer
U.S. Naval Ord. Lab.
Corona, Calif. 91720
1 Attn: Mr. V.E. Hildebrand (Code 453)

No. of Copies

AIR FORCE

Headquarters
Air Force Systems Command
Foreign Tech. Div.
Wright-Patterson AFB, Ohio
1 Attn: TDC (Mr. Zabatakas)
1 Attn: TDEED (Mr. W.L. Picklesimer)
1 Attn: TDATA (Mr. G.A. Long, Jr.)
1 Attn: TDCE (Mr. M.S.J. Graebner)

Headquarters, RTD
Bolling AFB
Washington, D.C. 20332
1 Attn: RTHC (Col. Richard Cosel)

Rome Air Dev. Center
Res. and Tech. Div.
Griffiss AFB, New York
1 Attn: EMASR (Mr. V.J. Coyne)
1 Attn: RAVEL-3 (Mr. G.R. Weatherup)
1 Attn: RALCS (Mr. S. DiGennaro)

Commander
USAF Security Systems
San Antonio, Texas
1 Attn: ORL (Mr. W. L. Anderson)

Headquarters, USAF
Off. of Assistant Chief of Staff, Intelligence
Washington, D.C. 20330
1 Attn: AFNICAA (Lt. Col. Long)
1 Attn: Policy & Prog. Gp., AFNINC

Hqs., N. Amer. Air Def. Command
Ent AFB
Colorado Springs 12, Colorado
1 Attn: NPSD-A (Col. M.R. Cripe)
1 Attn: NELC-AP

Hqs., AFCRL
L. G. Hanscom Field
Bedford, Mass.
1 Attn: CRUP (Dr. G.J. Gassman)
1 Attn: CRUI (Mr. W.F. Ring)

No. of Copies

Hqs., USAF
The Pentagon
Washington 25, D.C.
1 Attn: AFRDDF (Lt. Col. Eugene A. Novak)

Hqs., SAC
Offutt AFB
Omaha, Nebraska
1 Attn: Mr. Eugene Jackson

ARMY

Chief, Army Security Agcy.
Arlington Hall Station
Arlington, Va. 22212
1 Attn: ATOP-O (Mr. W. Mulroney)

Commanding Officer, Bldg. T-7
U.S. Army Material Command
Washington 25, D.C.
1 Attn: AMCRD-D

U.S. Army Elec. Labs.
Mt. View Office
P.O. Box 205
Mt. View, Calif. 94042
1 Attn: Mr. Joseph Bert

U.S. Army, SLAG
1B-657, The Pentagon
1 Washington, D.C. 20505

DOD

Dir., Adv. Res. Projects Agcy.
Washington 25, D.C.
1 Attn: Mr. Alvin Van Every

Director
Weapons Systems Evaluation Group
Office of the Dir. of Def.
Res. and Eng.
1 Washington 25, D.C.

Office of Assistant Chief of Staff for Intelligence
Dept. of the Army
Rm 2B457, The Pentagon
Washington 25, D.C.
1 Attn: Mr. Joseph Grady

No. of Copies

Office of the Assistant Dir.
Intelligence and Reconnaissance
Office of the Dir. of Def.
Res. and Eng.
Rm. 3E119, The Pentagon
Washington 25, D.C.
1 Attn: Mr. Howard A. Staderman

Dir., Def. Intelligence Agcy.
Washington, D.C. 20301
1 Attn: DIAAQ-2A (Capt. J. Stewart)
1 Attn: DIAST-B (Mr. T. Brooke)

Deputy Dir., Res. and Tech.
Office of the Dir. of Def.
Res. and Eng.
Rm. 3E1030, The Pentagon
Washington 25, D.C.
1 Attn: Dr. Chalmers W. Sherwin

Office of the Assistant Dir.
(Defense Systems)
Def. Res. and Eng.
Rm. 3D138, The Pentagon
Washington 25, D.C.
1 Attn: Mr. Daniel Fink

Dir., National Security Agcy.
Ft. George G. Meade, Md.
1 Attn: K-344 (Mr. Charles Gandy)
1 Attn: C3/TDL

Def. Doc. Center
Cameron Station
20 Alexandria, Va.

OTHER

ACF-E Industries
3355-52nd Ave.
Hyattsville, Md.
1 Attn: Mr. William T. Whelan

Aero Geo Astro Corp.
13624 Magnolia Ave.
Corona, Calif.
1 Attn: Donald Adrian

Astrophysics Res. Corp.
2444 Wilshire Blvd., Rm 512
Santa Monica, Calif.
1 Attn: Dr. Alfred Reifman

No. of Copies	
	HRB Singer, Inc. Science Park State College, Pa.
1	Attn: Library
	Institute for Def. Analyses 400 Army-Navy Drive Arlington, Va. 22202
1	Attn: Dr. Paul von Handel
	Inst. of Science and Tech. The Univ. of Michigan P.O. Box 618 Ann Arbor, Michigan
1	Attn: BAMIRAC Library
	Mass. Inst. of Tech. Center for Space Res. Bldg. 33-109 Cambridge, Mass.
1	Attn: Dr. J. V. Harrington
	Mass. Inst. of Tech. Lincoln Lab. Lexington 73, Mass.
1	Attn: Dr. J. H. Chisholm
	MITRE Corp.-E Bldg. Rm. 353 Bedford, Mass.
1	Attn: Mr. W. A. Whitcraft, Jr.
	National Bureau of Standards Boulder Labs. Boulder, Colorado
1	Attn: 85.20 (Mr. L.H. Tveten)
	Pickard and Burns, Inc. Res. Dept. 103 Fourth Ave. Waltham 54, Mass.
1	Attn: Dr. John C. Williams
	Princeton Univ. James Forrestal Res. Center Sayre Hall Princeton, N. J.
1	Attn: Dr. Edward Frieman

No. of Copies	
	RAND Corp. 1700 Main St. Santa Monica, Calif.
1	Attn: Dr. Ivan Selin
1	Attn: Dr. Cullen Crain
1	Attn: Library
	Raytheon Company Communication and Data Processing Operations 1415 Boston-Providence Turnpike Norwood, Mass.
1	Attn: Mr. L. C. Edwards
	Stanford Res. Inst. Menlo Park, Calif.
1	Attn: Dr. David Johnson
	Mr. Thurston B. Soisson Box 8164 SW Station
1	Washington, D.C.
	Sylvania Elec. Systems Electronic Def. Labs. P.O. Box 205 Mt. View, Calif.
1	Attn: Mr. John DonCarlos
	University of California Mathematics Dept. Berkeley 4, Calif.
1	Attn: Dr. Edmond J. Pinney
	Battelle-Defender Battelle Memorial Inst. 505 King Ave. Columbus, Ohio 43201
1	Attn: Doc. Center
	Dept of Elec. Eng. Radiolocation Res. Lab. University of Illinois Urbana, Illinois
1	Attn: 311 EERL (Mr. D.G. Detert)
	Bendix Corp. Bendix Radio Div. Baltimore 4, Md.
1	Attn: Mr. John Mortin

UNCLASSIFIED

Security Classification

DOCUMENT CONTROL DATA - R&D

(Security classification of title, body of abstract and indexing annotation must be entered when the overall report is classified)

1. ORIGINATING ACTIVITY *(Corporate author)*

Stanford Electronics Laboratories
Stanford University, Stanford, California

2a. REPORT SECURITY CLASSIFICATION
UNCLASSIFIED

2b. GROUP

3. REPORT TITLE

THE SYNTHESIS OF SWEEP-FREQUENCY GROUND BACKSCATTER BY DIGITAL COMPUTER

4. DESCRIPTIVE NOTES *(Type of report and inclusive dates)*

Technical Report

5. AUTHOR(S) *(Last name, first name, initial)*

T. A. Croft

6. REPORT DATE	7a. TOTAL NO. OF PAGES	7b. NO. OF REFS
January 1965	142	54

8a. CONTRACT OR GRANT NO.	9a. ORIGINATOR'S REPORT NUMBER(S)
Office of Naval Research Contract	Technical Report No. 84
b. PROJECT NO. Nonr-225(64)	SU-SEL-65-002
c.	9b. OTHER REPORT NO(S) *(Any other numbers that may be assigned this report)*
d.	

10. AVAILABILITY/LIMITATION NOTICES

Foreign announcement and dissemination by DDC not authorized.

11. SUPPLEMENTARY NOTES	12. SPONSORING MILITARY ACTIVITY
	ONR

13. ABSTRACT A high-frequency pulse radar often receives energy which has propagated through the ionosphere to the ground, scattered, and then returned to the radar again via the ionosphere. When this energy is displayed as a function of both time delay and operating frequency, the record is called sweep-frequency backscatter. In this report a digital computer technique is devised to synthesize such records in a manner which is quantitative in all parameters.

The synthesis is designed so that very few approximations are needed. Full allowance is made for the following: a spherical earth and ionosphere; a wide variety of electron-density variations in height and range; ionospheric absorption which varies with frequency, azimuth, and elevation; ground-scattering characteristics which vary with frequency, range, and the angle of incidence; ground-reflection coefficients which vary with frequency and range; the transmitted pulse shape, duration, and power level; receiver bandwidth and total received noise power. Only three approximations are made: the discrete number systems is substituted for continuous numbers; ray theory is used with the assumption that energy is distributed uniformly between adjacent closely spaced raypaths; the effect of the geomagnetic field on raypath range and group time delay is neglected.

The digital synthesis has two major uses. First, it is possible to vary a single parameter in a known way and then see the effect that the variation should have on ground backscatter. For example, a ripple of known characteristics can be inserted in the ionosphere at a known range and the resulting perturbation in the ground backscatter can be calculated.

(Cont'd. on page 2)

DD FORM 1 JAN 64 1473

UNCLASSIFIED

Security Classification

The second major use of the program is the synthesis of a close likeness of a specific experimental record. This synthetic record serves to confirm knowledge of the mechanisms which play a part in ground backscatter. For example, the ground-scatter coefficient varies with frequency, terrain type, and incidence angle in a manner which is not presently well understood. The process of making a synthetic record to match an experimental record will involve the trial of several hypothetical scatter functions until one is found which duplicates observed behavior. Since most of the other contributing mechanisms exhibit a predictable behavior, it will thus be possible to isolate the scatter pattern and study it independently.

14 KEY WORDS	LINK A		LINK B		LINK C	
	ROLE	WT	ROLE	WT	ROLE	WT
PROGRAMMING (COMPUTERS) IONOSPHERIC PROPAGATION MODELS (SIMULATION)						

INSTRUCTIONS

1. ORIGINATING ACTIVITY: Enter the name and address of the contractor, subcontractor, grantee, Department of Defense activity or other organization *(corporate author)* issuing the report.

2a. REPORT SECURITY CLASSIFICATION: Enter the overall security classification of the report. Indicate whether "Restricted Data" is included. Marking is to be in accordance with appropriate security regulations.

2b. GROUP: Automatic downgrading is specified in DoD Directive 5200.10 and Armed Forces Industrial Manual. Enter the group number. Also, when applicable, show that optional markings have been used for Group 3 and Group 4 as authorized.

3. REPORT TITLE: Enter the complete report title in all capital letters. Titles in all cases should be unclassified. If a meaningful title cannot be selected without classification, show title classification in all capitals in parenthesis immediately following the title.

4. DESCRIPTIVE NOTES: If appropriate, enter the type of report, e.g., interim, progress, summary, annual, or final. Give the inclusive dates when a specific reporting period is covered.

5. AUTHOR(S): Enter the name(s) of author(s) as shown on or in the report. Enter last name, first name, middle initial. If military, show rank and branch of service. The name of the principal author is an absolute minimum requirement.

6. REPORT DATE: Enter the date of the report as day, month, year, or month, year. If more than one date appears on the report, use date of publication.

7a. TOTAL NUMBER OF PAGES: The total page count should follow normal pagination procedures, i.e., enter the number of pages containing information.

7b. NUMBER OF REFERENCES: Enter the total number of references cited in the report.

8a. CONTRACT OR GRANT NUMBER: If appropriate, enter the applicable number of the contract or grant under which the report was written.

8b, 8c, & 8d. PROJECT NUMBER: Enter the appropriate military department identification, such as project number, subproject number, system numbers, task number, etc.

9a. ORIGINATOR'S REPORT NUMBER(S): Enter the official report number by which the document will be identified and controlled by the originating activity. This number must be unique to this report.

9b. OTHER REPORT NUMBER(S): If the report has been assigned any other report numbers *(either by the originator or by the sponsor)*, also enter this number(s).

10. AVAILABILITY/LIMITATION NOTICES: Enter any limitations on further dissemination of the report, other than those imposed by security classification, using standard statements such as:

(1) "Qualified requesters may obtain copies of this report from DDC."

(2) "Foreign announcement and dissemination of this report by DDC is not authorized."

(3) "U. S. Government agencies may obtain copies of this report directly from DDC. Other qualified DDC users shall request through _____."

(4) "U. S. military agencies may obtain copies of this report directly from DDC. Other qualified users shall request through _____."

(5) "All distribution of this report is controlled. Qualified DDC users shall request through _____."

If the report has been furnished to the Office of Technical Services, Department of Commerce, for sale to the public, indicate this fact and enter the price, if known.

11. SUPPLEMENTARY NOTES: Use for additional explanatory notes.

12. SPONSORING MILITARY ACTIVITY: Enter the name of the departmental project office or laboratory sponsoring *(paying for)* the research and development. Include address.

13. ABSTRACT: Enter an abstract giving a brief and factual summary of the document indicative of the report, even though it may also appear elsewhere in the body of the technical report. If additional space is required, a continuation sheet shall be attached.

It is highly desirable that the abstract of classified reports be unclassified. Each paragraph of the abstract shall end with an indication of the military security classification of the information in the paragraph, represented as *(TS)*, *(S)*, *(C)*, or *(U)*.

There is no limitation on the length of the abstract. However, the suggested length is from 150 to 225 words.

14. KEY WORDS: Key words are technically meaningful terms or short phrases that characterize a report and may be used as index entries for cataloging the report. Key words must be selected so that no security classification is required. Identifiers, such as equipment model designation, trade name, military project code name, geographic location, may be used as key words but will be followed by an indication of technical context. The assignment of links, roles, and weights is optional.